Effect of Silica Fume on Moisture Flow and the Advective-Dispersive Transport of Ionic Species in Unsaturated Concrete

A Thesis Submitted to the College of Graduate Studies and Research in Partial Fulfillment of the Degree of Master of Science in the Department of Civil and Geological Engineering, University of Saskatchewan, Saskatoon, Canada

By

Thamer Ramadani

PERMISSION TO USE

In presenting this thesis in partial fulfillment of the requirements for a Postgraduate degree from the University of Saskatchewan, I agree that the Libraries of this University may make it freely available for inspection. I further agree that permission for copying of this thesis in any manner, in whole or in part, for scholarly purposes may be granted by the professor or professors who supervised my thesis work or, in their absence, by the Head of the Department or the Dean of the College in which my thesis work was done. It is understood that any copying or publication or use of this thesis or parts thereof for financial gain shall not be allowed without my written permission. It is also understood that due recognition shall be given to me and to the University of Saskatchewan in any scholarly use which may be made of any material in my thesis.

Requests for permission to copy or to make other use of material in this thesis in whole or in part should be addressed to:

Head of the Department of Civil and Geological Engineering,
University of Saskatchewan
57 Campus Drive
Saskatoon, Saskatchewan
Canada, S7N 5A9

ABSTRACT

Under unsaturated conditions, both moisture flow and the transport of ions strongly depend on the degree of saturation in concrete. In the current literature, most theories and empirical models describe moisture flow and the transport of ions in concrete based on the assumption that concrete is fully submerged in a liquid phase. This simplistic assumption often leads to a systematic underestimation in the amount of ions, such as chlorides, especially in the case of concrete applications subjected to cyclic wetting and drying conditions. In this study, an experimental program was established to determine the key hydraulic parameters needed for modeling the moisture flow and the transport of ions in five types of concrete mixes under unsaturated conditions.

The required hydraulic parameters of the five concrete mixes include the saturated hydraulic permeability, the moisture retention function, and the dependency of the relative diffusion coefficient on degree of saturation. A centrifuge technique was used to determine the saturated hydraulic permeability of the five concrete mixes. The moisture retention data of all concrete mixes were determined using a vapour equilibrium technique. The moisture retention data were then used to determine the van Genuchten empirical parameters for an analytical characterization of the capillary pressure-degree of water saturation and the relative permeability-degree of saturation relationships. The dependency of the relative diffusion coefficient on the degree of water saturation was characterized for each type of concrete mix indirectly using an electrical resistivity technique. The experimental results of this study were used in different empirical models that have been originally developed for soils to examine whether they could be applied for concrete

The five concrete mixes used in this study were characterized by the usage of a different proportion of dry densified silica fume in each concrete mix. Those mixes were used to determine the effect of silica fume on the experimental and the empirical key hydraulic parameters considered in this study.

ACKNOWLEDGEMENTS

This work would not have been possible without the whole-hearted support and encouragement of many individuals. Their contribution deserved special mention. It is a pleasure to convey my gratitude to them all in my humble acknowledgment.

First, I want to thank the Department of Civil and Geological Engineering for giving me permission to commence this thesis in the first instance. I offer my sincerest gratitude to my supervisor, Prof. Mohamed Boulfiza, who has assisted me throughout my thesis with his patience, knowledge, and valuable support whilst allowing me the room to work in my own way. I am grateful to him.

I have to thank Professors Leon Wegner and Ikechukwuka Oguocha, the members of my advisory committee, for their expertise, constructive criticism, guidance and valuable comments during the course of this research.

I am grateful for the financial support provided by The Ministry of Higher Education in Saudi Arabia and The Natural Sciences and Engineering Research Council of Canada (NSERC).

I would like to thank Mr. Brennan Pokoyoway, Mr. Doug Fisher and Mr. Dale Pavier for their assistance and direction throughout the laboratory component of the research.

My parents, Abdullah Ramadani and Shahenaz Nasser, and my wife, Israa Baz, deserve special acknowledgement for encouraging me to pursue my degree. I have relied on their love and support throughout all my academic work. Their courage always inspired me. It is to them that I dedicate this work. I cannot end without thanking the friendly and cheerful group of fellow students, who to thank any others whom I may have missed, who have, directly or indirectly, contributed to my research.

Table of Contents

List of Tables

List of Figures

1. Introduction

1.1 General background

Concrete is one of the most used materials in several types of construction, and its long-term durability has become an important aspect that has to be taken into consideration both by the materials specialist and the structural engineer alike. Despite the fact that concrete materials have shown a good performance, in general, towards applied loads, in terms of their mechanical properties, concrete materials can also be very vulnerable to several environmental factors under some specific severe or harsh conditions. Examples of such severe conditions include moisture, air, and/or other aggressive environmental factors that can potentially cause several forms of deterioration in concrete structures and corrosion of reinforcing steel bars.

The corrosion of reinforcing steel bars, caused by the ingress of chloride ions into the concrete matrix, has become an important problem as it has significant side effects on reinforced concrete durability. When the concentration of chloride ions in the capillary pores reaches a threshold value at the rebar location, the chloride ions start to attack the protective layer (passivity layer) that develops on the steel surface in high pH solutions, to form rust. The formation of rust leads to a volume expansion in concrete elements, causing cracking, spalling, and loss of concrete cover. In addition, the severe formation of rust leads to a reduction in the cross-sectional area of the reinforcing steel bars, and hence ultimately leading to a reduction of the load-carrying capacity of concrete structures.

Most concrete structures operate under unsaturated conditions where the risk of corrosion is more severe than in the saturated case due to the availability of moisture and oxygen,

as well as the rapid ingress of chloride ions by advection under high capillary suctions. Under unsaturated conditions, concrete is typically subjected to repeated wetting and drying cycles where the transport of ions is driven not only by diffusion but by the simultaneous action of advective and diffusive transport mechanisms, resulting in an increase of ions concentration, such as chloride ions, in the capillary pores of the concrete matrix. However, the quality of concrete can play a very important role in reducing the ions penetration into concrete. In particular, the incorporation of pozzolanic materials into the concrete mix has shown significant improvements in reducing the porosity and the permeability of concrete, and hence, has been used as a means to reduce the penetration of ions.

1.2 Unsaturated water flow and transport of ions

Most reinforced concrete structures do not operate under fully saturated conditions. This is particularly the case of columns or dams that are permanently submerged in water, in their service environment. Thus, the spaces between the pores in a concrete matrix are in general not fully occupied by a liquid phase (Kelham 1988; Hall 1989; Hall 1994; Martys 1995). When a concrete element is under unsaturated conditions, the small pores within the concrete matrix would absorb water by a large capillary pressure produced by the contact of the small pores in the concrete matrix with the surrounding moisture or liquid phase. As a result, the dissolved ions in water would be transported along the moving liquid phase in the concrete matrix. In addition, the degree of water or moisture flow and the subsequent transport of dissolved ions in concrete matrix depends on the relative humidity conditions that impose different levels of vapor pressure and degrees of saturation on concrete elements. Therefore, a relation between the capillary pressure imposed by the environment and the degree of saturation in the concrete element, known as “the moisture retention function”, has to be determined at equilibrium in order to have

a more realistic model for simulating water flow and the transport of ions in concrete under unsaturated conditions. Moreover, data in describing the relationship between the capillary pressure and the degree of saturation of concrete are not easy to find in the available literature on concrete.

Diffusion of ions through the liquid and gaseous phases in the concrete pores is another important mechanism of ions transport under unsaturated conditions. Diffusion of ions in concrete is defined as the movement of ions under the effect of a concentration gradient from high concentration regions to low concentration regions. When concrete is fully saturated, the pores have continuous water phases, in which diffusion is the predominant mechanism controlling the transport of ions into concrete. However, under partially saturated or unsaturated conditions, the diffusion coefficient of ions is governed by the degree of saturation of concrete and is no longer constant (Bazant and Najjar 1972; Garboczi 1990; Saetta et al. 1993; McCarter et al. 2001). In addition, the diffusion rate of ions can either increase or decrease sharply as the degree of saturation or the moisture content in the concrete matrix changes (Richardson 2002). Therefore, the dependency of the effective diffusion coefficient on the degree of saturation of concrete is essential in order to simulate the transport of ions and moisture flow in unsaturated concrete. In the field of concrete, there is no standard test for determining the relation between the diffusion coefficient and the degree of saturation, and the data related to this issue are still limited up to date.

The geometrical and physical properties of concrete, such as pore size, pore distribution, hydraulic conductivity, and concrete mix design are also key factors that can characterize the rate of ions diffusion and moisture flow in concrete under both saturated and unsaturated conditions. Unfortunately, there are no standard tests here also for determining some of the hydraulic properties, such as hydraulic conductivity and

moisture retention function in the field of concrete. Therefore, tests from other fields, such as soil science and rock science, have been adapted and used to measure these basic physical properties of concrete.

1.3 **Silica fume and its effect on durability of concrete** (Siddique and Khan 2011)

Silica fume, also known as microsilica, is a byproduct produced by the smelting process in the silicon and ferrosilicon industries. The production process of silica fume involves melting the productions of silicon in electric arch furnaces to produce very fine non-crystalline silica. Silica fume can take two possible forms, dry and wet, and both forms of silica fume are classified as very active pozzolanic admixture due to its effect in enhancing the mechanical and the chemical properties of concrete to a great extent. The typical particles size of silica fume, less than 1 micro millimeter, is 100 times smaller than those of Portland cement, and when these particles of silica fume are used in a concrete mixture, they act as micro filling materials that fill the voids between the Portland cement particles. In addition, silica fume reacts with the calcium hydroxide, produced from the chemical reaction of Portland cement and water, to produce an additional type of binder material called calcium silicate hydrate (CSH). This calcium silicate hydrate is similar in its properties to the calcium hydroxide formed from Portland cement and the corresponding reaction is known as a pozzolanic reaction. More generally, pozzolans are usually defined as any siliceous or alumino-siliceous materials that, in a finely divided form and in the presence of moisture, chemically react with calcium hydroxide released by the hydration of Portland cement to form compounds possessing cementing properties.

There are three main effects that can explain the advantage of using silica fume for improving the durability of concrete. First, the presence of silica fume in a concrete

mixture reduces the volume of large pores due its effect on filling the large voids between the Portland cement particles. Furthermore, in comparison with the calcium silicate hydrate produced by the presence of silica fume, the calcium hydroxide formed from Portland cement is considered to be more vulnerable to the propagation of cracks affecting the strength and the durability of concrete structures. Therefore, the incorporation of silica fume in concrete mixes reduces the amount of calcium hydroxide formed from the reaction between Portland cement and water, and hence, increases the amount of calcium silicate hydrate. Another effect of silica fume on concrete is the enhancement of the transition zones between aggregates and cement particles. Silica fume increases the thickness of the transition zones and the bond strength between aggregates and cement particles resulting in a microstructural modification. All of these effects of silica fume reduce the permeability and the porosity of concrete and result in a reduction in the moisture movement and in the ingress of ions in concrete.

1.4 Objectives

The main objective of this research was to determine the effect of silica fume on the key parameters needed for modeling moisture flow and the ingress of ions into concrete under unsaturated conditions.

The specific objectives of this research were as follows:

1) Propose a rational theoretical framework that could capture the major aspects of moisture flow and the transport of ionic species in unsaturated concrete.
2) Identify appropriate experimental techniques and apply them for the determination of the key material parameters needed for modeling moisture flow and the transport of ions under unsaturated conditions; namely the saturated permeability coefficient, the capillary pressure-moisture relationship, and the

dependency of the effective diffusion coefficient on the degree of water saturation.

3) Use the experimental results of this study in different empirical constitutive models that have been originally developed for soils to examine whether they could be applied for the representation of concrete properties or not. In particular, the adequacy of the van Genuchten-Mualem model to represent the unsaturated hydraulic conductivity parameters and water retention data needed to be assessed. The Millington and Quirk model that has been successfully applied in many soils applications for representing the dependence of the diffusion coefficient on the degree of saturation also needed to be assessed in the case of concrete. Depending on whether the available models in the literature can represent the experimental data generated in this study, more realistic empirical models will be developed, if needed.

4) Discuss the effects of using different proportions of a supplementary cementing material, namely silica fume, on the key hydraulic parameters, including its effect on the saturated permeability coefficient, the relative permeability coefficient, the moisture retention data, the relative diffusion coefficient, and the dependency of the effective diffusion coefficient on the degree of water saturation.

1.5 Scope

This main focus of this study was to assess the effect of silica fume on the water flow and transport of ions in concrete under saturated and unsaturated conditions. Further to the above objectives, the following bullet points provide a brief description of the scope and limitations of this study:

- The type of raw materials used in this study, including aggregates, Portland cement, silica fume, and sand, were the same for all the considered concrete mixes.
- Only four different proportions of silica fume were considered in this study. These proportions were 5% silica fume, 10% silica fume, 15% silica fume, and 20% silica fume.
- The water-cementitious ratio was fixed at a value of 0.4 for all the five concrete mixes considered in this study.
- The effect of loading or cracking was not considered in this research.

1.6 Methodology

The research methodology was divided into two main stages: A laboratory-testing phase followed by a phase of constitutive modeling of the hydraulic properties of concrete

a) Laboratory tests

The experimental program was intended to identify several key hydraulic parameters, including saturated permeability coefficient, moisture retention function and dependency of diffusion coefficient on the degree of saturation needed for simulating the transport of moisture and diffusion of ions under unsaturated conditions for different qualities of concrete samples.

b) Constitutive modeling of the hydraulic properties of concrete

The experimental results were compared with several analytical and empirical models found in the literature in order to examine the validity of those models for concrete. New empirical models were sought for instances where the models currently available did not work.

2. Literature Review

Moisture movement coupled with transport of chemical species in concrete is one of the main causes of deterioration of concrete structures. This chapter presents a review of current knowledge, empirical models and experimental methods relevant to the main transport properties of unsaturated concrete. The main properties and transport mechanisms affecting moisture movement and ions transport include permeability, capillary absorption, and diffusion.

2.1 Moisture movement in concrete

Moisture movement associated with the transport of ions in concrete is one of the major causes of deterioration for concrete structures. There are two major types of moisture conditions in which water flow occurs in a concrete matrix: namely, saturated and unsaturated conditions. When voids in concrete are completely filled by the pore water solution, the condition is called “saturated”, and when the pores are filled by both gas and liquid, the condition is called “unsaturated”.

2.1.1 Water flow under saturated conditions

Darcy’s Law is one of the well-known equations describing moisture movement under saturated conditions. Darcy’s Law states that the volumetric flow rate through a porous medium in one dimension is proportional to the cross-sectional area and the hydraulic gradient. Mathematically, Darcy’s Law is expressed as:

$$Q = -K_s A \frac{dh}{dl} \tag{2.1}$$

where Q is the volumetric discharge ($\frac{m^3}{s}$), K_s is the saturated hydraulic conductivity, also called coefficient of permeability ($\frac{m}{s}$), A is the cross-sectional area (m^2), dh is the hydraulic head (m) = ($P/\rho_w.g$) + z, P is the fluid pressure ($\frac{N}{m^2}$), ρ_w is the fluid density ($\frac{kg}{m^3}$), g = acceleration due to gravity ($\frac{m}{s^2}$), z is the elevation (m), dl is the flow path length (m), and $\frac{dh}{dl}$ is the hydraulic gradient.

The hydraulic conductivity, also called coefficient of permeability, is a function of both the properties of the fluid and the properties of the porous medium. Another concept of permeability, which is independent of fluid properties, is known as the intrinsic coefficient of permeability. The intrinsic coefficient of permeability is a function of the properties of the porous medium only, without considering the properties of the liquid. Equation (2.2) shows the relation between the saturated coefficient of permeability, K_s, and the intrinsic coefficient of permeability, k:

$$K_s = \frac{k\ \rho_w\ g}{\mu} \tag{2.2}$$

where k is the intrinsic permeability (m^2), and μ is the dynamic viscosity of fluid ($\frac{kg}{m \cdot s}$).

Darcy's Law can be rewritten in terms of volume flux, q (m/s), as:

$$q = \frac{Q}{A} = -K_s \frac{dh}{dl} \tag{2.3}$$

Although the volume flux, also known as Darcy's flux, has the velocity units, it does not actually describe the velocity of the fluid traveling through all the pores in a porous medium system because of the existence of some other portions in the porous medium that are not completely filled by liquid.

The law of mass conservation is applicable in any mass transport process and this leads to a partial differential equation of the flow which, when solved, gives the hydraulic head and the flow rate in the flow domain. The continuity equation states that the divergence of mass flux equals change in mass in a control volume. For steady state, in which the water is considered to be incompressible (constant density of water ρ_w), the continuity equation is written as:

$$\Delta . q = 0 \tag{2.4}$$

2.1.2 Water flow under unsaturated conditions

In most applications, the concrete matrix of reinforced concrete structures is not fully saturated by the liquid phase (pore solution). In particular, concrete structures that are subjected to cyclic wetting and drying conditions have specific mechanisms in transporting the water and subsequently ions into concrete matrix. The degree of saturation of concrete strongly depends on the relative humidity of the environment and on the previous exposure of concrete to moisture. If the moisture content in a concrete specimen is less than the saturation level, water with its associated ions can be absorbed by large capillary forces that are caused by the contact of very small pores of concrete with the liquid phase. This mechanism of moisture flow is frequently repeated when concrete structures are subjected to cyclic wetting and drying conditions, resulting in a gradual increase of ion concentration over time, such as chlorides, inside the concrete matrix. This increase of an ion's concentration occurs under these conditions as a result of the progressive evaporation of moisture inside the concrete matrix. In general, there are two major approaches that can be used to model moisture flow in unsaturated porous media, the single-phase flow models and the multiphase models. Both approaches are described in this literature survey.

2.1.2.1 Single-phase flow system

One of the well-known equations that describe the unsaturated flow of liquids in porous media is the modified Richards' equation (Richard and Lorenzo 1931). Richards' equation is a general non-linear partial deferential equation, which was developed by extending Darcy's law to describe the water movement in unsaturated and non-swelling soil:

$$\frac{\partial(\emptyset S_l)}{\partial t} = -\nabla \cdot \left[\frac{k \cdot k_r}{\mu_l}(\nabla P_l - \rho_l g)\right] \tag{2.5}$$

where $\emptyset$ is the porosity, S_l is the saturation of the liquid phase, t is the time, ∇ is the divergence of a three dimensional vector field of the flow, k is the intrinsic permeability, k_r is the relative permeability of liquid, μ_l is the dynamic viscosity of liquid, P_l is the liquid phase pressure, ρ_l is the liquid phase density, and g is the acceleration due to the gravity.

The relative permeability of the liquid, k_r is a function of the unsaturated hydraulic conductivity, K and the saturated hydraulic conductivity, K_s (also called the saturated permeability), as it is shown in Equation (2.6):

$$K(h, x) = K_s(x) \cdot k_r\,(h, x) \tag{2.6}$$

Richards' equation considers only the flow of water in the liquid phase of a porous medium and neglects the effect of the vapor phase. It assumes that the vapor inside a porous medium is infinitely mobile, and it ignores the effect of displaced vapor during water flow. This assumption is justified in most soils' applications (Šimůnek et al. 2008), and it has also been shown under this assumption that the moisture content can be evaluated in cement-based materials (E. Samson et al. 2005 and S. Whitaker 1998).

Therefore, the wetting phase equation is only necessary to describe flow of liquid in a porous medium system by Richards' equation.

In order to solve Richards' equation, the unsaturated hydraulic properties of the porous medium under consideration have to be determined, including the capillary pressure-degree of saturation relationship, $P_c(h)$ (also known as water retention function) and the unsaturated hydraulic conductivity, $K\ (h)$. These properties can be expressed in terms of several possible analytical models available that have been proposed in the literature for porous media, such as (Brooks and Corey 1964; van Genuchten 1980; Vogel and Císlerová 1988; Kosugi 1996; Durner 1994).

However, in order to express the unsaturated hydraulic properties of the medium of interest by one of the above-mentioned models, other hydraulic properties of the porous medium need also to be determined experimentally. These properties are the saturated hydraulic conductivity K_s, and the moisture retention function.

In 1976, Mualem developed a statistical model to estimate the pores' distribution in soil, and Van Genuchten used this model in 1980 to predict the unsaturated hydraulic conductivity parameters of a porous medium in terms of the porous medium's water retention data by implementing some predictive equations. The van Genuchten- Mualem model (Mualem 1976; van Genuchten 1980) is represented by the following equations:

$$k_r = S_e \left[1 - \left(1 - S_e^{\frac{1}{m}}\right)^m\right]^2 \tag{2.7}$$

$$P_c = -\frac{1}{\alpha}\left[S_e^{\frac{1}{m}} - 1\right]^{\frac{1}{n}} \tag{2.8}$$

$$S_e = \frac{S_l - S_{lr}}{1 - S_{lr}} \tag{2.9}$$

where S_e is the effective saturation of liquid, P_c is the capillary pressure of the porous medium, m, α, n are empirical parameters affecting the shape of the hydraulic functions of the porous medium, S_l is the degree of saturation in porous medium, and S_{lr} is the residual saturation of the porous medium.

There are also several other analytical models found in the soil's literature by which the unsaturated hydraulic properties of a porous medium in single-phase flow system could be predicted (Brooks and Corey 1964; Vogel and Císlerová 1988; Kosugi 1996; Durner 1994). However, The van Genuchten-Mualem analytical model was selected in this research from among other analytical models because it has been extensively used in soils sciences and has been validated for concrete by several researchers **(**Mainguy et al. 2001; Monlouis et al. 2004; Pont et al. 2004).

2.1.2.2 Multiphase flow system

In addition to the single-phase flow approach, the multiphase flow approach sometimes is also used to describe unsaturated flow in the porous medium of interest when two or more immiscible phases are present. This is the case for concrete when both the liquid pore solution and gas phase coexist. Darcy's Law, which has been applied to describe the single flow in a porous medium, can be generalized to describe multiphase flow or unsaturated flow in a porous medium under the assumption that the flow of a phase in the presence of another phase can be viewed as a single phase flow through a reduced network of pores (Scheidegger 1974). Assuming that each phase has its own phase pressure, the one-dimensional mass flux of liquid and gas can be written as:

$$\begin{cases} q_l = -\dfrac{k \cdot k_{rl}}{\mu_l}(\nabla \cdot P_l - \rho_l g) \\ q_g = -\dfrac{k \cdot k_{rg}}{\mu_g}(\nabla \cdot P_g - \rho_g g) \end{cases} \tag{2.10}$$

where q_l (q_g) is the volumetric flux in the liquid (gas) phase, k is the intrinsic permeability, k_{rl} (k_{rg}) is the relative permeability of the liquid (gas) phase, μ_l (μ_g) is the dynamic viscosity of the liquid (gas), ∇P_l (∇P_g) is the divergence of the fluid pressure in the liquid (gas) phase, ρ_l (ρ_g) is the density of the liquid (gas) in the phase, and g is the acceleration due to the gravity.

The relative permeability of the liquid (gas), k_{rl} (k_{rg}), in Equation (2.10) above quantifies the interference of one phase with the other, which has a value between 0 and 1. In addition, the pressure in the liquid or the gas phase, is the sum of the capillary pressure of the liquid (gas) phase, P_{cl} (P_{cg}), and the pressure of a reference phase P, usually taken as the gas phase P_g:

$$\begin{vmatrix} P_l = P + P_{cl} \\ P_g = P + P_{cg} \end{vmatrix} \tag{2.11}$$

The capillary pressure is defined as the difference between the non-wetting phase pressure (gas) and the wetting phase (liquid). In the case of concrete, the capillary pressure depends on the degree of saturation and takes the form as in Equation (2.12)

$$P_c(S_l) = P_g - P_l \tag{2.12}$$

The movement of each phase, the gas and the liquid, in an unsaturated porous medium, such as concrete, occurs under the combined effect of gravity and pressure forces. In this case, the mass of the fluid within the porous medium of interest for a specified period of time can be described by the mass balance equation. The general mass balance equation describing the movement of each phase in unsaturated porous media takes the form of Equation (2.13) (Scheidegger 1974; Dullien 1992):

$$\begin{cases} \dfrac{\partial(\emptyset\rho_l S_l)}{\partial t} = -\nabla\cdot(\rho_l q_l) - F_l \\ \dfrac{\partial(\emptyset\rho_g S_g)}{\partial t} = -\nabla\cdot\left(\rho_g q_g\right) - F_g \end{cases} \tag{2.13}$$

where $\emptyset$ is the porosity, ρ_l (ρ_g) is the density of the liquid (gas) phase, $S_l(S_g)$ is the saturation of the liquid (gas) phase, t is the time, $\nabla\cdot(\rho_l q_l)$ ($\nabla\cdot\left(\rho_g q_g\right)$) is the divergence of the liquid (gas) flux, and F_l (F_g) is a source or sink term for the liquid (gas) phase.

It is clear from Equations (2.10), (2.11), and (2.13) that the capillary pressure-degree of saturation and the relative permeability-degree of saturation relationships are essential for the modeling of moisture flow in unsaturated porous media. These properties can be expressed in terms of several possible analytical models that have been proposed in the literature for porous media, such as (Brooks and Corey 1964; van Genuchten 1980; Vogel and Císlerová 1988; Kosugi 1996; Durner 1994). As discussed previously in the single flow approach, the van Genuchten mathematical model (Mualem 1976; van Genuchten 1980), which has been extensively used in soil sciences and has been validated for concrete by several researchers **(**Mainguy et al. 2001; Monlouis et al. 2004; Pont et al. 2004), was selected in this study to characterize the capillary pressure-degree of saturation and the relative permeability-degree of saturation relationships for concrete.

2.2 Ion transport

Advection and diffusion are the two major mechanisms of ionic mass transport in porous media. Under saturated conditions, the mechanism for the transport of ions, such as chlorides, could be either by diffusion or by advection-diffusion depending on whether the pore water-solution phase is stagnant or moving. When the pressure gradient is negligible, the liquid phase would be stagnant and ionic transport takes place through diffusion under a concentration gradient as the only driving force. Under unsaturated

conditions, advection (or convection) through capillary sorption is always present and transport of ionic species occurs by both advection and diffusion.

2.2.1 Transport of ions by diffusion

Diffusion can be defined as the transport of ions under the effect of a concentration gradients. In the diffusion process, ions move from regions of high concentration of ions into regions of low concentration of ions. For steady sate conditions of diffusion in a porous medium system, Fick's first law describes the rate of ion diffusion flow as in Equation (2.14).

$$J = -D_{eff} \nabla \cdot C \tag{2.14}$$

where J is the mass transport rate due to diffusion Flux $\left(\frac{kg}{m^2 \cdot s}\right)$, D_{eff} is the effective diffusion coefficient of the porous medium $\left(\frac{m^2}{s}\right)$, ∇ is the divergence of a three-dimensional vector field of the concentration, C is the concentration of the ionic species of interest dissolved in the pore solution $\left(\frac{kg}{m^3}\right)$ (of pore solution). The negative sign in the equation indicates that the flux occurs along a negative concentration gradient.

Under transient or unsteady state conditions of diffusion, Fick's second law governs the change of concentration of ions in a porous medium over the time, t:

$$\frac{\partial(\emptyset S_l C)}{\partial t} = -\nabla \cdot J \tag{2.15}$$

The left side of Fick's second law above describes the rate at which ions intrude into a porous medium's matrix, and the right side of the equation represents the divergence of ions' flux in the pores' solution. In a porous medium system, the available cross-sectional area for the diffusion to occur in the aqueous phase is reduced by the volume fraction of the gas phase spaces inside the porous medium.

The volume fraction of the void spaces is known as porosity $\emptyset$. Therefore, Fick's second law changes to the following equation:

$$\frac{\partial(\emptyset S_l C)}{\partial t} = D_{eff}\nabla^2 \cdot C \tag{2.16}$$

The boundary conditions of the equation above are the initial condition C (x >0, t= 0) =0 (the initial concentration of ions is zero), and the boundary condition C (x= 0, t >0) = C_s (the surface concentration is constant at C_s) for semi-infinite medium. Using these boundary conditions, it can be shown that the solution to Equation (2.16) is given by (Crank 1975):

$$C_{x,t} = C_s\left[1 - \text{erf}\left(\frac{x}{4D_{eff}t}\right)\right] \tag{2.17}$$

where $C_{x,t}$ is the concentration of ions ($\frac{kg}{m^3}\ of\ pore\ solution$) at a specific depth, x and after a specific time, t, C_s is the concentration $\left(\frac{kg}{m^3}\right)$ of the surface solution, and (erf) is the error-function. The above solution is only valid if the surface concentration and the diffusion coefficient are constant in space and time.

As discussed previously, the ions diffusion process can only be well explained if the matrix of concrete is relatively fully saturated. However, the diffusion process in unsaturated conditions has a different mechanism because of the continuity of water inside the pores of concrete is not fully achievable. Therefore, in unsaturated conditions, the effective diffusion behaviour is significantly affected by the degree of saturation in a porous medium (Millington and Quirk 1961; Sallam et al. 1984; Shackelford 1991). The relation between the effective diffusion coefficient and the degree of saturation is represented by the following equation:

$$D_{eff} = D_0\emptyset\beta \tag{2.18}$$

where $D_0$is the diffusion coefficient in solution (e.g. the ionic diffusion in bulk water), $\emptyset$ is the porosity, and β is a pore structure parameter, known as tortuosity.

The parameter β reflects the shape or the geometry of the ion diffusion paths in a porous medium, in which the pore structures are not uniform or tortuous. For example, if it were assumed that all pores were straight and uniform in a porous medium's matrix, the β parameter would be equal to one under saturation conditions. This geometry factor is a function of the degree of saturation and the pore structures of a porous medium. The geometry factors can be predicted by using different empirical models. The most well known model of these models in soil science is The Millington-Quirk model (1961) (Millington and Quirk 1961), which has been frequently used in partially saturated media systems. The geometry factor is expressed in Millington and Quirk (1961) as:

$$\beta = \emptyset^{\frac{4}{3}} S_l^{\frac{10}{3}} \tag{2.19}$$

where $\emptyset$ is the porosity, and S_l is the degree of saturation in a porous medium.

2.2.2 Transport of ions by advection

Advection is the process of transporting ions as a result of bulk water movement, in which they are dissolved. It is mathematically described in terms of moisture flux through a porous medium and the concentration of dissolved chemical species, such as chloride ions:

$$\begin{cases} J'\,(Sat) = C \cdot q \\ J'\,(Unsat) = C \cdot q_l \end{cases} \tag{2.20}$$

where $J'\,(Sat)$ is the saturated advective flux $\left(\frac{kg}{m^2 \cdot s}\right)$, $J'\,(Unsat)$ is the unsaturated advective flux$\left(\frac{kg}{m^2 \cdot s}\right)$, q is the saturated moisture flux, given by Darcy's equation, and q_l

is the unsaturated moisture flux or the moisture flux in the liquid phase, and C is the concentration of the dissolved chemical species $\left(\frac{kg}{m^2}\right)$.

The unsaturated moisture flux in a porous medium is given by the equation below, which was developed from Darcy's law to be generalized to unsaturated water flow for the liquid phase (Scheidegger 1974).

$$q_l = -\frac{k \cdot k_{rl}}{\mu_l}(\nabla \cdot P_l - \rho_l \cdot g) \tag{2.21}$$

where k is the intrinsic permeability, k_{rl} is the relative permeability of the liquid phase, μ_l is the dynamic viscosity of the liquid, P_l is the pressure of the liquid phase, ρ_l is the density of the liquid phase, and g is the acceleration due to the gravity.

As the advection and the diffusion processes are more common mechanisms in unsaturated conditions, it is important to distinguish the dominance of one mechanism over the other. In this situation, the Peclet number, which is a dimensionless number describing the relative strength of advection and diffusion, can be used. When the Peclet number is less than one (Pe < 1), the diffusion process is the dominant mechanism, but if the Peclet number is greater than one (Pe >1), then advection is the dominant mechanism (Martys 1995). However, It was found that in most practical situations, the Peclet number (Pe) for concrete is greater than ten (Pe >10) in unsaturated conditions, indicating the dominance of advection (Puyate and Lawrence 1998).

2.3 Models for predicting ion transport

There are two major types of models that are typically used to simulate the transport of ions and the movement of moisture in unsaturated concrete. These models include diffusion models and advection-diffusion models. Each of these models involves

different types of governing equations and different assumptions about the boundary conditions. The diffusion models and the advection-diffusion models are discussed in the following sections in the case of a single-phase flow system where only the liquid phase can flow under a pressure gradient while the gas phase is assumed to remain stagnant. In addition, a brief discussion is also provided about multiphase multicomponent models where the flow takes place in both the liquid phase and the gas phase together with the transport of multiple ionic species

2.3.1 Diffusion models

Diffusion models have been extensively used in the concrete literature to simulate the ingress of ions, such as chlorides. Most of those models are based on Fick's second law, Equation (2.16), under the assumption that the porous medium is fully saturated by water and diffusion is the only mechanism controlling the transport of ions.

However, these pure diffusion models tend to underestimate the concentration of ions penetrating the porous medium of interest when simulating situations where repeated cycles of wetting and drying conditions are presented. This underestimation of the ionic concentration is due to the fact the increase in concentration caused by water evaporation during the drying cycle and by advection during the wetting cycle is not accounted for. It is a well-known fact that under wetting and drying conditions, the diffusion of ions is significantly dependent on the moisture distribution in the porous medium of interest as well as the conditions of the service environment (relative humidity, temperature, concentration of chemical species, etc.).

Only few authors have considered the effect of humidity conditions and degree of saturation on the effective diffusion coefficient in the published diffusion models. The

typical approach in all those cases has been to make the effective diffusion coefficient dependent on the humidity conditions or the degree of saturation of concrete. For example, Saetta et al. (1993) proposed an equation to describe the effect of relative humidity on the chloride ions diffusion coefficient (Saetta et al. 1993), Equation (2.22):

$$D_{cl} = D_{eff} \frac{1}{\left[1 + \frac{(1 - RH)^4}{(1 - RH_c)^4}\right]} \tag{2.22}$$

where D_{cl} is the chloride ions diffusion coefficient at the relative humidity of interest, RH is the relative humidity, and RH_c is the humidity at which the saturated diffusion coefficient is reduced by half, $D\ (RH_c) = 0.5\ D_{eff}\ (100\%)$.

2.3.2 Advection-diffusion models

The advection-diffusion models are based on a partial differential equation that describes the transport of ions into a porous medium, such as soils or concrete, by both diffusion and advection mechanisms.

Under saturated conditions, the advection-diffusion equation is expressed in terms of the total mass flux of diffusion and advection. A bulk movement of fluid in a porous medium system causes the advective mass flux, while the diffusive mass flux is caused by the concentration gradient within the pore solution. Under saturated conditions, the diffusion-advection equation takes the form of the following equation:

$$\phi \frac{\partial C}{\partial t} = D_{eff} \nabla^2 \cdot C - q \nabla \cdot C \tag{2.23}$$

where the left side of Equation (2.23) above describes the change in the concentration of ions over time, and the right side describes the diffusive and the advective mass flux.

Under unsaturated conditions, the physical domain available for the transport of ions is reduced because the available cross-sectional area in a porous medium system for the liquid phase is reduced. Therefore, the diffusive flux and the advective flux under unsaturated conditions are dependent on the saturation of the liquid phase in addition to the porosity of a porous medium system. As a result, the advection-diffusion equation under unsaturated conditions is changed and expressed in the following equation:

$$\frac{\partial(\phi S_l C)}{\partial t} = \nabla \cdot \left(D_{eff} \cdot \nabla C - q_l C\right) \tag{2.24}$$

where q_l is the moisture flux, expressed in Equation (2.21), and S_l is the degree of saturation of the porous medium.

2.3.3 Multiphase-Multicomponent models

Multiphase multicomponent models are often used to determine the flow in porous media where two or more immiscible phases are present in the porous medium of interest. In the case of concrete, the two types of fluid that typically occupy the pore volume are water and gas. The gas phase is treated as a mixture of air and water vapour while the liquid phase is considered to be mostly water. The term "multicomponent" indicates the transport of one or more components, such as ionic species, in the liquid and the gas phase. The transport mechanisms in the case of multiphase multicomponent approaches are discussed in this section of the literature survey.

In the non-isothermal multiphase system, it is often assumed that the porous medium is under local equilibrium because the velocities of the flow in the pores are assumed to be small and compared to the kinetics of the phase transitions that can take place. In addition, the effects of heterogeneity of the constitutive relationships are not considered most of the time. The component mass equation, which was developed under the assumption of

thermodynamic phase equilibrium, for water, gas, and components takes the form of Equation (2.25):

$$\begin{cases} \dfrac{\partial d_w}{\partial t} + \nabla \cdot M_w = F_w \\ \dfrac{\partial d_a}{\partial t} + \nabla \cdot M_a = F_a \\ \dfrac{\partial d_i}{\partial t} + \nabla \cdot M_i = F_i \end{cases} \tag{2.25}$$

where d_w (d_a, d_i) is the bulk density of the water (air, component), M_w (M_a, M_i) is the net mass flux of water (air, component), F_w (F_a, F_i) is the mass source for water (air, component), and t is the time.

The bulk density for each phase, namely water and gas, is given by

$$\begin{cases} d_w = \phi(X_{wl}\rho_l S_l + X_{wg}\rho_g S_{g)} \\ d_a = \phi(X_{al}\rho_l S_l + X_{ag}\rho_g S_{g)} \\ d_i = \phi(X_{il}\rho_l S_l + X_{ig}\rho_g S_{g)} \end{cases} \tag{2.26}$$

where X_{wl} (X_{al}) is the mass fraction of water (air) in the liquid phase, X_{wg} (X_{ag}) is the mass friction of water (air) in the gas phase, X_{il} (X_{ig}) is the mass fraction of the component of interest in the liquid (gas) phase, ρ_l (ρ_g) is the density of liquid (gas) phase, S_l (S_g) is the liquid (gas) phase saturation, and ϕ is the porosity of the porous medium.

The pore space in the porous medium is assumed to be fully saturated by the fluid phases (gas and liquid). Therefore, the summation of liquid saturation and the gas saturation takes the form, Equation (2.27):

$$S_l + S_g = 1 \tag{2.27}$$

The net mass fluxes of water, air, and component are assumed to be a superposition of the fluxes in each phase as:

$$\begin{cases} M_w = M_{wl} + M_{wg} \\ M_a = M_{ag} \\ M_i = M_{il} + M_{ig} \end{cases} \tag{2.28}$$

where M_{wl} (M_{wg}) is the net mass flux of water in the liquid (gas) phase, M_{ag} is the net mass flux of air in the gas phase, and M_{il} (M_{ig}) is the mass of the component of interest in the liquid (gas) phase. The dissolved air in the liquid phase has been neglected in Equation (2.28).

Each phase flux can be written as a sum of the advective flux and the diffusion flux as:

$$\begin{cases} M_{wl} = X_{wl}\rho_l q_l + J'_{wl} \\ M_{wg} = X_{wg}\rho_g q_g + J'_{wg} \\ M_g = X_{ag}\rho_g q_g + J'_{ag} \\ M_{il} = X_{il}\rho_l q_l + J'_{il} \\ M_{ig} = X_{ig}\rho_g q_g + J'_{ig} \end{cases} \tag{2.29}$$

where J'_{wl} (J_{wg}) is the diffusive flux of water in the liquid (gas) phase, J'_{ag} is the diffusive flux of the air in the gas phase, and J'_{il} (J'_{ig}) is the diffusive flux of the component of interest in the liquid (gas) phase. The diffusion fluxes of air, water and component can be written as in shown Equation (2.30).

$$\begin{cases} J'_{wl} = \phi\beta_l\rho_l D_{wl}\nabla \cdot X_{wl} \\ J'_{wg} = \phi\beta_g\rho_g D_{wg}\nabla \cdot X_{wg} \\ J'_{ag} = \phi\beta_g\rho_g D_{ag}\nabla \cdot X_{ag} \\ J'_{il} = \phi\beta_l\rho_l D_{il}\nabla \cdot X_{il} \\ J'_{ig} = \phi\beta_g\rho_g D_{ig}\nabla \cdot X_{ig} \end{cases} \tag{2.30}$$

where J'_{wl} (J'_{wg}) is the diffusive flux of water in the liquid (gas) phase, J'_{ag} is the diffusive flux of air in the gas phase, J'_{il} (J'_{ig}) is the diffusive flux of the component of interest in the liquid (gas) phase, D_{wl} (D_{wg}) is the diffusion coefficient of water in the liquid (gas) phase, D_{ag} is the diffusion coefficient of air in the gas phase, and D_{il} (D_{ig}) is the diffusion coefficient of the component of interest in the liquid (gas) phase.

2.4 Effect of Silica fume on the hydraulic properties of concrete

Among the effects of silica fume on the properties of concrete, the reduction of the permeability to water and the diffusivity of ionic species are of particular interest. Several studies have reported reduction in the water permeability when silica fume was added to the concrete. For example, Gjrov (1993) found that the water permeability coefficient of a lean concrete mixture reduced from 4×10^{-4} to 1×10^{-7} m/s when 9% silica fume was used. Hooton (1993) also stated that the water permeability of a high strength concrete mix reduced from 1.8×10^{-14} m/s to 1×10^{-17} m/s when 10% of silica fume was added to the concrete mix. Moreover, the addition of silica fume has also been reported to reduce the diffusion of ionic species in concrete. Perraton et al. (1988) observed a significant reduction in the diffusion coefficient of the chloride ion in concrete as the dosage of silica fume increased from 5% to 20% by weight of cement. All of these observations indicated that silica fume has shown considerable enhancement in the microstructural composition of concrete due to the pozzolanic reaction of silica fume with calcium hydroxide discussed previously in Section 1.3.

Four different proportions of silica fume ranging from 5% to 20% by the total cementitious materials were selected in this study to assess the effect of these proportions on the key hydraulic parameters of concrete. More specifically, the effect of silica fume on the saturated permeability coefficient, the relative permeability coefficient, the moisture retention data, the relative diffusion coefficient, and the dependency of the effective diffusion coefficient on the degree of water saturation will be assessed.

2.5 Experiments

As discussed in the previous sections, in order to successfully model the flow of water and the transport of ions in unsaturated conditions, it is essential to experimentally measure the key transport properties and their dependency on the degree of saturation of the porous material of interest. Once such information is available, realistic evaluations of the durability, performance, and service life of porous materials, such as concrete, could be easily carried out. An overview of the current experimental methods, available in the literature of porous media, is discussed in the following sections.

2.5.1 Hydraulic transport properties

In order to accurately model water flow and the transport of ions in porous materials under unsaturated conditions, it is important to measure their key hydraulic transport properties. In the field of concrete, there are several experimental techniques found in the literature to measure the hydraulic transport properties (Basheer 2001)**,** such as the saturated hydraulic permeability coefficient and the capillary-driven moisture transfer. However, none of those experiments is still recognized as a standard experiment for concrete materials. Experimental methods found in different fields of science are needed to determine the hydraulic transport properties of concrete, such as saturated permeability coefficient and capillary pressure-moisture content relationship. The measurement of the hydraulic properties of porous materials and their some associated experimental methods are discussed in the following sections.

2.5.1.1 Saturated permeability coefficient

The saturated permeability coefficient of concrete is defined as the resistance of concrete to allow fluids to penetrate its surface as a result of pressure gradient (The Concrete Society 1988, Perraton and Aitcin 1992). The typical value of the saturated permeability coefficient of concrete falls in the range of 10^{-12} m/s, lower than those of soils and several types of rocks, such as sand and sandstone rocks. However, the magnitude of the saturated permeability coefficient of concrete is influenced by several factors, such as the type, size and distribution of aggregates, temperature and curing conditions (Kitowski and Wheat 1997). Several experimental techniques have been used to measure the saturated permeability coefficient of concrete, but none of them is recognized as a standard test method.

One technique, very widely used in soil science (Ludirdja et al. 1989), involves measuring the saturated permeability coefficient of concrete by placing water above a concrete specimen of known volume, and the drop in the height of the water tube above the specimen is monitored and measured over time. After completing the process of measuring the height of the water tube, Darcy's Law is then used to calculate the saturated permeability coefficient. This experimental technique, however, has a major disadvantage that the time of the experiment might take weeks or longer because concrete in general has very low permeability in comparison with other porous materials.

In order to shorten the time for measuring the saturated permeability coefficient of concrete, an additional pressure to the fluid is applied by using a special experimental setup to force the liquid into the concrete, in addition to the use of an effective sealing to prevent or reduce the leakage of fluid (Martys 1995). In this type of experimental techniques, the saturated permeability coefficient is calculated based upon knowing the

specimen geometry and the measurements of flow rate with its associated applied pressure using Darcy's Law and the calculation of coefficient of permeability. When an additional pressure is applied in the water flow, the drop in the height of the water tube is incorporated in the calculation of the saturated permeability coefficient, as shown in the Equation (2.31):

$$K_s = \frac{aL}{At} \ln \frac{h_0}{h_t} \tag{2.31}$$

where a is the cross-sectional are of the water tube (m^2), L is the length of the specimen parallel to the direction of flow (m), A is the cross-sectional area of the specimen (m^2), t is the time of the flow (t), h_0 is the initial height of the water tube (m), and h_t is the height of the water tube (m) at time t.

Several experimental methods proposed have been in the published literature for measuring the saturated hydraulic permeability coefficient under the action of an additional applied pressure. Among these methods, procedures are particularly suitable for measuring the saturated hydraulic permeability coefficient of concrete. These methods are the permeability cell method and the centrifuge method. The two methods are discussed in the following sections.

a) Permeability cell method

A typical permeability cell for concrete, shown in Figure 1, consists of a set of inlet and outlet to control the flow direction into the specimen under a controllable pressure. In addition, an effective sealing material, such as rubber or epoxy, is used in the permeability cell to prevent any leakage of liquid. By measuring the charge and the discharge of liquid in the permeability cell, the saturated hydraulic permeability coefficient is then calculated by using Darcy's Law based on the specimen geometry, the fluid properties, the flow rate, and the applied pressure.

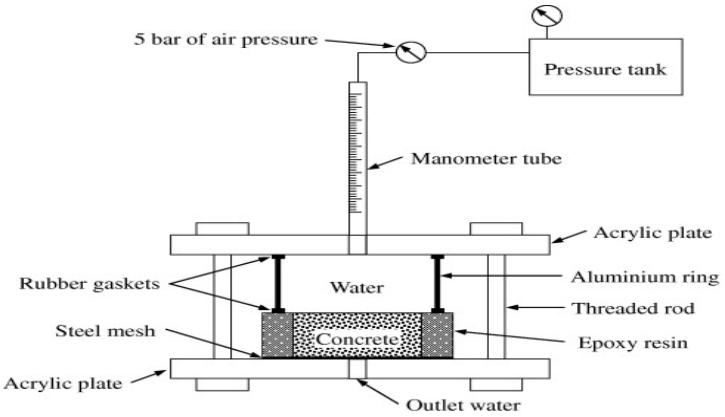

Figure 2.1: An example of typical permeability cell (Basheer 2001).

b) Centrifuge method

In the centrifuge method, a rotational speed is applied to the specimen and to the fluid above it to generate a fluid flow through the specimen under the action of an accelerated-gravity environment. The acceleration, a_r, of the applied rotational speed is calculated based on knowing the centrifuge operative radius, R_{cen}, and the magnitude of the applied rotational speed, ω_r, as illustrated in Equation (2.32):

$$a_r = \omega_r^2 \cdot R_{cen} \tag{2.32}$$

The increase in the specimen's acceleration is used to determine the centrifuge scale factor, N, as in the following equation:

$$N = \frac{a_r}{\mathrm{g}} \tag{2.33}$$

The scale factor is then introduced in the calculation of the saturated hydraulic conductivity coefficient according to Equation (2.34):

$$K_s = \frac{1}{N}\frac{aL}{At}\ln\frac{h_0}{h_t} \tag{2.34}$$

After considering the time frame to carry out this research and the availability of the equipment for the two above-mentioned experimental methods, it was decided that the centrifuge method would be used in this research to measure the saturated hydraulic permeability coefficient for concrete.

2.5.1.2 Capillary pressure-moisture content relationship

The moisture retention data or the relationship between capillary pressure and moisture content in concrete is described as the ability of concrete to intake or uptake water at given capillary pressure and degree of saturation. As discussed in the previous sections, the determination of this relationship is essential for predicting the unsaturated moisture flow in porous materials. Therefore, several experimental methods, proposed in the literature, could be used to determine the moisture retention data of porous materials such as concrete.

There are two main experimental techniques that are typically used to determine the moisture retention data. The two experimental techniques are discussed in the following sections.

a) Pressure Membrane Technique

The principle of this technique is based on finding capillary pressure P_c (MPa), defined as the pressure difference between the pore-air pressure P_a (MPa), and the pore-water pressure P_w (MPa), as illustrated in the following equation:

$$P_c = P_a - P_w \tag{2.35}$$

The procedures of the pressure membrane technique involve using a high-pressure chamber, in which a saturated specimen is placed in contact with a saturated porous membrane resting on a screen disk plate. The bottom of the membrane is exposed to the atmospheric pressure and connected to a small tube to collect the water outside the pressure chamber. Initially, the experimental technique starts with maintaining the pore-water pressure constant, usually at a magnitude of zero. After that, the desired air pressure is applied to the pressure chamber to force the saturated specimen to drain the water across the saturated membrane and subsequently out of the pressure chamber through the tube. When the drainage of water through the tube stops, the specimen is considered to be in equilibrium at the desired capillary pressure. After the specimen reaches equilibrium, the sample is taken out of the pressure chamber to measure its degree of saturation. Finally, the capillary-driven moisture relationship is determined based on knowing the applied air pressure, the capillary pressure, and the degree of saturation.

The pressure membrane technique has always been used in soil science, and the capillary pressure obtained by this technique is up to 14 MPa (Richards 1941). However, concrete materials require larger capillary pressure than those of soils to overcome the suction force, especially in dry conditions. Therefore, the pressure membrane technique can only be used for concrete in high relative humidity conditions or if concrete has a high degree of saturation.

b) Vapour equilibrium technique

The vapour equilibrium technique is used to measure the moisture retention data of porous materials, such as soil and concrete. The procedure of this technique start by the creation of different relative humidity environments using saturated salt solutions. After

that, saturated specimens of the porous medium of interest are placed in the created environmental chamber, and left for the liquid inside each specimen to be released until its vapour pressure becomes equal to that of the surrounding humidity environment. The total suction in each specimen is then calculated based on the measurements of the vapour phase pressure in equilibrium with the liquid phase pressure in each humidity environment. For a given temperature, the total suction is calculated using Kelvin's equation:

$$P_c = \left[\frac{RT}{\mathrm{M}}\right] \ln\left[\frac{\rho}{\rho_s}\right] \tag{2.36}$$

where P_c is the total suction (MPa), R is the ideal gas constant, M molecular weight of water vapour (0.01802 $\frac{Kg}{Mol}$), T is the temperature of the liquid phase in Kelvin (C^0+273.16) (T), ρ is the water vapour pressure in equilibrium with liquid phase (Pa), ρ_s is the saturated water vapour pressure (Pa) at a given temperature (T).

If the osmotic pressure, which is the hydrostatic pressure produced by a solution in the pore volume due to a difference in concentration of the solute, is negligible, the total suction, P_c, in Kelvin's equation above is then considered to be equivalent to the capillary pressure of concrete. In the case of concrete, the osmotic pressure is very small compared to the capillary pressure. Therefore, the water retention data can be calculated without considering the osmotic pressure in Kelvin's equation.

The degree of saturation of each specimen, S_l, is calculated based on the measurements of initial saturated weight of each specimen, m_s (g), the weight of each specimen after reaching equilibrium in each controlled humidity condition, m_h (g), and the oven dry weight of each specimen, m_d (g). The degree of saturation of each specimen is calculated according to Equation (2.37):

$$S_l = \frac{m_h - m_d}{m_s - m_d} \times 100 \tag{2.37}$$

Since the pressure required to remove water from concrete pores is greater than that obtained by most techniques (Martys 1995), the vapour equilibrium technique has been widely used for measuring the moisture retention data of concrete (Romero et al. 2001; Tang and Cui 2005). In addition, the values of the suction pressure in this technique are in the range of 3 to 1000 MPa (Romero et al. 2001; Tang and Cui 2005). Therefore, it was decided that the vapour equilibrium technique would be used to measure the water retention data of concrete in this research.

2.5.2 Dependency of the diffusion coefficient on the degree of saturation

The determination of the dependency of diffusion coefficient on the degree of saturation in porous materials is essential for predicting moisture flow and the ingress of ions under unsaturated conditions, in addition to the other usual basic properties of porous materials, such as porosity, hydraulic conductivity, and moisture retention data. Measurement of the diffusion coefficient is typically carried out by using Fick's first law in steady state experiments, and by using Fick's second law in transient state experiments.

However, in the current literature, there are only very few authors who have investigated the effect of degree of saturation on the diffusion coefficient in concrete under unsaturated conditions. In addition, because of the difficulties in the experimental setup and in maintaining the required boundary condition during the experimental program consistently, such as maintaining a specific degree of saturation during the experiment, there is no direct experimental technique found in the literature to measure the dependency of the diffusion coefficient on the degree of saturation in concrete (Conca and Wright 1990**)**. Therefore, indirect experimental techniques are needed in order to

construct a relationship between diffusion coefficient and degree of saturation in materials of low porosity, such as concrete.

The most common used indirect experimental technique, found in the literature, to measure the diffusion coefficient at different degrees of saturation in concrete is the resistivity technique (Atkinson et al. 1984; Conca and Wright 1990), discussed in the following section.

a) Resistivity technique

The resistivity technique can be used to determine the dependency of diffusion coefficient on the degree of saturation in concrete. The effective diffusion, D_{eff}, is related to the electrical conductivity, σ (Siemens/m), of a porous material and to the pore structure parameter by the following Equation (Atkinson et al. 1984):

$$\frac{D_{eff}}{D_o} = \frac{\sigma}{\sigma_o} = \emptyset\beta \tag{2.38}$$

where D_{eff} is the effective diffusion coefficient, σ is the electrical conductivity, D_o is the diffusivity of ions in the pore solution, σ_o is the conductivity of the pore solution, and $\emptyset$ is the porosity.

The electrical resistivity, ρ (ohm), of a porous material is then calculated based on measuring the electrical conductivity of the porous medium as in the following equation:

$$\rho = \frac{1}{\sigma} \tag{2.39}$$

The electrical resistivity is defined as the ability of a unit cube of a material to resist an applied electrical current between its two opposite faces. Therefore, the resistance, R

(ohm), of a material of a known cross-sectional area A (m^2), and a length L (m), can be calculated as expressed in the following equation.

$$\rho = \frac{RA}{L} \tag{2.40}$$

In the resistivity technique, two types of tests could be used to measure the resistivity of porous materials, involving either direct electrical current (DC) or alternating electrical current (AC) (Monfore 1968). The use of a direct electrical current (DC) results in polarization of the electrolyte. The development of this polarization potential causes the applied current to be reduced by an unknown value (Monfore 1968). Therefore, in order to reduce the effect of polarization potential on the applied current, the measurements of the currents has to be taken at two different applied voltages, and the effect of polarization has to be incorporated in the calculation of the resistivity. If it is assumed that the polarization potential is constant at different applied voltages, the potential polarization, V_P, is then calculated using Equation (2.41) (Monfore 1968).

$$V_P = \frac{V_1 I_2 - V_2 I_1}{I_1 - I_2} \tag{2.41}$$

where V_1 & V_2 are the two applied voltages, and I_1&I_2 are the related currents.

The electrical resistance of a porous material is related to the potential polarization by the following equation.

$$R = \frac{V - V_P}{I} \tag{2.42}$$

where V is the applied voltage, V_P is the polarization potential, and I is the current.

In the resistivity technique, the resistivity of a porous medium is usually measured based on the assumption that the porous medium is fully saturated with liquid. However, in the case of concrete, if the conductivity of the pore fluid is constant over time, the bulk

conductivity of concrete is then dependent only on the degree of saturation of the pore. Therefore, the resistivity of concrete is strongly influenced by the degree of saturation of the pores. Using either direct current or alternating current, it has been shown in several studies that the resistivity of concrete falls in the range of 10^4 (ohm-cm) for moist concrete, and that the resistivity of dry concrete falls in the range of 10^{11} (ohm-cm) (Monfore 1968).

2.6 Literature review summary

Darcy's Law, which was developed essentially to describe single-phase water flow in saturated porous media, could also be used to describe moisture flow in unsaturated concrete. Richard's equation is one of the well-known extensions of Darcy's Law for describing single-phase moisture flow in unsaturated porous materials.

In order solve Richard's equation, the unsaturated hydraulic properties of the porous medium at hand, including the relative permeability, the liquid-capillary pressure relationship, and the unsaturated hydraulic conductivity, have to be determined first using appropriate techniques. One of the analytical models that are used frequently in the literature to represent unsaturated hydraulic properties is the van Genuchten- Mualem model.

In addition, Darcy's Law, which has been applied to describe the single flow in a porous medium, can be generalized to describe the multiphase flow or the unsaturated flow in a porous medium. The movement of each phase, gas and liquid, occurs under the combined action of gravity and pressure forces. Therefore, the mass of the fluid within the porous medium of interest for a specified period of time can be described by the mass balance equation. However, in order to solve the mass balance equation, it is essential to

characterize the capillary pressure-degree of saturation and the relative permeability-degree of saturation relationships using several analytical models available in the literature, including the van Genuchten- Mualem model.

Transport of ions in porous media can be driven by two main mechanisms: diffusion and advection. Diffusion is the mechanism by which the transport of ions occurs under the effect of a concentration gradient. Under saturated conditions, it is usually fair to assume that diffusion is the only dominant mechanism responsible for the ingress of ions in concrete. Diffusion can be described by Fick's fist law for steady state conditions and Fick's second law for transient state conditions. Under unsaturated conditions, the effective diffusion coefficient becomes a function of the saturation of the porous medium, and hence is not a constant. Advection is the mechanism by which the transport of dissolved ions in a porous medium occurs as a result of bulk monument of the solvent fluid. Under saturated conditions, the ionic advective flux is described in terms of the saturated moisture flux, while the advective flux in unsaturated conditions is described in terms of the unsaturated moisture flux. In contrast to saturated conditions, advection is always dominant in variably saturated conditions.

On the other hand, diffusion models are essentially built based on the assumption that concrete is fully saturated with the pore solution, and that diffusion is the only dominant mechanism. Those pure diffusion models have sometimes been applied to the case where the effect of cyclic wetting-drying conditions where advection and evaporation are very important mechanisms and still not accounted for leading to an underestimation of the concentration of ions in the porous medium system. However, very few studies have attempted to include the effect of humidity and degree of saturation on the effective diffusion coefficient. Advection-diffusion models can be developed to simulate the ingress of ions into the porous medium under either saturated conditions or unsaturated

conditions. In unsaturated conditions, both the diffusive flux and the advective flux are dependent on the saturation of the liquid phase in a porous medium.

In addition to the diffusion and advection-diffusion models, multiphase-multicomponent models are often used to simulate the flow in a situation where the flow takes place in both the liquid phase and the gas phase together with the transport of multiple ionic species. In those types of models, each phase flux can be written as a sum of the advective flux and the diffusion flux.

In order to accurately model the moisture flow and the transport of ions in unsaturated porous materials, several experimental parameters need to be determined including the hydraulic properties of the porous medium and their dependency on the degree of saturation. The hydraulic properties of concrete, such as the saturated hydraulic permeability and the moisture retention data, can be determined using different suitable experimental techniques as discussed in the preceding sections. The two experimental techniques selected in this research to measure the hydraulic properties of concrete were the centrifuge technique for the saturated hydraulic permeability coefficient and the vapour equilibrium technique for the moisture retention data. Finally, the dependency of the diffusion coefficient on the degree of saturation in concrete was determined using the resistivity technique.

3. Materials and Experimental Methods

Five different types of concrete mixes were carefully prepared to perform three different experimental tests to determine several parameters needed for modelling the moisture flow and the transport of ions in unsaturated concrete. In the five concrete mixes, different proportions of silica fume were used to characterize each concrete mix of the five concrete mixes. The experimental methods included the centrifuge technique for measuring the saturated permeability coefficient of the concrete mixes, the vapour equilibrium technique for measuring the moisture retention data of the concrete mixes, and the resistivity technique for measuring the dependency of the diffusion coefficient on the degree of water saturation of the concrete mixes.

3.1 Materials selection and concrete mixtures

Normal Portland cement (CSA A5 Type 10) was used as a cementitious material in the five concrete mixes. Type 10 normal Portland cement is used in most concrete applications where no additional chemical or physical cementitious properties are required. The chemical composition and the mineral composition of the normal Portland cement are shown in Table 3.1 and Table 3.2.

Table 3.1: Chemical composition of type 10 normal Portland cement (CSA A5 Type 10).

Chemical composition	**Composition (%)**
SiO_2	20.7
AL_2O_3	3.68
CaO	63
Fe_2O_3	2.95
MgO	4.21
Na_2O	0.14
K_2O	0.59
SO_3	2.62
$Free\ CaO$	1.02
Loss on ignition	2.7

Table 3.2: Mineral composition of type 10 normal Portland cement: (Canadian Portland Cement Association).

Mineral symbol	**Composition %**
C_3S	50
C_2S	24
C_3A	11
C_4AF	8

Moreover, dry densified silica fume (ASTM C1240) was used partially as a supplementary cementing material in only four mixes of the five concrete mixes. Dry silica fume is used in concrete mixtures as a micro-filling material that fills the voids between the cement particles to reduce the permeability of concrete. In addition, as a pozzolanic material, silica fume reacts with other cementitious materials in the concrete matrix to produce additional amounts of calcium silicate hydrate (CSH). As discussed in

Section 1.3, this additional amount of CSH increases the strength and reduces the permeability of the concrete matrix. The general physical and chemical properties of the dry densified silica fume used in the four concrete mixtures are presented in Table 3.3.

Table 3.3: Properties of the dry densified silica fume used in the concrete mixes.

Chemical/ Physical Properties	**Description**
Form	Powder
Colour	Grey
pH	Neutral
Melting point	1550 to1700 C^o
Flammability	Does not ignite
Bulk Density	2100 to 2300 $\frac{kg}{m^3}$
Solubility in water at 20C^o	Miscible

The raw materials used in the five concrete mixes included coarse and fine aggregates, water, and superplasticizer. All of these raw materials were produced and examined according to the Canadian Standards Association (CSA) and to the American Society for Testing and Materials (ASTM). The sources of these raw materials and their specifications standards are shown in Table 3.4.

Table 3.4: Raw materials sources and specifications standards.

Material	Source	Specifications Standard
Portland cement	Lafarge (Type 10)	1. CSA-A5
Silica Fume	Master Builder	1. ASTM C-1240
Coarse Aggregate	Lafarge (Gavel)	1. ASTM C-136 2. ASTM C-29 3. ASTM C-127
Fine Aggregate	Pit run (Coarse sand)	1. ASTM C-136 2. ASTM C-129
Water	Tap Water	N/A
Superplasticizer	Master Builder	1. ASTM C-260

In this study, each of the five concrete mixes was labelled by its amount of dry densified silica fume, partially replaced the Portland cement. The five concrete mixes were labelled as Mix A (0% Silica fume), Mix B (5% Silica fume), Mix C (10% Silica fume), Mix D (15% Silica fume), and Mix E (20% Silica fume). In addition, according to the Standard Practice for Selecting Proportions for Normal, Heavyweight, and Mass Concrete (ACI 211.1-91), a water-cementitious ratio of 0.4 was chosen for all the five concrete mixes based on the assumption that a concrete cover is exposed to severe exposure of seawater.

The mix proportions for all the five concrete mixes were selected according to the procedures of the general practice of ACI 211.1-91. The mix design of each concrete mix is illustrated in Table 3.5.

Table 3.5: Mix designs of the five concrete mixtures.

Mix type	**Mix A (0%SF)**	**Mix B (5%SF)**	**Mix C (10%SF)**	**Mix D (15%SF)**	**Mix E (20%SF)**
Portland cement kg/m^3	518	531	503	475	447
Silica fume kg/m^3	0	28	56	84	112
Coarse aggregate kg/m^3	867	867	867	867	867
Water kg/m^3	207	221	221	221	221
Superplasticizer kg/m^3	5.18	5.6	7	7	8
Fine aggregate kg/m^3	706	660	647	636	626

After measuring the required weight of each raw material, all the raw materials of each mix type, except superplasticizer, were mixed manually for approximately 5 to 10 minutes until each concrete mixture became visually homogeneous. The superplasticizer was then mixed with each concrete mixture for approximately 3 minutes to improve the workability of mixtures. After that, each concrete mixture was cast into two types of plastic cylindrical moulds ($\Phi\ 75mm \times 150mm$ and $\Phi 50\ mm\ \times\ 100mm$) according to ASTM C-31. At the end of the mixing process, the fresh concrete properties of all five mixtures were measured following the steps of ASTM C-31. The fresh properties of all five concrete mixes are shown in Table 3.6.

Table 3.6: Fresh properties of the concrete mixtures.

Mix type	**Mix A (0%SF)**	**Mix B (5%SF)**	**Mix C (10%SF)**	**Mix D (15%SF)**	**Mix E (20%SF)**
Slump (mm)	65	63	56	50	47
Air content %	3.3	3.1	2.8	2.5	2.5
Unit weight kg/m^3	2350	2390	2410	2450	2460

After 24 hours from casting the concrete mixtures in the cylindrical moulds, concrete cylinders were demolded and submerged in saturated limewater for curing. The purpose of using saturated limewater was to prevent the lime inside the concrete cylinders from leaching out. After 28 days of curing, four concrete cylinders were selected from each mix-type to measure their compressive strength according to ASTM C-39. Figure 3.1 shows an illustrative picture of the compressive strength test performed on the concrete cylinders. In addition, two concrete samples were selected from each type of mix to conduct the porosity test according to ASTM C-642. The values range of the compressive strength and the porosity results of all five concrete mixes are presented in Table 3.7.

Figure 3.1: Compressive strength test.

Table 3.7: Compressive strength and porosity of the five concrete mixes.

Mix type	**Mix A (0%SF)**	**Mix B (5%SF)**	**Mix C (10%SF)**	**Mix D (15%SF)**	**Mix E (20%SF)**
Compressive strength	41 - 51 MPa	48 - 50 MPa	46 - 50 MPa	45 - 57 MPa	46 - 50 MPa
Porosity	14.1 - 14.4 %	13.1 - 13.9 %	12.2 - 12.9 %	10.7 - 10.9 %	10.1 - 10.6 %

3.2 Centrifuge technique

As discussed previously in Section 2.4.1.1, the centrifuge technique was selected to measure the saturated permeability coefficient of concrete. Compared with other

techniques, the centrifuge technique provides a shorter time of testing. In addition, the applied force on a sample generated by this technique is designed to be equivalent to the gravity force with independency of any other surrounding forces such as gravity (Conca and Wright 1990).

3.2.1 Equipment and concrete samples

a) Centrifuge machine

A centrifuge machine, in the geotechnical lab, was selected to conduct the test on the five concrete mixes discussed in Section 3.1. As shown in Figure 3.2, the machine used in this study consisted mainly of a rotor with six swing buckets attached, and two compatible soil sample holders designed to carry soil samples inside two of the six swing buckets. The general specifications of the centrifuge machine used in this study are presented in Table 3.8.

Figure 3.2: The centrifuge machine.

Table 3.8: The general specifications of the centrifuge machine.

Specification	Comment
Model	J6-HC Centrifuge- Beckman Coulter
Rotor type	JS-4.2 Swinging bucket
Operative arm radius range (cm)	19 – 25.4
Angular velocity range (RPM)	50 – 6000

When running the centrifuge machine, the rotor produces an adjustable angular velocity, ranging from 50 to 6000 RPM, to force all the swing buckets and their compatible soil sample holders to spin horizontally. Figure 3.3 shows a general illustrative schematic diagram of a sample in the centrifuge machine.

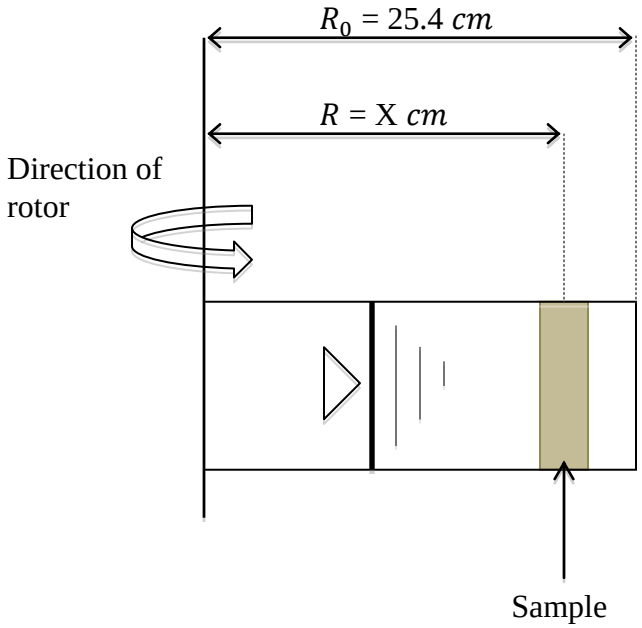

Figure 3.3: Schematic diagram of a sample in the centrifuge machine.

a) Preparations of sample holders

In the centrifuge machine, the soil sample holders, used inside the swinging buckets, are essentially designed to carry soil samples during test. Therefore, additional special concrete sample holders were designed and manufactured to be compatible with the soil sample holders. The design of a concrete sample holder involves using an aluminium tube with a smaller outlet diameter designed for holding a concrete sample. In the outlet of the aluminium tube, a water resistant epoxy is injected by a needle in the gap between the inner wall of the aluminium tube and the outer wall of the concrete sample's surface to prevent any leakage of fluid during the test. In addition, an acrylic tubal lid with a rubber O-ring attached was specially designed and manufactured to be threaded in the inlet of the aluminium tube and to monitor the drop of water level during the test. The details of both the soil sample holder and the concrete sample holder are illustrated in Figure 3.4 and Figure 3.5.

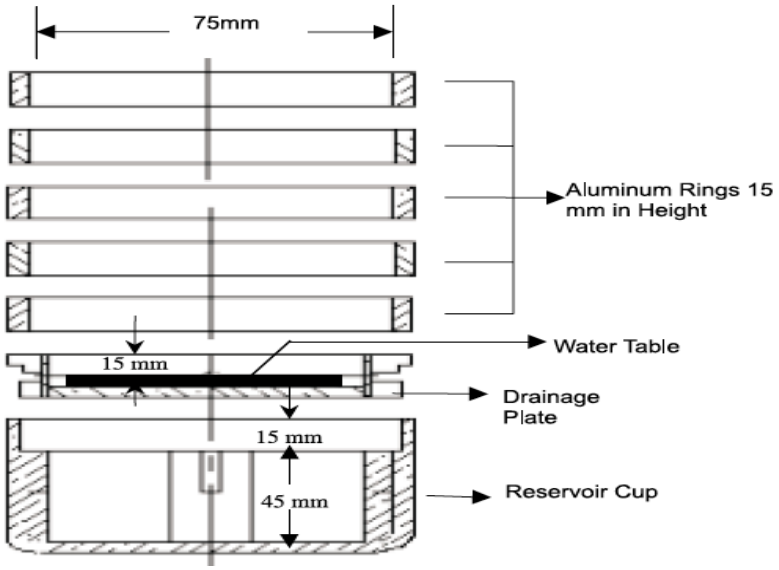

Figure 3.4: Soil sample holder (Khanzode 2002).

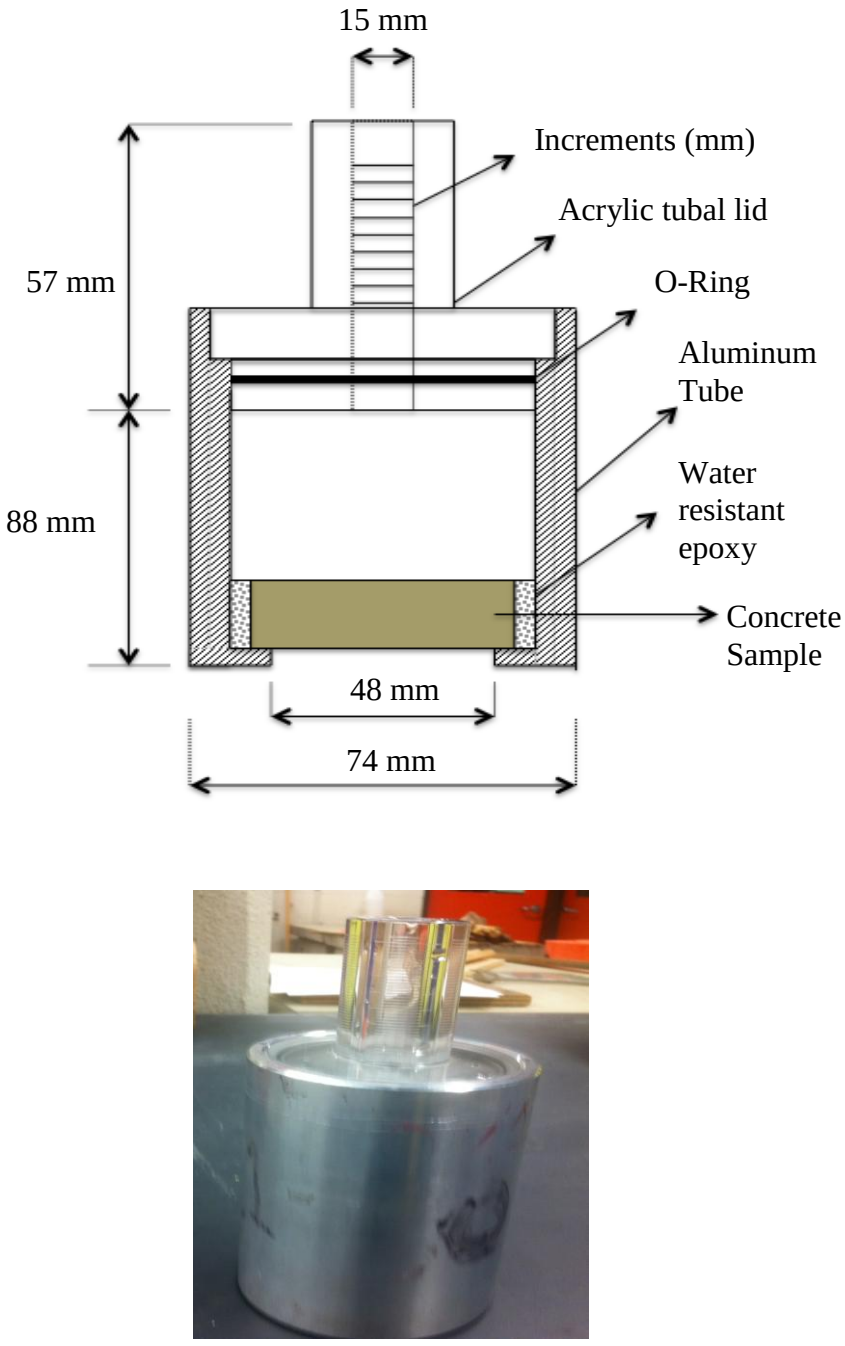

Figure 3.5: Concrete sample holder.

b) Preparations of concrete samples

After 56 days of curing, concrete disks of 50 mm diameter and 15 mm thickness were cut from cast concrete cylinders of 50 mm diameter and 100 mm length. The mix designs of these concrete samples were presented in Table 3.5.

3.2.2 Testing method

Before starting the test, each concrete sample was carefully placed in the outlet of each concrete sample holder, and then was sealed using water resistant epoxy, as illustrated in Figure 3.5. The epoxy used in each concrete sample holder was allowed to cure for at least 24 hours. Each concrete sample holder with its concrete sample sealed was submerged in a water tank for at least 72 hours to saturate the concrete samples. After that, each concrete sample holder with its concrete sample sealed was taken out of the water tank. Water was then poured inside the concrete sample holders between the concrete samples and the tube of the acrylic lids. When each concrete sample holder was filled with water, it was ensured that the air bubbles in each concrete sample holder were vacuumed to eliminate any disruption in the flow of water during test. The initial height, 56 ± 0.5 mm, of water in the tube of each acrylic lid was recorded, and the tube of each acrylic lid was covered with nylon using rubber O-ring. At the start of the test, each two concrete sample holders with their concrete samples sealed were inserted in the two available soil sample holders and then in the centrifuge swinging buckets

All the centrifuge tests were conducted on 15 concrete samples (three concrete samples per each mix-type), from the five concrete mixes discussed in Section 3.1, at a constant temperature of 24 ± 0.5^{0}C However, each centrifuge test was conducted separately on a pair of concrete samples from each mix because there were only two available soil

sample holders. Depending on the type of the concrete mix used in each test, each pair of concrete samples was centrifuged at different angular speeds for at least 24 hours. During the centrifugation time of each concrete mix, the data were collected periodically. The centrifugal angular speeds and the periods of collecting the data are presented for each concrete mix in Table 3.9. After collecting the data, it was insured that the water coming out of each concrete sample was collected in the reservoir cups of the soil sample holders. In a few cases, when a concrete sample had some invisible minor cracks or the sealant inside a concrete sample holder was not properly done, the water in the tube of the acrylic lid was emptied within an hour of the experiment. As a result, if the water in the tube of the acrylic lid was emptied within an hour of the experiment, the concrete sample was discarded.

Table 3.9: Centrifugation speeds and periods of checking data.

Mix type	**Mix A (0%SF)**	**Mix B (5%SF)**	**Mix C (10%SF)**	**Mix D (15%SF)**	**Mix E (20%SF)**
Centrifugation speed (RPM)	2600	2800	2800	2800	2900
Periods of checking data during at least 24 hours (hr)	4	4	6	10	14

The data required to calculate the saturated permeability of concrete included the initial and the final heights of the water in the tube of acrylic lids, the dimensions of the concrete samples, and the centrifugation time of each concrete mix. The dimensions of the concrete samples were initially measured before placing them in their concrete sample holders.

3.3 Vapour equilibrium technique

As discussed in Sections 2.1.2.1 and Section 2.1.2.2, the determination of moisture retention function of concrete is required for understanding the unsaturated flow of water in concrete materials. Since concrete materials require large suction pressures to desorb or absorb fluids, the vapour equilibrium technique was selected. The vapour equilibrium technique provides suction pressures ranging from 3 to 1000 MPa by using different saturated salt or acid solutions.

3.3.1 Equipment and concrete samples

a) Preparation of solutions

As illustrated in Table 3.10, eleven types of saturated salt solutions were prepared in the laboratory according to the European Standard (ISO/DIS 1257 1996) to create different relative humidity desorption environments, ranging from RH = 8.2% to 97.3%. Each saturated solution was then kept in a plastic box at a normal room temperature of $24 \pm 0.5^{0}C$ to impose its corresponding equilibrium desorption environment on concrete samples.

Table 3.10: Relative humidity and suction values of the saturated solutions used.

Solution symbol	Type of salt	RH (%)	Total suction (MPa)
1	Potassium Sulphate	97.3	3.7
2	Potassium Nitrate	93.5	9.2
3	Potassium chloride	84.3	23.3
4	Sodium Chloride	75.3	38.6
5	Potassium Iodide	68.9	50.8
6	Sodium Bromide	57.6	75.2
7	Potassium Carbonate	43.2	114.4
8	Magnesium Chloride	32.9	151.9
9	Potassium Acetate	22.5	203.3
10	Lithium Chloride	11.3	297.1
11	Sodium Hydroxide	8.2	340.8

The purpose of using the saturated salt solutions, provided in Table 3.10, was to create a specific humidity environment above each solution. However, if a porous material is presented in one of these humidity environments, it will give off or absorb moisture, causing the equilibrium relative humidity to shift (Labuza 1963). Therefore, it was ensured that there was always some excess amount of salts used in each saturated solution to maintain its corresponding relative humidity condition constant during test. In addition, a humidity probe of ± 1 RH % accuracy was frequently used to check the relative humidity of each humidity environment. Figure 3.6 shows the process of measuring a relative humidity condition of a saturated solution kept in a plastic container.

Figure 3.6: Measuring the relative humidity conditions of a saturated solution.

b) Preparation of concrete samples and solutions container

After 56 days of curing, concrete samples of 50 mm diameter and 6 mm thickness were cut from the cast concrete cylinders, discussed in Section 3.1, using a wet saw. The five mix designs of these concrete samples were listed in Table 3.5. From each mix, 33 concrete samples were selected to conduct the vapour equilibrium test on them. The 33 samples of each mix were then divided into 3 samples per a saturated salt solution of the eleven saturated solutions provided in Table 3.10.

For each concrete mix, eleven wide mouth plastic boxes were selected to separately carry the eleven saturated solutions illustrated in Table 3.10. In each cap of the plastic boxes' caps, two holes with two rubber stoppers attached were made. As shown in Figure 3.7, the first hole was made to suspend three concrete samples inside each plastic box using the rubber stoppers and a copper wire, while the other hole was made to insert a humidity probe inside each plastic box for measuring the relative humidity condition. The copper wire used to tie the concrete samples was selected to avoid any rusting during the experiment. In addition it was ensured that the concrete samples were separated from each other using rubber O-rings of a diameter (10 mm) smaller than the diameters of the

concrete samples. The purpose of using these rubber O-rings was to provide a sufficient gap between the concrete samples for air circulation inside each humidity box.

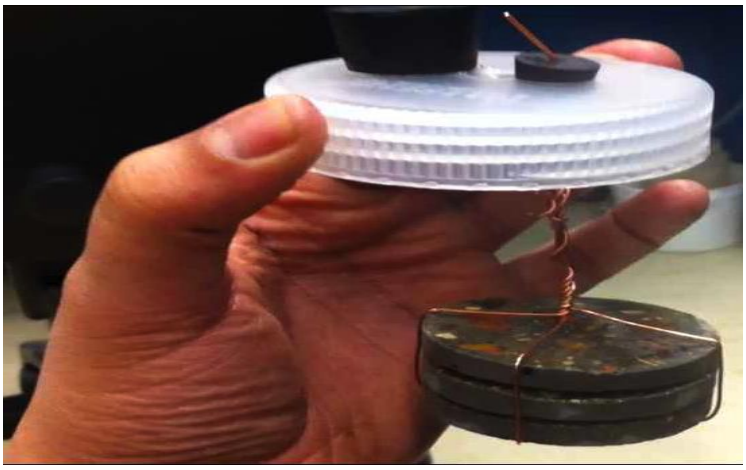

Figure 3.7: Suspension of concrete samples.

3.3.2 Testing method

Before starting the experiment, all the concrete samples were submerged in saturated limewater for at least a week in order to measure the saturated surface dry weights (SSD), m_s, of each concrete sample. The mass of all samples was measured to the nearest 0.001gm. The concrete samples were then taken out of limewater and tied together as shown in Figure 3.7. After that, the concrete samples were submerged in saturated limewater again temporarily to saturate them before starting the experiment. At the start of the experiment, three concrete samples from each type of mix were taken out of the saturated limewater and immediately suspended inside each humidity plastic box. While suspending the concrete sample, it was ensured that concrete samples were not directly in contact with the solutions inside the humidity boxes. In addition, it was also ensured that the cap of each humidity box was closed firmly to prevent any loss of moisture from the concrete samples.

All the concrete samples were kept inside the humidity boxes for 28 days to allow the water content inside each concrete sample to reach equilibrium. During the 28 days, the relative humidity and the temperature inside each humidity box were checked every three days. Upon reaching equilibrium, the concrete samples were taken out of the humidity boxes, and the equilibrium humidity, m_h, and weights of the concrete samples were measured. The concrete samples were then put in an oven at a temperature of 105^0C for 24 hours in order to measure their oven dry weights, m_d. At the end of the experiment, the degree of water saturation of each concrete sample was measured using Equation (2.37), and the capillary pressure of each humidity environment was measured using Kelvin's equation, Equation (2.36).

3.4 Resistivity technique

The dependency of the ion diffusion coefficient on degree of saturation is one of the important key parameters needed to model the transport of ions in an unsaturated porous medium. Therefore, the resistivity technique was selected to indirectly determine the dependency of ions diffusion coefficient on degree of saturation in concrete. The resistivity technique is a well-known indirect method used to determine the diffusion coefficient of a porous material by measuring its electrical conductivity (Atkinson et al. 1984).

3.4.1 Equipment and concrete samples

a) Preparation of electrical circuits

The items of the experimental setup used in this study included two DC voltage suppliers, two voltmeters, two ammeters, electrical wires, four brass disks ($\Phi 50mm \times 4mm$), and

four plastic clamps. Two DC electrical circuits were built from these items to conduct the test on two concrete samples at the same time. As shown in Figure 3.8, each electrical circuit consists of electrical wires connected to one voltage supplier, one voltammeter, one ammeter, and two brass plates. The voltammeter was used to measure the voltage between the two brass disks, while the ammeter was used to measure the corresponding current of an applied voltage in the electrical circuit. The two brass plates used in each electrical circuit were design and manufactured to constrain a concrete sample between them using two plastic clamps during the experiment. In addition, two plastic bags were used to cover each concrete sample in each electrical circuit to eliminate the moisture loss in each concrete sample during the experiment.

Figure 3.8: Electrical circuit built to measure the resistivity of a concrete sample.

b) Preparation of concrete samples

After 56 days of curing, concrete disks of 50 mm diameter and 6 mm thickness were cut from the cast concrete cylinders, discussed in Section 3.1. The mix designs of these

concrete samples were listed in Table 3.5. From each mix type, 33 concrete samples were selected and submerged in limewater in order to conduct the experiments. After submerging each of the 33 concrete samples for at least a week, the saturated surface dry weight (SSD), m_s, of each concrete sample was carefully measured. The mass of all the samples was measured to the nearest 0.001gm

3.4.2 Testing method

Before starting the experiment, 33 concrete samples from each type of mix, were put in the eleven humidity boxes, as explained in Section 3.1, for 28 days. The purpose of using these humidity boxes was to create eleven different degrees of water saturation over all the concrete samples. Upon reaching equilibrium, three concrete samples were taken out from each humidity box to measure their equilibrium humidity weight, m_h. At the start of the test, a 0.5 water-cement ratio cement paste was prepared and coated on only one face of each brass plate in the electrical circuits. Since cement paste has low electrical resistivity (2 Ωm) compared with concrete (Whittington et al. 1981), the cement paste was used to have an intimate contact between a concrete sample and the brass plates in each electrical circuit. In addition, the combination of cement paste and the brass cement would provide a uniform distribution of current across a concrete sample. From the three concrete samples suspended in each humidity box, two concrete samples were used to conduct the resistivity test in the two available electrical circuits at the same time, while the third sample was kept in a plastic bag temporarily to preserve its moisture content. After testing the first two concrete samples, the third concrete sample was immediately used in the test.

Two different voltages, 2.5V and 5V, were applied to each concrete sample, and the corresponding electrical current of each voltage was recorded. In order to preserve the

moisture contents of a concrete sample during the test, these two values of voltage were selected to avoid overheating the concrete samples during each test. During the tests, the electrical current of each voltage was allowed to decay for few minutes until it reached to an equilibrium state for recording it. Figure 3.9 shows the process of measuring the electrical resistivity of concrete samples. The polarization potential was then measured using Equation (2.41). It was noticed that the drop in polarization potential, approximately 1V, was less than the two applied voltages. After measuring the polarization potential, the electrical resistance and the electrical resistivity of each concrete sample was calculated using Equations (2.42) and (2.40). At the end of the experiments, the concrete samples were washed with water and put in an oven at 105 C^0 for 24 hours in order to measure their oven dry weights, m_d. After that, the degree of water saturation of each sample was calculated using Equation (2.37). At the end, the resistivity measurements of each concrete mix type were then used to calculate the relative diffusion coefficient at different degrees of water saturation, explained in Section 4.3 in Chapter 4.

Figure 3.9: The process used to measure the resistivity of concrete.

3.5 Overall summary of Chapter 3

Three different experimental tests were conducted on five concrete mixes, explained in Section 3.1, to experimentally determine several key parameters needed to model the transport of moisture and ions in unsaturated conditions. These parameters included the saturated permeability coefficient of concrete, the moisture retention data of concrete, and the dependency of effective diffusion coefficient on degree of saturation of concrete.

The first experimental technique used to determine the saturated permeability coefficient of the five concrete mixes was the centrifuge technique. A centrifuge machine was selected to conduct the experiment on three concrete samples per mix. In this method, concrete sample holders were specially designed and manufactured in order to conduct the test.

The second experimental technique used to determine the moisture retention data of the five concrete mixes was the vapour equilibrium technique. From each mix type, 33 concrete samples were subjected to eleven desorption humidity environments at a constant temperature of 24 ± 0.5^{0}C. The eleven desorption humidity environments were prepared using eleven different saturated salt solutions kept in separate plastic boxes. At the end of the experiment, the degree of water saturation of each sample was determined. In addition, the capillary pressure of each humidity environment was calculated using Kelvin's equation.

The resistivity technique was used to characterize the dependency of the effective diffusion coefficient on the degree of water saturation of the five concrete mixes. 33 concrete samples from each mix were placed in eleven humidity environments, discussed in the vapor equilibrium technique, to create different degree of water saturation.

Electrical circuits were built to apply two different voltages, 2.5V and 5V, on each concrete sample at different degree of water saturation. The electrical resistivity of each concrete sample was then determined based on measuring the corresponding current of each applied voltage. At the end, the diffusion coefficients of all concrete samples at different degrees of water saturation were measured for each concrete sample.

4. Results and Discussion

4.1 Saturated permeability coefficient

The saturated permeability coefficients of the five types of concrete mixes were determined using a centrifuge technique, as described in Sections 3.1 and 3.2. The five concrete mixes considered in this study were Mix A (0%SF), Mix B (5%SF), Mix C (10%SF), Mix D (15%SF), and Mix E (20%SF). For each type of mix, the centrifuge test was carried out for three concrete samples, the average of which was taken as the saturated permeability coefficient for that mix.

The initial data of the saturated permeability coefficient measurement of each concrete sample included the initial and the final heights of water level in the water tube, the centrifugation time, the angular velocity of the centrifuge machine, and the dimensions of the concrete sample and its holder. Based on knowledge of all these parameters, the saturated permeability coefficient of each concrete mix was then calculated using Equations (2.32), (2.33), and (2.34), shown below for convenience:

$$a_r = \omega_r^2 \cdot R_{cen} \tag{2.32}$$

$$N = \frac{a_r}{\mathrm{g}} \tag{2.33}$$

$$K_s = \frac{1}{N}\frac{aL}{At}\ln\frac{h_0}{h_t} \tag{2.34}$$

where ω_r is the applied rotational speed, $R_{cen}$is the centrifuge operative radius, N is the scale factor, a_r is the acceleration, g is the acceleration due to the gravity, K_s is the saturated permeability, a is the cross-sectional area of the water tube, L is the length of the specimen parallel to the direction of flow, A is the cross-sectional area of the specimen, t is the time of the flow, h_0 is the initial height of the water tube, and h_t is the height at t.

The analysis of the saturated permeability coefficients of the five mixes is presented in Table 4.1. The saturated permeability coefficients of each type of concrete mix were statistically analyzed to determine the reliability of the experimental method used in this study. First, the coefficient of variation of each mix type was calculated based on the measured mean value of each saturated permeability coefficient. As shown in Table 4.1, 5.1% to 9.8% was the range of coefficients of variation for the measured saturated permeability coefficient.

Table 4.1: Saturated permeability coefficients of the five concrete mixes.

Mix type	**Mix (A) 0%SF**	**Mix (B) 5%SF**	**Mix (C) 10%SF**	**Mix (D) 15%SF**	**Mix (E) 20%SF**
Centrifuge Speed (RPM)	2600	2800	2800	2800	2900
Angular velocity (rad/s)	272	293	293	293	304
Acceleration (a) (m/s^2)	13737	15932	15932	15932	17091
Scale factor N	1400	1624	1624	1624	1742
Periods of checking data during at least 24 hours (hr)	4	4	6	10	14
Mean of saturated permeability coefficients (m/s)	7.0E-12	4.4E-12	3.7E-12	1.8E-12	1.2E-12
Maximum saturated permeability coefficient (m/s)	7.8E-12	4.6E-12	3.8E-12	2.0E-12	1.3E-12
Minimum saturated permeability coefficient (m/s)	6.6E-12	4.3E-12	3.4E-12	1.7E-12	1.3E-12
Standard deviation (m/s)	6.7E-13	2.2E-13	2.3E-13	1.7E-13	1.2E-13
Coefficient of variation (%)	9.5	5.1	6.1	9.4	9.8

In addition, error bars were constructed in a graph to reflect the variability of data in each type of mix. As shown in Figure 4.1 the margin of error in each type of mix is in an acceptable range. Based on the statistical analysis of data, it was found that the centrifuge method used in this study was a suitable technique for measuring the saturated permeability coefficient of concrete. However, it is worth noticing that just like with any experimental test, several possible sources of error could be at the origin the observed error margins for this test. Among the most important technical and human sources of errors that could be considered in the this technique one can mention, errors associated with microstructural differences (such as defects) between samples, errors associated with an accurate recording of the dimensions of each concrete sample, errors in recording the height of the water level in each concrete sample holder, errors in the accuracy of the angular speeds provided by the centrifuge machine.

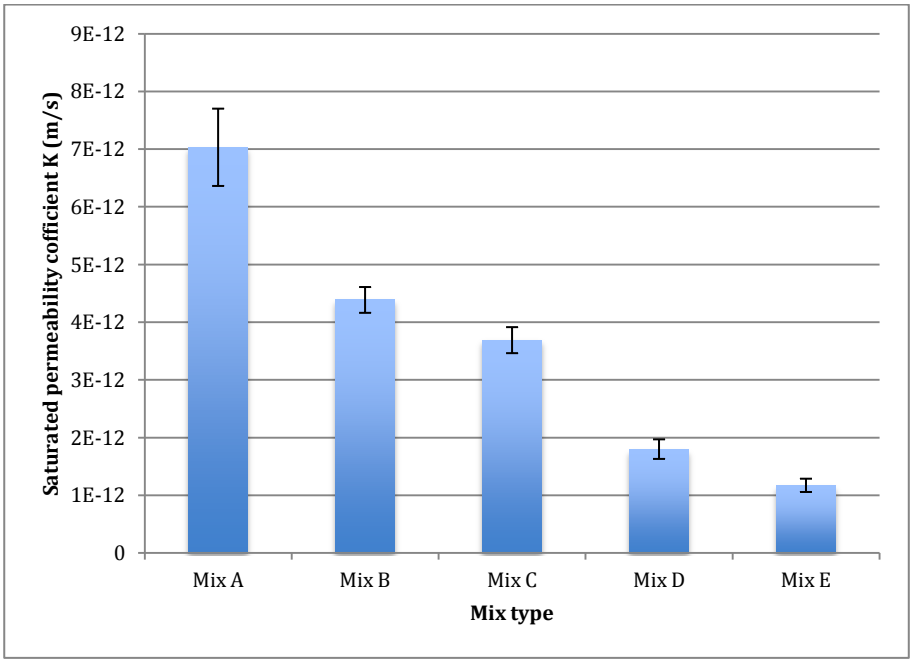

Figure 4.1: The measured saturated permeability coefficients with error margins for Mix A (0%SF), Mix B (5%SF), Mix C (10%SF), Mix D (15%SF) and Mix E (20% SF).

The saturated permeability coefficients of all concrete mix samples were plotted on the same graph to check if there was any overlapping between the results of the various mix types. As shown in Figure 4.2, no overlapping between the various mixes can be seen, indicating that each mix type had a visible effect on the value of the saturated permeability coefficient.

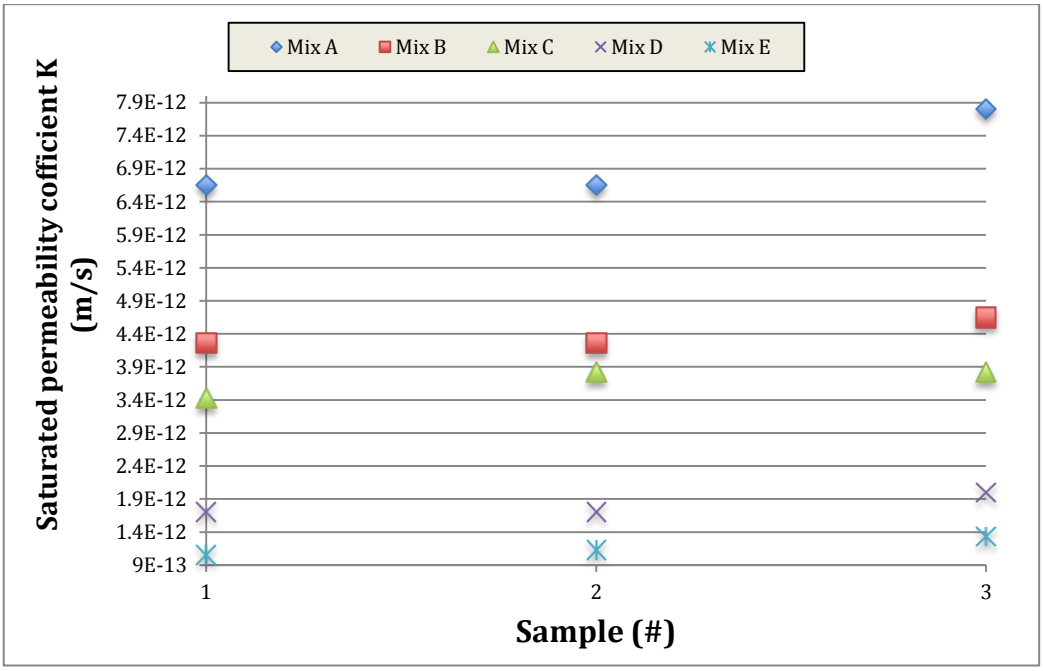

Figure 4.2: The measured saturated permeability coefficients for Mix A (0%SF), Mix B (5%SF), Mix C (10%SF), Mix D (15%SF) and Mix E (20%SF).

In comparison with other experimental techniques found in the literature, the advantage of using the centrifuge technique in this study was clearly noticed in terms of speed. The time of measuring the saturated permeability coefficient for concrete went down from one day or more to only several hours. In fact, the concrete sample holder that was specially designed for and used in this study (see Figure 3.4) has shown that even under a high angular speed of 4000 RPM there was no leakage of water, resulting in a significant

reduction of the experimental time. Although the concrete sample holder used in this study was suitable for usage under a high angular speed of 4000 RPM, a maximum angular speed of 2900 RPM was chosen because the centrifuge machine used in this study could overheat fairly quickly when an angular speed of more than 2900 RPM was used.

4.1.1 Effect of silica fume on results:

The incorporation of different proportions of dry densified silica fume in four concrete mixes had a significant effect on the measured saturated permeability coefficients. Compared with the mean saturated permeability coefficient of Mix A (0%SF), the replacement of 5% and 10% of type 10 Portland cement with silica fume decreased the mean saturated permeability coefficients of Mix B and Mix C by 37% and 47%, respectively. However, the replacement of 15% and 20% of type 10 Portland cement with silica fume decreased the mean saturated permeability coefficients of Mix D and Mix E by 74% and 83%, respectively. The reduction in the saturated permeability coefficient of concrete made with silica fume could be attributed to the effect of silica fume in reducing the connection between the pores in concrete, resulting in difficulty for water to penetrate the concrete matrix.

Moreover, to clearly reflect the effect of the addition of silica fume on the measured saturated permeability coefficient, the saturated permeability data were converted to normalized saturated permeability with respect to the saturated permeability of Mix A (0%SF). Figure 4.3 shows that that an increase in silica fume from 0% to 20% decreased the saturated permeability coefficient by six times.

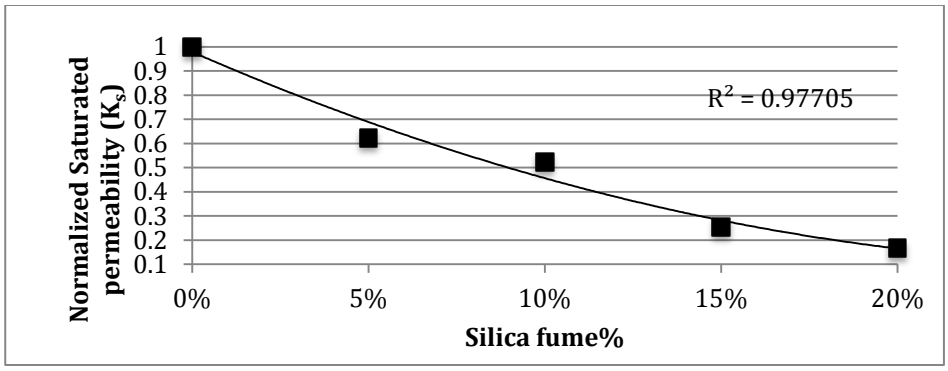

Figure 4.3: Normalized saturated permeability with respect to Mix A (0%SF) and the percentages of silica fume for Mix A (0%SF), Mix B (5% SF), Mix C (10%SF), Mix D (15%SF) and Mix E (20%SF) with respect to Mix A (0%SF).

According to Figure 4.3, the approximate empirical relation between the silica fume percentage and the saturated permeability could be expressed according to Equation (4.1):

$$K_s(\%SF) = K_{so}[11.6\,(SF\%)^2 - 6.4(SF\%) + 1] \quad (4.1)$$

where $K_s(SF\%)$ is the saturated permeability coefficient at a given percentage of silica fume, K_{so} is the saturated permeability when silica fume is not introduced into the concrete mix, and (%SF) is the silica fume percentage.

4.2 Moisture retention data

The moisture retention data of the five concrete mixes were determined by creating eleven different desorption relative humidity environments using the vapour equilibrium technique. The five concrete mixes considered in this study were Mix A (0% Silica fume), Mix B (5% Silica fume), Mix C (10% Silica fume), Mix D (15% Silica fume), and Mix E (20% Silica fume). In addition, the van Genuchten analytical model (van Genuchten 1980) was used to represent the required empirical retention parameters for concrete to

characterize the capillary pressure- degree of water saturation relationship and the relative permeability- degree of water saturation relationship.

For each type of mix, thirty-three saturated concrete samples were subjected to eleven different desorption relative humidity environments. For every relative humidity, the average value of three concrete samples was used to compute the degree of water saturation using Equation (2.37). Equation (2.37) is represented here for the convenience of the reader:

$$S_l = \frac{m_h - m_d}{m_s - m_d} \times 100 \tag{2.37}$$

It was noticed that at about 97.3% RH the corresponding equilibrium mass weight of each concrete sample, m_h, was found to be lower than its saturated mass weight, m_s. This reduction in mass at this high relative humidity level indicates that all concrete samples were likely saturated with water before conducting the vapour equilibrium technique.

Figure 4.4 shows the relation between the degree of water saturation of all five concrete mixes and their corresponding relative humidity environments. It was noticed that the degree of saturation of the five concrete mixes was approximately in the range of 20% to 97%. In addition, as the relative humidity of the eleven desorption environments increases, the degree of water saturation of the concrete mixes also increases. As can be seen in Figure 4.4, the relations between the degree of water saturation and the relative humidity of all concrete mixes were almost linear.

The data of all five concrete mixes were statically analyzed to verify the reliability of the experimental method used in this study. The maximum coefficient of variation of the measured degree of water saturation of all concrete mixes was 5.7%, indicating that the method used to create the different degrees of water saturation in the concrete samples is

reliable. In addition, error bars were plotted to check that each error margin for a given degree of water saturation was within an acceptable range. As shown in Figure 4.4, the error margins for each concrete mix are very small compared to their respective average degree of water saturation, indicating that the distribution of moisture inside each concrete sample was reproducible with a relatively high degree of accuracy. However, just like for the centrifuge technique described in the previous section, several sources of errors that can lead to the observed error margins for this test can be identified. Among the most important technical and human sources of errors one can mention, errors associated with microstructural differences (such as defects) between samples, errors associated with an accurate recording of mass weight for each concrete sample, together with errors in the accuracy of the humidity probe used to measure the corresponding relative humidity of each salt solution used in the humidity chambers.

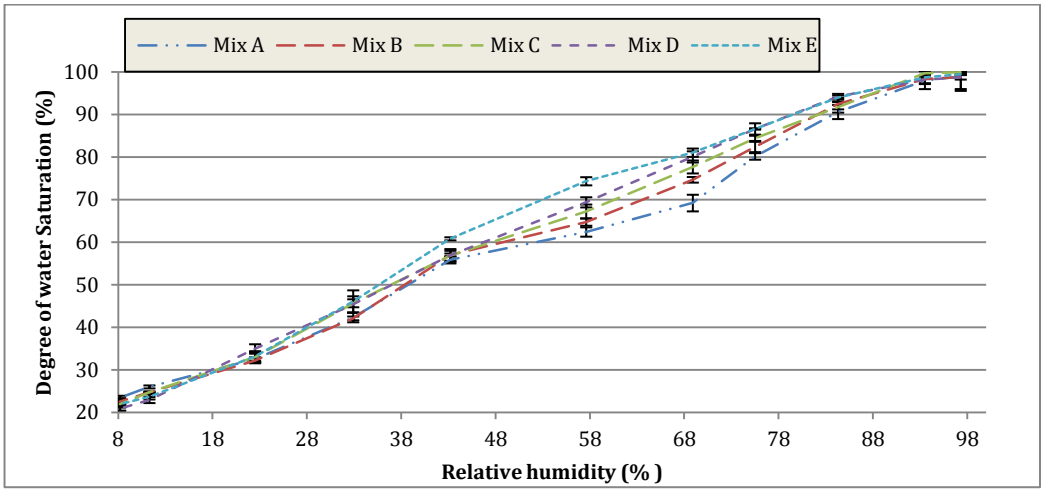

Figure 4.4: Relative humidity-degree of water saturation relationships for Mix A (0%SF), Mix B (5%SF), Mix C (10%SF), Mix D (15%SF) and Mix E (20%SF).

The capillary suction-degree of water saturation relationship for each concrete mix was also determined. The relative humidity of environmental chamber was converted to a

specific capillary suction using Kelvin's equation, Equation (2.36), at a given degree of water saturation. The equation is represented here by:

$$P_c = \left[\frac{RT}{\mathrm{M}}\right] \ln\left[\frac{\rho}{\rho_s}\right] \tag{2.36}$$

where P_c is the total suction (MPa), R is the ideal gas constant, M molecular weight of water vapour (0.01802 $\frac{kg}{Mol}$), T is the temperature of the liquid phase in Kelvin (^{0}C+273.16) (T), ρ is the water vapour pressure in equilibrium with liquid phase (Pa), ρ_s is the saturated water vapour pressure (Pa) at a given temperature (T).

Figure 4.5 shows the variations of degree of water saturation as a function of capillary suction for the five concrete mixes. It was noticed that as the degree of water saturation in the five concrete mixes decreases, the capillary suction environments increases.

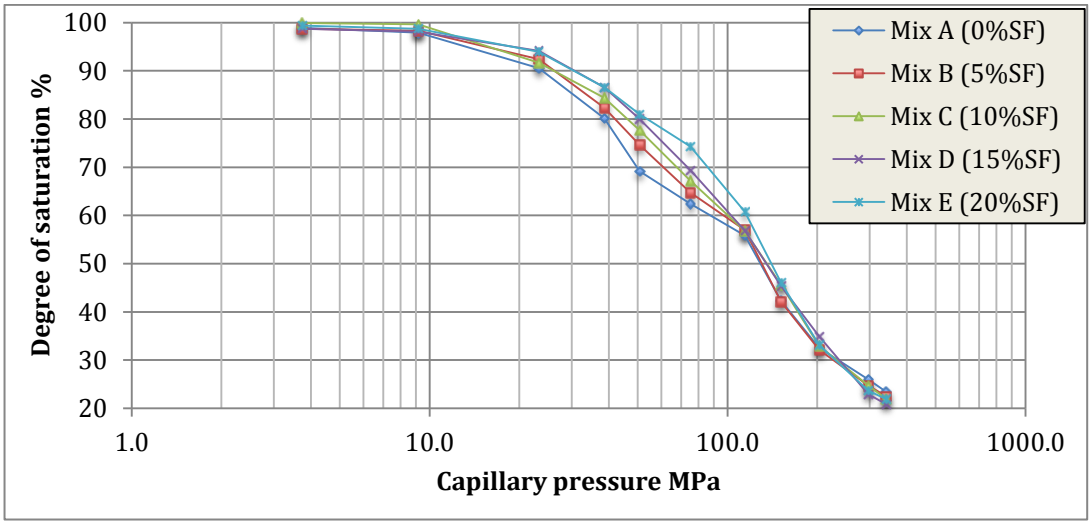

Figure 4.5: Capillary suction-degree of water saturation relationships for Mix A (0%SF), Mix B (5%SF), Mix C (10%SF), Mix D (15%SF) and Mix E (20% SF).

Several available analytical models have been proposed in the literature to represent moisture retention data for various porous materials. In this study, the van Genuchten

analytical model (1980) was selected, among other models, to provide a continuous representation of the retention curve of concrete.

The experimental moisture retention data was used in a regression analysis to determine the material parameters, m and α, for each type of concrete mix. These empirical retention parameters were fitted to the experimental retention data using a nonlinear, least square, curve fitting computer program known as RETC (van Genuchten et. al. 1991). Table 4.2 shows the empirical retention parameters obtained for each concrete mix. No standard method could be found in the present literature for defining the residual water saturation for concrete. Therefore, the residual saturation values, shown in Table 4.2, were treated as fitted empirical parameters only and taken as 0.1 for each type of concrete mix. In real conditions, concrete material rarely achieves a residual state. Therefore, the chosen residual saturation value of 0.1 is not of much importance.

Table 4.2: Empirical van Genuchten retention parameters for concrete.

Mix type	$\boldsymbol{\alpha}$ **(1/MPa)**	$\boldsymbol{m}$	$\boldsymbol{S_{lr}}$	$\boldsymbol{S_l}$
Mix A (0%SF)	0.02147	0.38714	0.1	1
Mix B (5%SF)	0.01809	0.3963	0.1	1
Mix C (10%SF)	0.01595	0.4269	0.1	1
Mix D (15%SF)	0.01373	0.46108	0.1	1
Mix E (20%SF)	0.01208	0.48216	0.1	1

The empirical parameter α is defined as the inverse of the air-entry value or the bubbling pressure, describing generally the porosity, the pore size diameter, the tortuosity, and the connectivity of pore in a porous material. When the values of the parameter α, shown in Table 4.2, were obtained for all concrete mixes, they were compared with the typical

inverse air-entry values provided by van Genuchten for soils, presented by the curve fitting program RETC program (van Genuchten et. al. 1991). It was noticed that the parameter α values for all concrete mixes were higher than those of soils, such as sand and clay, by about four orders of magnitude. This could be attributed to the significant differences between concrete and soils in terms of their microstructures, such as porosity, tortuosity, distribution of pores, and pore size.

The empirical retention parameters and the degree of water saturation range of a porous material can be used to determine the capillary pressure-degree of saturation relationship as illustrated in van Genuchten analytical model, in Equation (2.8). Equation (2.8) is represented here by:

$$P_c = -\frac{1}{\alpha}\left[S_e^{\frac{1}{m}} - 1\right]^{\frac{1}{n}} \tag{2.8}$$

where P_c is the capillary pressure, S_e is the effective degree of saturation, and m, α, n are empirical parameters affecting the shape of the hydraulic functions of the porous medium.

A comparison, shown in Figures 4.6 (a), (b), (c), (d), and (e), was made between the experimental capillary pressure-degree of water saturation data and the van Genuchten capillary pressure- degree of water saturation data for each type of concrete mix. As shown in these figures, there is a good agreement between the experimental data and the van Genuchten data at high degree of water saturation for all types of mixes. However, as the degree of water saturation decreases to about 0.4, the van Genuchten model starts to provide poor representation of capillary pressure values, especially for Mix A (0%SF) and Mix B (5%SF). Some researchers have reported this type of poor representation (Meyer et al. 2004; Khaleel et al. 1995).

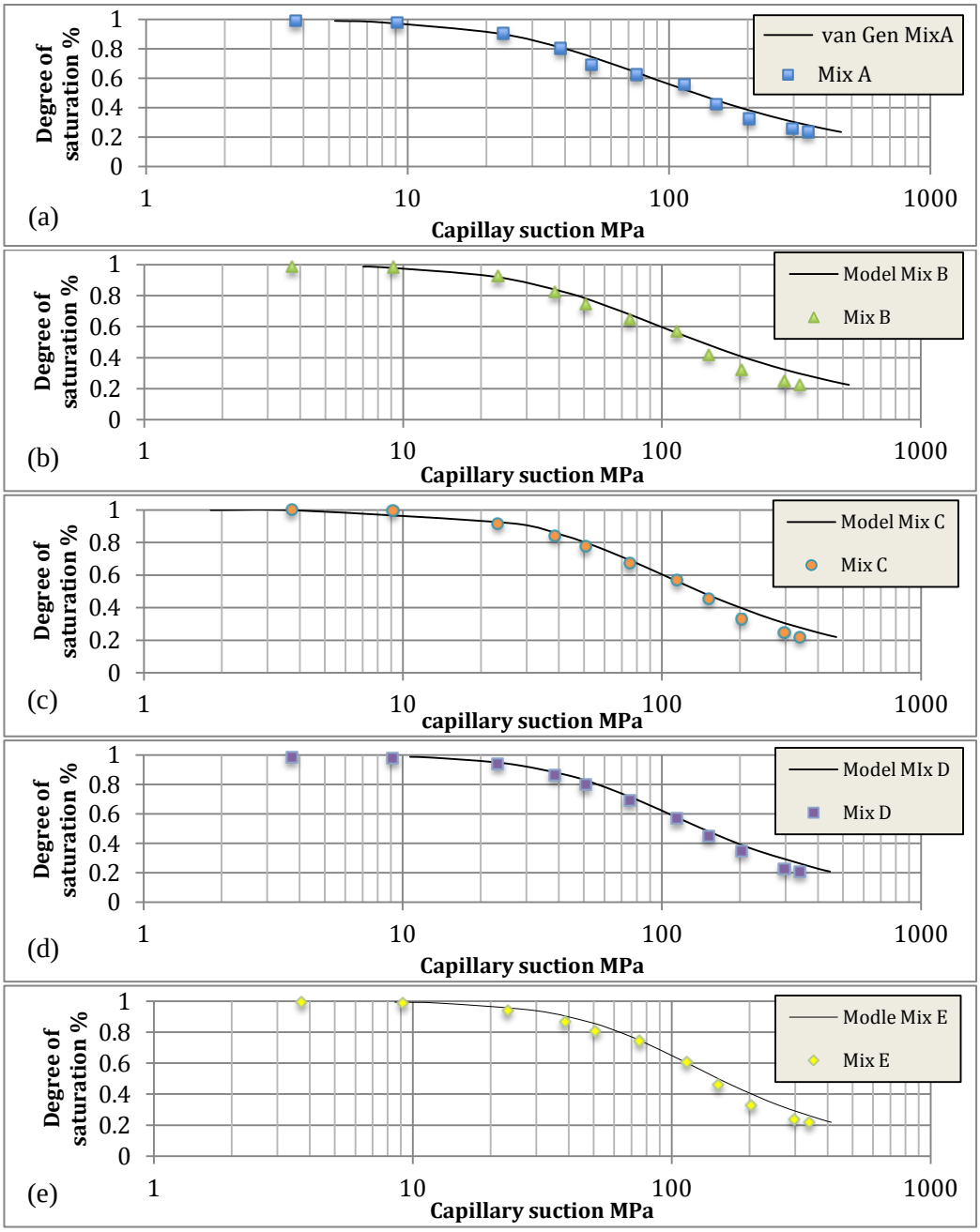

Figure 4.6: Experimental and van Genuchten moisture retention data for (a) Mix A (0%SF), (b) Mix B (5%SF), (c) Mix C (10%SF), (d) Mix D (15%SF) and (e) Mix E (20%SF).

The relative permeability of water- degree of saturation relationship was characterized for each type of concrete mix using the van Genuchten-Mualem model (Mualem 1976; van Genuchten 1980). The van Genuchten empirical retention parameters, shown in Table 4.2, were used in Equation (2.7) to determine the relative permeability of water-degree of saturation relationship for each type of mix. Equation (2.7) is represented here by:

$$k_r = S_e \left[1 - \left(1 - S_e^{\frac{1}{m}}\right)^m\right]^2 \tag{2.7}$$

where k_r is the relative permeability of water, S_e is the effective degree of saturation, and m is the pore-size distribution index.

Figure 4.7 shows the relative permeability of water at different degrees of saturation, ranging from nearly 1 to 0.2, for each type of concrete mix. Figures 4.7 (a), (b), (c), (d), and (e) show that the relative permeability of water decreases as the degree of saturation of concrete decreases. For all the five types of concrete mixes, at high degree of water saturation the curve of relative permeability of water shows a linear decrease, followed by a nonlinear decrease at lower degrees of saturation.

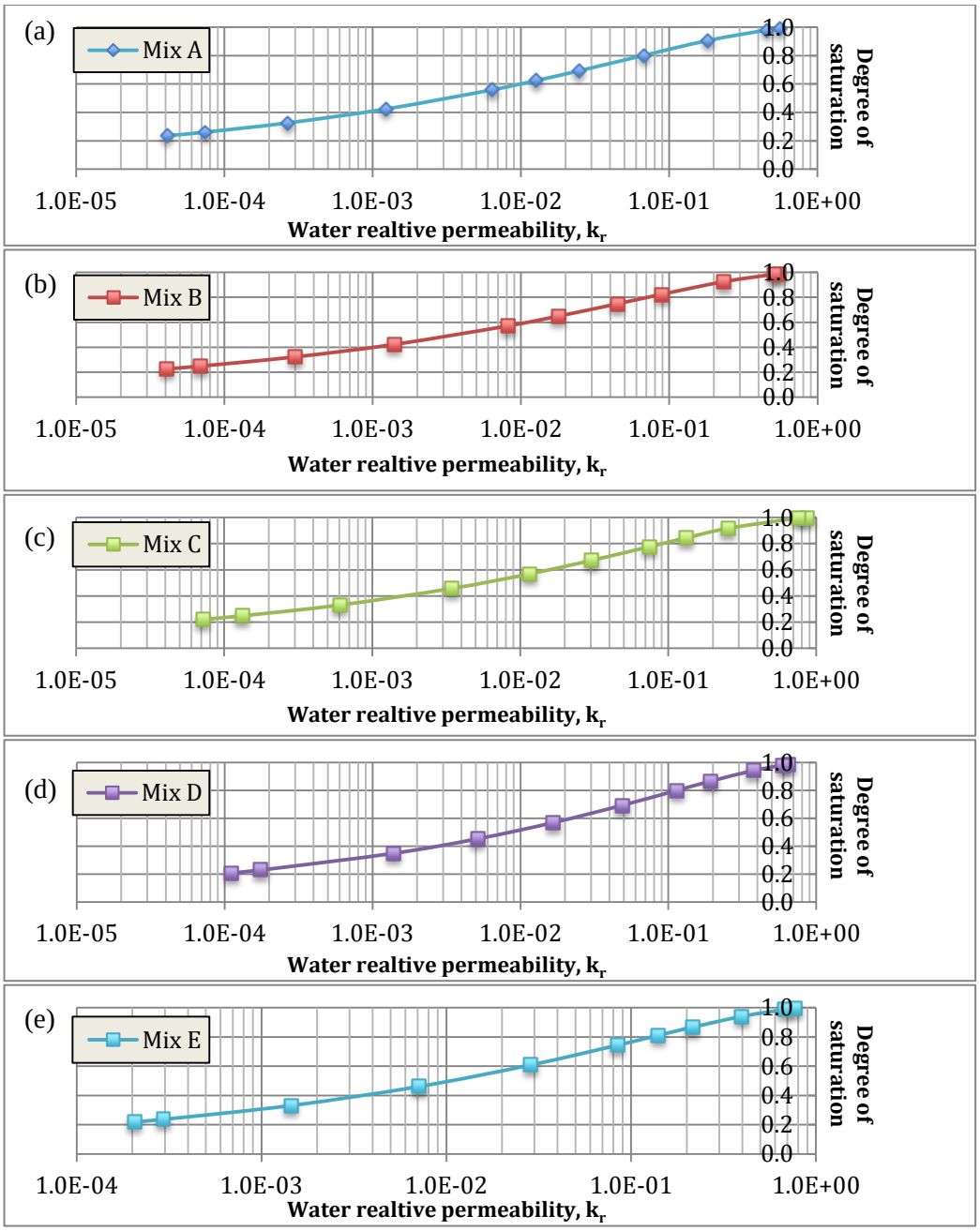

Figure 4.7: Water relative permeability curves for (a) Mix A (0%SF), (b) Mix B (5%SF), (c) Mix C (10% SF), (d) Mix D (15%SF) and (e) Mix E (20%SF).

4.2.1 Effect of silica fume on results:

The replacement of a specific amount of silica fume with type 10 normal Portland cement in concrete has a significant effect on the size and the distribution of pores in concrete. This effect is clearly shown in the experimental degree of water saturation data, The van Genuchten empirical parameters, and the relative permeability of water obtained by the van Genuchten model.

The degree of water saturation data of Mix B (5%SF), Mix C (10%SF), Mix D (15%SF), and Mix E (20%SF) are higher than the degree of saturation data of Mix A (0%SF). As shown in Figure 4.5, concrete samples with higher silica fume content were more difficult to desaturate at the levels between 100% to 40% relative humidity. This could be attributed to the presence of smaller size pores in concrete with higher silica fume content, which in turn require larger capillary pressures to desaturate.

In addition, it was noticed that the parameter α, obtained by the van Genuchten model, was also smaller in concrete with higher silica fume content. This indicates that when silica fume is used in concrete, the size of pores becomes small enough to prevent air bubbles from entering the samples. To clearly reflect the effect of silica fume percentage on the empirical parameter α, the α values for all the concrete mixes were normalized with respect to Mix A (0%SF). As shown in Figure 4.8, the increase in silica fume percentage from 0% to 20% decreased the value of parameters α by 1.8 times.

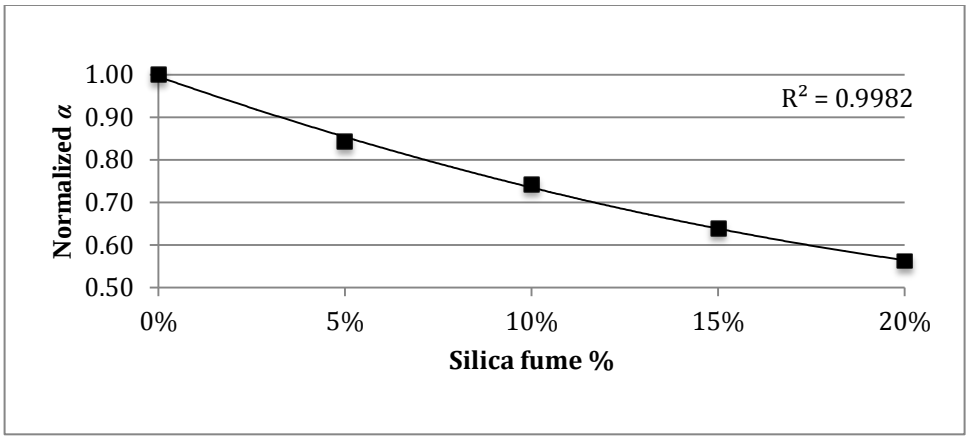

Figure 4.8: The normalized empirical parameter, α, with respect to Mix A (0%SF) and the percentage of silica fume for Mix A (0%SF), Mix B (5% SF), Mix C (10%SF), Mix D (15%SF) and Mix E (20% SF) with respect to Mix A (0%SF).

According to Figure 4.8, the empirical relationship between the silica fume percentage and the inverse of the air-entry value can be expressed as in Equation (4.2).

$$\alpha(\%SF) = \alpha_o[4.5(\%SF)^2 - 3.1(\%SF) + 1] \quad (4.2)$$

where α $(SF\%)$ is the inverse of the air-entry value at a given silica fume percentage, α_o is the inverse of the air-entry value when silica fume is not introduced into the concrete mix, and (%SF) is the percentage of silica fume.

Moreover, as presented in Table 4.2, the empirical parameter m, the pore-size distribution index, increased as the percentage of silica fume increased from 0% to 20% in the five concrete mixes. This increase in m could be attributed to the effect of silica fume on increasing the pores' distribution inside the concrete matrix. Figure 4.9 reflects the effect of silica fume on the empirical parameter m of the five concrete mixes. As shown in Figure 4.9, the increase in silica fume percentage from 0% to 20% increased the empirical parameter m by 1.25 times.

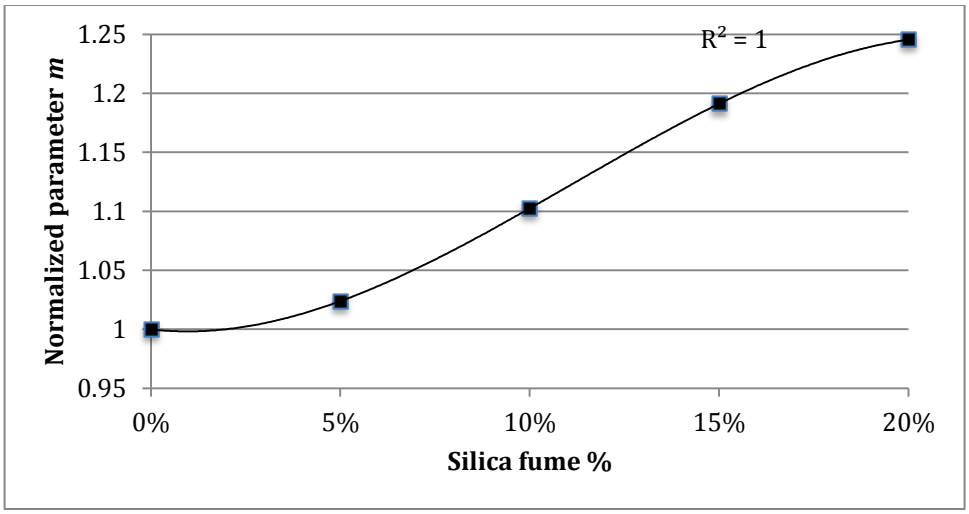

Figure 4.9: The normalized empirical parameter, m, with respect to Mix A (0%SF) and the percentage of silica fume for Mix A (0%SF), Mix B (5% SF), Mix C (10%SF), Mix D (15%SF) and Mix E (20% SF) with respect to Mix A (0%SF).

According to Figure 4.9, the approximate empirical relationship between the silica fume percentage and the parameter m can be expressed as:

$$m\ (SF\%) = m_o[-59.5(\%SF5)^3 + 19.9(\%SF)^2 + 0.37(\%SF) + 1] \qquad (4.3)$$

where $m\ (SF\%)$ is the empirical parameter, m, at a given silica fume percentage, m_o is the empirical parameter m when silica fume is not introduced into the concrete mix, and $(\%SF)$ is the silica fume percentage.

Also, as shown in Figure 4.7, the values of the relative permeability of water, over a wide range of degrees of water saturation, were also larger in concrete mixes with higher silica fume content. This could be attributed to the effect of silica fume on reducing the size of pores, which makes it difficult for water to exit from the concrete matrix.

4.3 Dependence of the effective diffusion coefficient on saturation

The dependency of the effective diffusion coefficient on the degree of water saturation in concrete was determined for the five concrete mixes presented in Section 3.1 using a resistivity technique. As presented in Section 3.1, the five concrete mixes considered in this study are Mix A (0%SF), Mix B (5%SF), Mix C (10%SF), Mix D (15%SF), and Mix E (20%SF). The experimental results for all concrete mixes were compared with the predictions obtained from the Millington and Quirk model to evaluate the applicability of the Millington and Quirk model to the case of concrete.

As shown in Figure 4.10, the electrical resistivity values for all the five types of concrete mixes were obtained at various degrees of water saturation. The considered degrees of saturation for all concrete mixes ranged from 1 to 0.2.

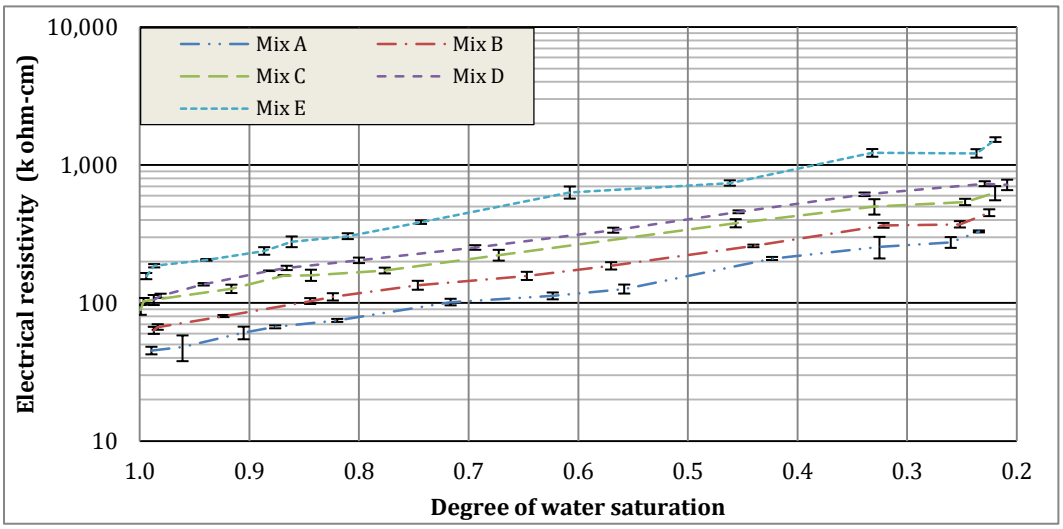

Figure 4.10: Electrical resistivity measurements at different degrees of water saturation for Mix A (0%SF), Mix B (5%SF), Mix C (10%SF), Mix D (15%SF) and Mix E (20%SF).

It is clearly shown in Figure 4.10 that as the degree of water saturation of concrete became high, the electrical resistivity of all the five types of concrete mixes decrease. This decrease in electrical resistivity at high degree of water saturation indicates that the mobility of ions in concrete pores becomes easier at a high degree of water saturation.

The electrical resistivity results for each type of concrete mix were statistically analyzed to reflect the variability of data at a given degree of water saturation. As shown in Figure 4.10 an error bar was calculated at every resistivity measurement to check if the variability of data of each concrete sample was within an acceptable range. All the error bars showed acceptable margins of errors, indicating that the errors made during the process of measuring the electrical resistivity of each sample were not significant. However, just like for the other two techniques that have been described in the previous sections, several sources of errors that can lead to the observed error margins for this test can be identified. Among the most important technical and human sources of errors one can mention, errors associated with microstructural differences (such as defects) between samples, as well as errors associated with the recording of either the electrical current or the voltage provided by the voltage suppliers.

The electrical resistivity results were then converted to normalized electrical resistivity values, shown in Figure 4.11, with respect to the smallest electrical resistivity value at the highest degree of water saturation ($S_l \approx 1$) for each type of mix. The normalized electrical resistivity was calculated using the following equation:

$$N_P = \frac{\rho}{\rho_s} \tag{4.4}$$

where ρ_s is the smallest electrical resistivity measured at the highest degree of saturation of each type of concrete mix.

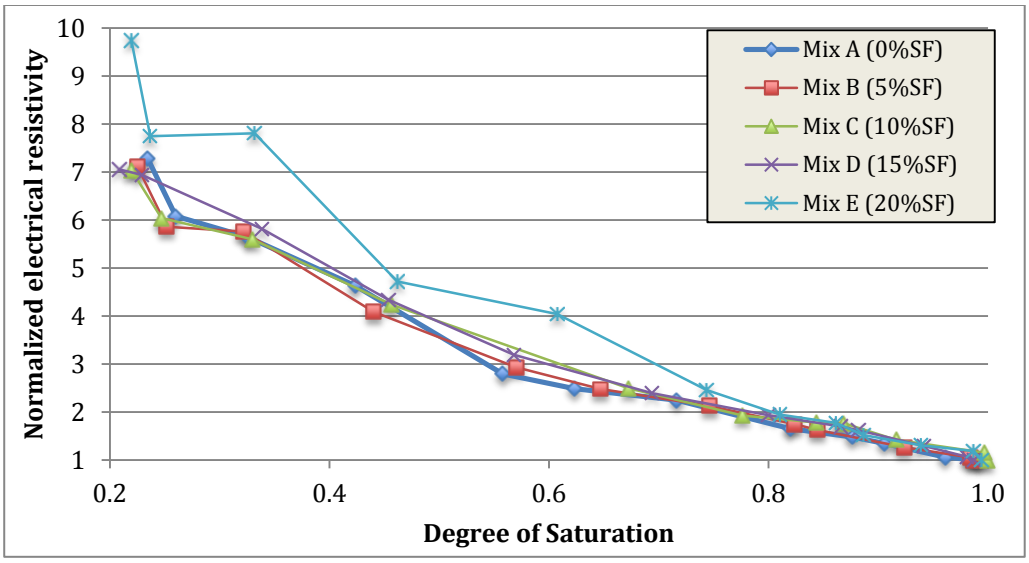

Figure 4.11: Normalized electrical resistivity and degree of saturation for Mix A (0%SF), Mix B (5%SF), Mix C (10%SF), Mix D (15%SF) and Mix E (20%SF).

As discussed in Section 2.4.2, the electrical conductivity and the effective diffusion coefficient are related to each other (Atkinson et al. 1984). In addition, the electrical conductivity measurements can be used to calculate the relative diffusion coefficient. Polder et al (2002) and Martys (1999) have showed in concrete that there is a good agreement between the experimental electrical conductivity and the relative diffusion coefficient.

The normalized electrical resistivity measurements were then used in Equation (2.38) in order to calculate the normalized electrical conductivity and, analogously, the relative diffusion coefficient of each type of concrete mix at different degrees of water saturation. The relative diffusion coefficients were calculated based on in the following equation:

$$D_r(S_l) = \frac{1}{N_P(S_l)} = \frac{\sigma(S_l \leq 1)}{\sigma(S_l \approx 1)} = \frac{D_{eff}(S_l \leq 1)}{D_{eff}(S_l \approx 1)} = \tau(S_l \leq 1) \qquad (4.5)$$

where D_r is the relative diffusion coefficient, $N_P(S_l)$ is the normalized electrical

resistivity at a given degree of saturation, σ is the electrical conductivity, S_l is the degree of saturation, D_{eff} is the effective diffusion coefficient, and $\tau\,(S_l)$ is the saturation dependent tortuosity.

Equation (4.5) assumes that tortuosity $\beta\,(S_l)$ can be written as:

$$\beta\,(S_l) = \tau_o \cdot \tau(S_l) \tag{4.6}$$

where τ_o is the value of tortuosity at saturation and $\tau(S_l)$ is the saturation dependent tortuosity. Under saturation conditions, S_l =1, and $\tau(S_l)$=1.

As shown in Figures 4.12 (a), (b), (c), (d), and (e), the relation is characterized at lower degrees of saturation by a decrease in the relative diffusion coefficient as the degree of water saturation decreases. For all five concrete mixes, it was noticed that in the range of 1 to 0.8 of degree of water saturation, the decrease in the relative diffusion coefficient was rapid. However, below about 0.6 degree of water saturation, the decrease in relative diffusion coefficient for all concrete mixes was less steep. The relation between the diffusion coefficient and water saturation was therefore nonlinear.

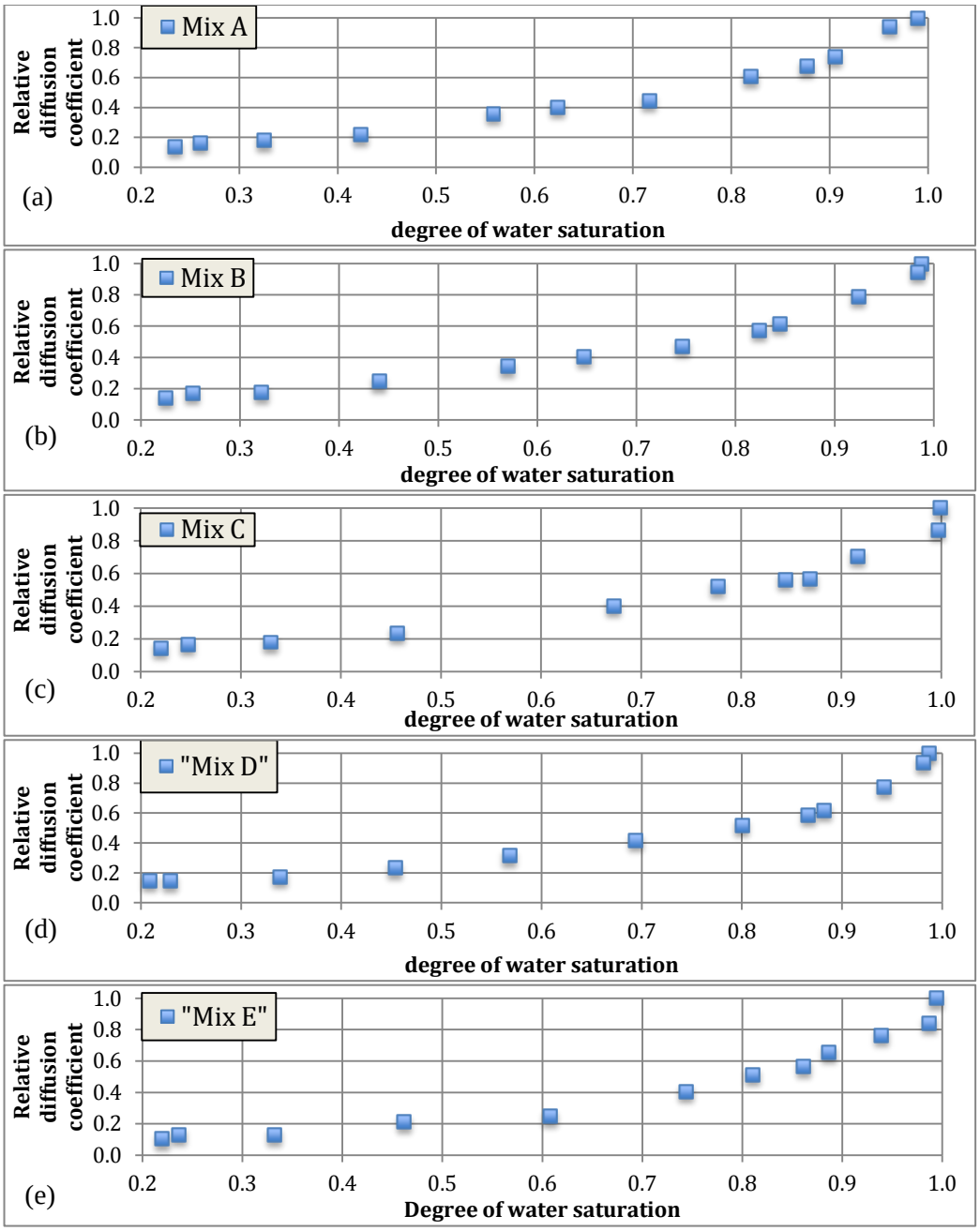

Figures 4.12: Experimental relative diffusion coefficients for (a) Mix A (0%SF), (b) Mix B (5%SF), (c) Mix C (10%SF), (d) Mix D (15%SF), and (e) Mix E (20%SF).

The relative diffusion coefficient-degree of water saturation relationship for concrete was compared with experimental data for sand from Barbour et al. (1996), as shown in Figure 4.13. In comparison with all concrete mixes, the relative diffusion coefficient curve of sand shows a nearly linear drop as the degree of water saturation decreases. In addition, all the relative diffusion coefficient curves for all five concrete mixes were found to be smaller than the sand results, confirming the major microstructural differences, such as porosity and distribution of pores, between sand and concrete.

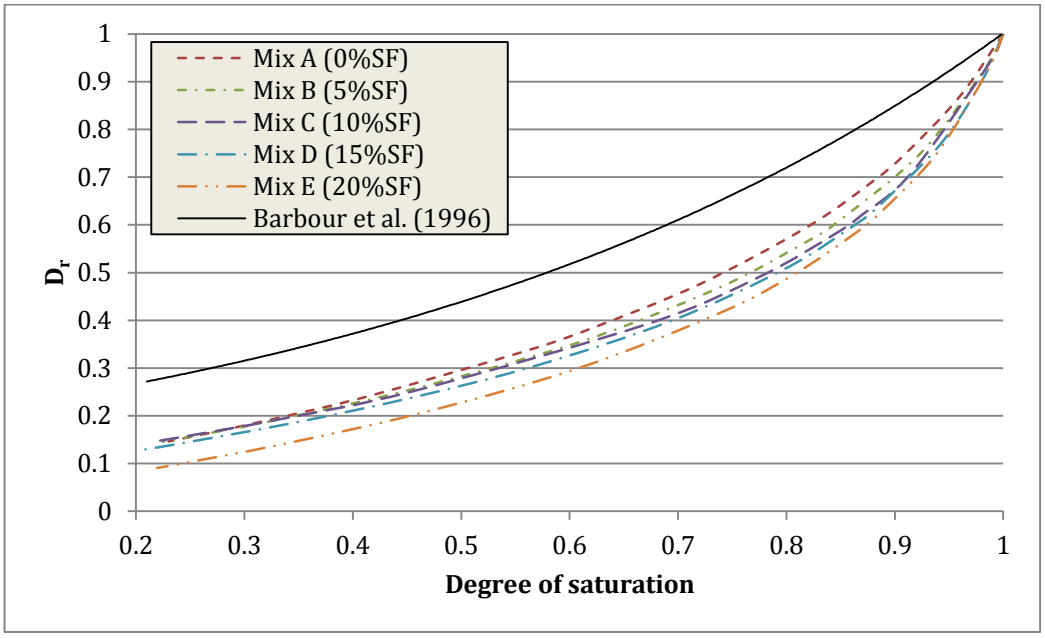

Figure 4.13: Relative diffusion coefficient of sand and concrete mixes, Mix A (0%SF), Mix B (5%SF), Mix C (10%SF), Mix D (15%SF), and Mix E (20%SF).

The Millington and Quirk (1961) empirical model was also compared with the experimental data. In order to make the comparison, the normalized saturation dependent tortuosity, $\tau(S_l)$, had to be calculated with respect to porosity, as illustrated in the following empirical equation:

$$\tau(S_l) = \frac{\beta}{\emptyset^{4/3}} = S_l^{10/3} \tag{4.7}$$

Figures 4.14 (a), (b), (c), (d), and (e) show a comparison between the experimental results and the Millington and Quirk (1961) results. As shown in Figure 4.14, the Millington and Quirk (1961) results are close to the experimental results at high degrees of water saturation. However, below about a degree of water saturation of 0.7, the relative diffusion coefficient curve of the Millington and Quirk model started to deviate from the experimental result and to underestimate the relative diffusion coefficients at low degrees of water saturation.

Although the Millington and Quirk (1961) empirical model is widely used in the literature, it is still not regarded as the most accurate equation over very wide ranges of variation of the degree of saturation (Davis et al. 2004). In addition, it was concluded by Schaefer et al. (1995) that the Millington and Quirk (1961) model severely underestimates the effective diffusion coefficient in several types of soils.

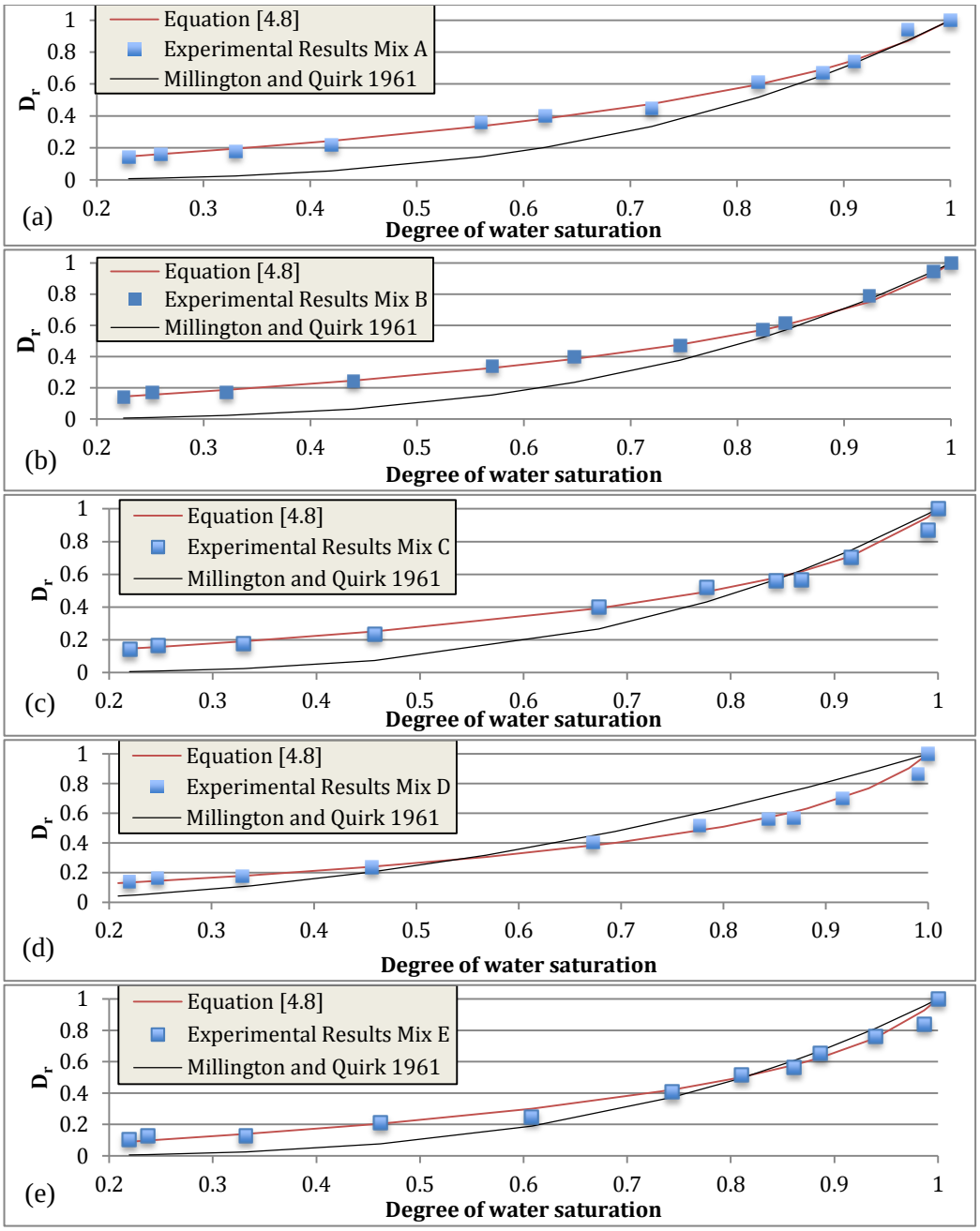

Figures 4.14: The relative diffusion coefficient, $D_{r,}$ of the normalized MQ, equation (4.8), and the experimental results for (a) Mix A (0%SF), (b) Mix B (5%SF), (c) Mix C (10%SF), (d) Mix D (15%SF), and (e) Mix E (20%SF).

Since the Millington and Quirk (1961) equation is an empirical equation that was developed based experiments and observations for soils and rocks rather than basic theories, another empirical equation was developed in this study using a regression analysis and was carried out to represent the saturation dependent tortuosity, $\tau(S_l)$ or the relative diffusion coefficient, such that a better agreement with the experimental results of this study could be achieved. The best empirical equation was determined as a function of the degree of water saturation, shown in Equation (4.8):

$$\tau(S_l) = D_r(S_l) = a\,\mathrm{Ln}\left[b(S_l - 1) + e^{1/a}\right] \tag{4.8}$$

where $\tau(S_l)$ is the saturation dependent tortuosity, $D_r(S_l)$ is the relative diffusion coefficient at a given degree of saturation, S_l is the degree of water saturation, and a and b are empirical factors affected by the silica fume percentage.

The empirical factors a and b shown in Equation (4.8) are considered to have constant values of -0.4 and -0.794, respectively, if silica fume is not used, for Mix A (0%SF). However, when silica fume is used, the empirical factors, a and b, become functions of the silica fume percentage. The empirical relations between the silica fume and the factors a and b are expressed in Equations (4.9) and (4.10). Figures 4.15 (a) and (b) show the relation between the silica fume percentage and the empirical factors.

$$a = 3 \times 10^{-6}(\%SF)^3 - 6 \times 10^{-4}(\%SF)^2 + 1.39 \times 10^{-2}(\%SF) - 0.4 \tag{4.9}$$

$$b = -7 \times 10^{-5}(\%SF)^3 + 1 \times 10^{-3}(\%SF)^2 + 5 \times 10^{-4}(\%SF) - 0.794 \tag{4.10}$$

where a and b are the empirical factors used in Equation (4.8) and $(\%SF)$ is the percentage of silica fume.

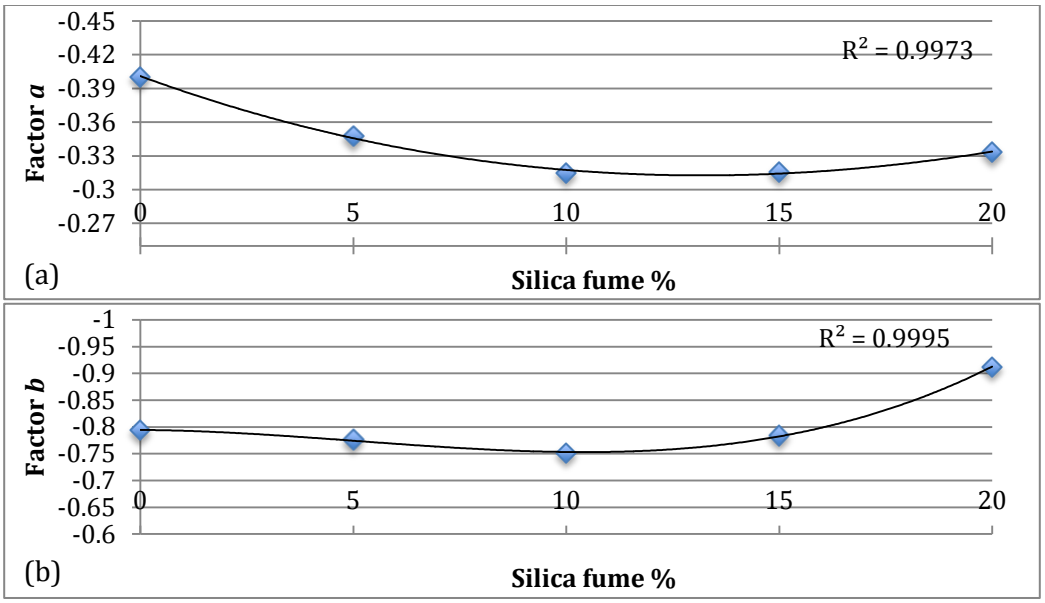

Figure 4.15: The relation between the empirical factors (a) a and (b) b of Equation (4.8) and the percentage of silica fume.

Table 4.3 shows the values of the empirical factors a and b obtained for Mix A (0%SF), Mix B (5%SF), Mix C (10%SF), Mix D (15%SF), and Mix E (20%SF). In addition, Table 4.4 shows a statistical analysis regarding the significance of the empirical factors a and b.

Table 4.3: The empirical factors a and b, used in Equation (4.8).

Mix type	**Factor a**	**Factor b**
Mix A (0%SF)	-0.400	-0.794
Mix B (5%SF)	-0.345	-0.776
Mix C (10%SF)	-0.315	-0.751
Mix D (15%SF)	-0.316	-0.784
Mix E (20%SF)	-0.333	-0.912

Table 4.4: A statistical analysis regarding the significance of the empirical factors a & b

Mix type	Factor	Standard error	t-Statistic	P-value
Mix A (0%SF)	a	0.036	-9.82	8.83E-7
	b	0.060	-12.68	6.56E-8
Mix B (5%SF)	a	0.027	-13.74	2.40E-7
	b	0.037	-21.54	4.70E-9
Mix C (10%SF)	a	0.024	-11.29	9.50E-8
	b	0.072	-9.71	4.91E-7
Mix D (15%SF)	a	0.013	-23.20	5.00E-10
	b	0.032	-24.34	3.11E-10
Mix E (20%SF)	a	0.030	-10.56	9.54E-7
	b	0.075	-11.99	2.93E-7

Figures 4.14 (a), (b), (c), (d) and (e) also show that the empirical equation developed in this study, Equation (4.8), provided better agreement with the experimental results than the Millington and Quirk (1961) empirical equation with a maximum relative absolute error and a minimum correlation coefficient of 4.25% and 0.994, respectively. This indicates that Equation (4.8) provided a good estimation of the relative diffusion coefficients as the percentage of silica fume changed between the five concrete mixes. Table 4.5 shows a statistical comparison between the experimental results and those of Equation (4.8).

Table 4.5: A comparison between the results of the empirical Equation (4.8) and the experimental results.

Mix Type	Mix (A)	Mix (B)	Mix (C)	Mix (D)	Mix (E)
Correlation coefficient (R^2)	0.996	0.998	0.995	0.998	0.994
Root mean-squared error (%)	2.60	1.57	3.06	1.39	3.31
Mean absolute error (%)	1.90	1.14	1.98	1.15	2.38
Relative absolute error (%)	3.68	2.27	4.00	2.25	4.25

Although the empirical equation proposed in this study, Equation (4.8), provides better agreement with the experimental results than the Millington and Quirk (1961) empirical equation, it might not accurately estimate the relative diffusion coefficient-degree of water saturation relationship for concrete with different qualities (for example, water cement ratio, mineral admixture, etc.). Therefore, modification might be needed in future studies for Equation (4.8) in order to estimate the relative diffusion coefficient-degree relationship for concrete with different qualities.

An additional comparison was also made between the experimental results, the results of Equation (4.8), and the Saetta et al. (1993) empirical model, Equation (4.11), to illustrate the differences between the empirical equations in estimating the relative diffusion coefficient over a wide range of relative humidity levels. In order to compare the experimental results and the results of Equation (4.8) with the Saetta et al. (1993) model, the relative diffusion coefficients over a range of relative humidity levels were calculated for each type of mix.

$$D_r(RH) = \frac{1}{\left[1 + \frac{(1 - RH)^4}{(1 - RH_c)^4}\right]} \tag{4.11}$$

where $D_r(RH)$ is the effective diffusion coefficient at a given relative humidity level,

RH, and RH_c is the relative humidity at which D_r drops to halfway between its maximum and minimum values, $D_r(RH_c)$ =0.5 $D_r(RH \approx 100\%)$.

Figures 4.16 (a), (b), (c), (d), and (e) show comparisons between the results of the Saetta et al. (1993) empirical equation, the experimental data, and the empirical Equation (4.8) over a wide range of relative humidity levels. Compared to the experimental results, the Saetta et al. (1993) curve overestimates the relative diffusion coefficient at high relative humidity levels of about 100% to 70%. In addition, the Saetta et al. (1993) curve tends to underestimate the relative diffusion coefficient below about 60% relative humidity level. The differences between the experimental results and the Saetta et al. (1993) model could be attributed to the differences in the experimental techniques used by each study. As can be seen in Figure 4.16, clearly the results of the empirical Equation (4.8) are in better agreement with the experimental results than those of the Saetta et al. (1993) model.

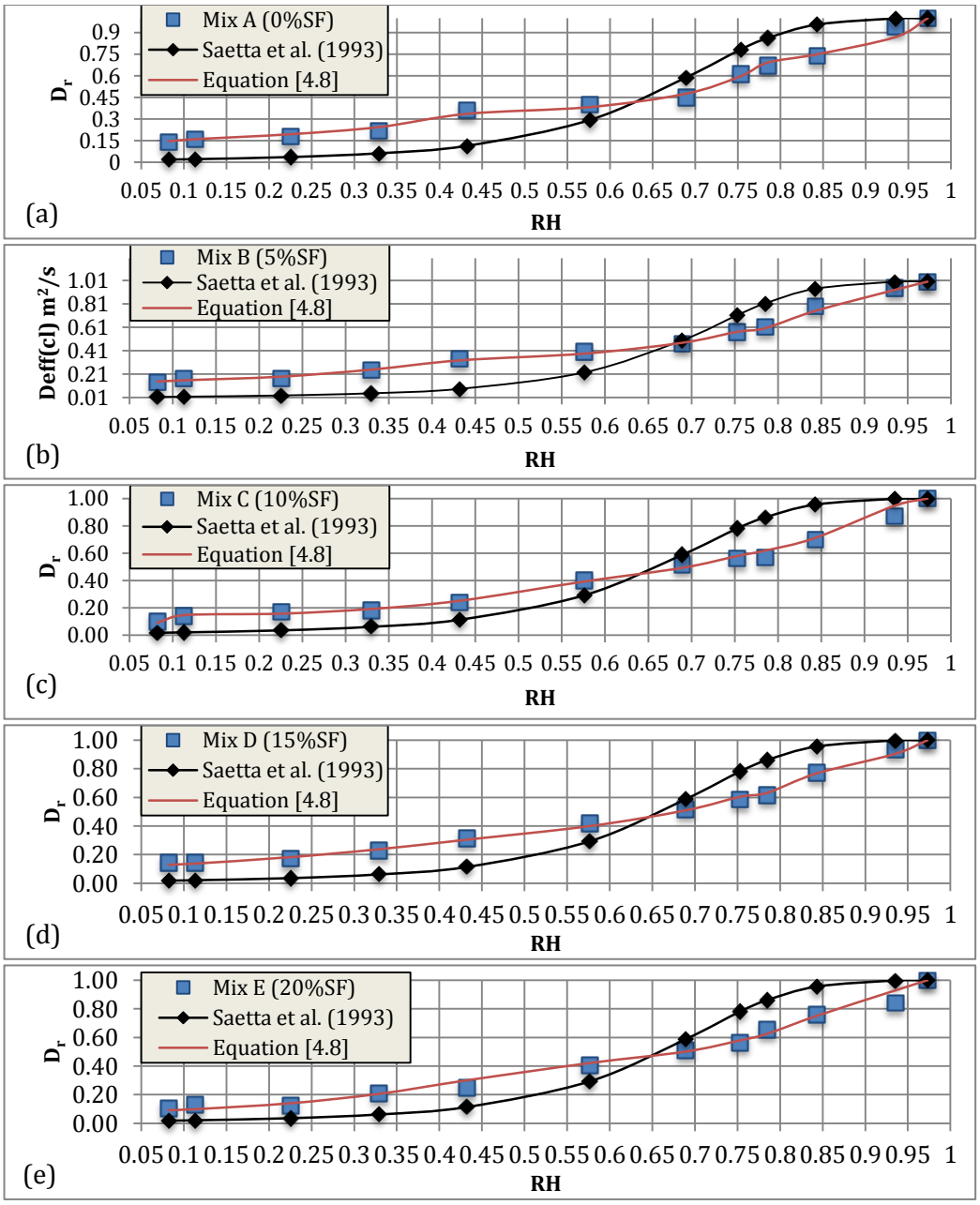

Figure 4.16: Relative diffusion coefficients of the experimental data, the Saetta et al. (1993), and Equation (4.8) for (a) Mix A (0%SF), (b) Mix B (5%SF), (c) Mix C (10%SF), (d) Mix D (15%SF), and (e) Mix E (20%SF).

4.3.1 Effect of silica fume on results:

The four different proportions of silica fume used in this study, namely, Mix B (5%SF), Mix C (10%SF), Mix D (15%SF), and Mix E (15%SF), have shown significant effects of silica fume on the relative diffusion coefficient-degree of water saturation relationship. In comparison with Mix A (0%SF), the addition of 5%, 10%, 15%, and 20% silica fume reduced the relative diffusion coefficient results of mixes B, C, D, and E, respectively. As shown in Figures 4.12 (a), (b), (c), (d), and (e), in the range between 1 to about 0.6 of degree of water saturation, Mix B (5%SF), Mix C (10%SF), and Mix D (15%SF) have lower relative diffusion coefficient values compared to Mix A (0%SF). As the degree of saturation decreases below 0.5, the relative diffusion coefficient curves for mixes A (0%SF), B (5%SF), C (10%SF), and D (15%SF) become almost the same. It was also found that the replacement of 20% Portland cement with silica fume in Mix E led to the smallest relative diffusion coefficients in comparison with all other concrete mixes. The reduction in the relative diffusion coefficient of all the concrete mixes made with silica fume could be attributed to the effect of silica fume on porosity and the tortuosity of the five concrete types.

4.4 Overall summary of Chapter 4

The saturated permeability coefficient was determined for each mix of the five concrete mixes considered in this study using a centrifuge technique. The mean saturated permeability coefficient was 7.0E-12 m/s for Mix A (0%SF), 4.4 E-12 m/s for Mix B (5%SF), 3.7 E-12 m/s for Mix C (10%SF), 1.8 E-12 for Mix D (15%SF), and 1.2E-12 m/s for Mix E (20%SF). The saturated permeability coefficient values obtained by the centrifuge technique in this study were found to fall within the range of typical values for concrete with comparable mix designs as reported in the published literature.

It was noticed that as the proportion of silica fume used in each concrete mix increased, the mean saturated permeability coefficient decreased. The results showed that the increase in silica fume percentage from 0% to 20% reduced the saturated permeability coefficient by six times.

The moisture retention curves were generated for the five concrete mixes using the vapour equilibrium technique. It was shown in the results that the degree of saturation of all concrete samples increased when the relative humidity increased. In addition, the results showed a decrease in capillary pressure when the degree of water saturation increased. The experimental moisture retention data were then used in the van Genuchten empirical model to determine the moisture retention parameters for each type of mix. After determining the empirical moisture retention parameters for all the concrete mixes, the relative permeability of water-degree of water saturation relationship was fully characterized for each type of mix. It was noticed that the relative permeability of water increased as the degree of water saturation increased.

The effects of using different proportions of silica fume on the capillary pressure, the relative permeability of water, and the empirical parameters of the van Genuchten model were evaluated. The addition of silica fume in concrete showed that a larger capillary pressure was needed to desaturate the concrete samples at relative humidity levels between 100% to 40%, resulting in higher degrees of water saturation in the concrete mixes made with silica fume. In addition, the results showed that as the percentage of silica fume increased in concrete, the relative permeability of water increased. The increase in silica fume percentage from 0 to 20% showed a decrease in the inverse of the air-entry value, α, by 1.8 times and an increase in the pore distribution index, m, by 1.25 times

The dependency of the relative diffusion coefficient on the degree of water saturation of concrete was characterized for each type of concrete mix using the electrical resistivity technique. The experimental electrical resistivity measurements were converted to normalized electrical resistivity to calculate the electrical conductivity and the relative diffusion coefficient at various degrees of water saturation for each type of mix. The results showed that a nonlinear decrease in the relative diffusion coefficient resulted as the degree of water saturation decreased. After that, the experimental relative diffusion coefficient results were compared with other experimental results obtained for sand. The relative diffusion coefficients of concrete were found to be higher than the coefficients of the considered sand, confirming the major microstructural differences between sand and concrete

In addition, the experimental relative diffusion results were compared with those predicated by the Millington and Quirk model to examine the applicability of that model to concrete. It was noticed that the experimental relative diffusion coefficient curves were close to the Millington and Quirk curve at high degrees of water saturation, but below about a value of 0.7 of degree of water saturation, the drop in the Millington and Quirk curve was more rapid than the experimental curves, except for Mix E (20%SF). In addition, an empirical equation was proposed in this study to estimate the relative diffusion coefficient as a function of saturation and amount of effect of silica fume used in the mix. The overall agreement between the results of this empirical equation and the experimental results were found to be better than the Millington and Quirk empirical model for all five concrete mixes with a maximum relative absolute error and a minimum correlation coefficient of 4.2% and 0.994, respectively. Moreover, an additional comparison with experimental results was also made to illustrate the differences between the Saetta et al. (1993) empirical equation and the empirical equation proposed in this study for estimating the relative diffusion coefficient over various relative humidity

levels. Compared with the experimental results, it was found that the results of the Saetta et al. (1993) empirical equation overestimated the relative diffusion coefficient at high relative humidity levels, and below about 70% relative humidity, the Saetta et al. (1993) equation started to underestimate the relative diffusion coefficient. It was also noticed in the comparison that there is a good agreement between the results of the empirical equation developed in this study and the experimental results.

Finally, it was noticed that the addition of silica fume reduced the relative diffusion coefficient values for Mix B (5%SF), Mix C (10%SF), and Mix D (20%SF) especially in the range of 1 to about 0.6 of water saturation degree. Mix E, made with 20% silica fume, showed smaller relative diffusion coefficient values than all the other concrete mixes.

5. Conclusions and Recommendations

A general summary of the work and conclusions of the research are presented in this chapter. In addition, recommendations are provided for future research in the same area.

5.1 Summary of work

The basic theories and equations explaining the transport of moisture and ions in unsaturated porous media were discussed. In addition, several experimental techniques available in the soils and the concrete literatures were discussed in terms of their capability of determining the key hydraulic parameters needed for modeling moisture flow and the transport of ions, such as chlorides, in unsaturated concrete.

Three experimental techniques were performed to determine the saturated permeability coefficient, the moisture retention function, and the dependency of the effective diffusion coefficient on the degree of water saturation of five different concrete mixes. The five concrete mix designs involved using a fixed water-cement ratio of 0.4 for all the concrete mixes but with different proportions of densified silica fume, Mix A (0% silica fume), Mix B (5%silica fume), Mix C (10% silica fume), Mix D (15% silica fume), and Mix E (20% silica fume).

The saturated permeability coefficients were experimentally determined for the five concrete mixes by using a centrifuge technique. A novel concrete sample holder was specifically developed for this study to avoid leakage of water between the concrete sample and its holder at high angular speed. The experimental technique was performed on three concrete samples from each concrete mix. The effect of using different proportions of silica fume on the saturated permeability coefficient was evaluated and

discussed for each concrete mix type.

The moisture retention functions of the five concrete mixes were determined using a vapour equilibrium technique. The experimental technique was carried out on 33 concrete samples from each of the five concrete mixes at a room temperature of 24 ± 0.5^{0}C. The 33 concrete samples of each type of mix were subjected to eleven relative humidity levels (desorption environments) using eleven types of saturated salt solutions kept in closed plastic containers. After determining the moisture retention functions of all the five concrete mixes, the results were correlated with the van Genuchten model to determine the empirical retention parameters of each concrete mix type. The van Genuchten parameters were then used to empirically characterize the capillary pressure-degree of water saturation relationship and the relative permeability-degree of water saturation relationship. The effects of using various silica fume proportions on the capillary pressure, the relative permeability, and the empirical parameters of the van Genuchten model were discussed and evaluated for each concrete mix type.

The dependency of the effective diffusion coefficient on the degree of water saturation was characterized using a resistivity technique. The electrical resistivity values of three concrete samples, from each of the five mixes, at different degrees of water saturation were determined using a DC voltage. Two different voltages were applied to each concrete sample, 2.5V and 5V, in order to measure the corresponding currents separately. The relative diffusion coefficient-degree of water saturation relationship was characterized and compared with other data found in the soils and concrete literature to illustrate the difference between the relative diffusion coefficient of concrete and the relative diffusion coefficient of sand, for example, over a wide range of degrees of water saturation. In addition, the results of Millington and Quirk (1961) empirical model were compared with the experimental results to examine the validity of this empirical model

for concrete. An empirical equation was proposed in this study to predict the relative diffusion coefficient of concrete at over a wide range of degrees of water saturation and the effect of silica fume addition. An additional comparison was made between the experimental relative diffusion coefficients, those obtained by the Saetta et al. (1993) empirical equation, and the empirical equation proposed in this study to illustrate the differences between the models in estimating the relative diffusion coefficient for concrete. The effect of using different proportions of silica fume on the relative diffusion coefficient was discussed.

5.2 Important findings

The mean saturated hydraulic permeability was 7.0E-12 m/s for Mix A (0%SF), 4.4E-12 m/s for Mix B (5%SF), 3.7E-12 m/s for Mix C (10%SF), 1.8E-12 m/s for Mix D (15%SF), and 1.2E-12 m/s for Mix E (20%SF). The saturated permeability coefficient values obtained in this study were found to be within the range of values typically observed for concrete samples with comparable mix designs. The maximum coefficient of variation in the measured saturated hydraulic permeability was 9.8% using a centrifuge technique. This value of coefficient of variation indicates that the centrifuge technique used in this study has a good potential for estimating the saturated hydraulic permeability of concrete in relatively short times compared with other traditional techniques.

It was shown in the saturated permeability results that the addition of silica fume decreased the saturated hydraulic permeability. An increase in the silica fume content from 0% to 20% decreased the saturated permeability coefficient by 6 times.

The results of the vapor equilibrium technique used in this study showed that the degrees of water saturation of all concrete samples were high at high relative humidity levels. In

addition, the capillary pressure results of all concrete mixes increased as the relative humidity decreased. The dependency of the relative permeability on the degree of water saturation was also characterized. For all the five types of concrete mixes, the relative permeability curves showed a nonlinear decrease with decreasing saturation levels.

At high relative humidity levels, it was found that the degrees of water saturation increased as the silica fume content in the concrete mixes increased. For the van Genuchten empirical parameters, the addition of silica fume reduced the value of the inverse of the air-entry value, α, and increased the value of the pore-size distribution index, m. It was also found from the results that the values of the relative permeability were larger in concrete mixes with higher silica fume content.

The experimental relative diffusion coefficient results were found to be higher at high degrees of water saturation. For all the five concrete mixes, it was noticed that in the range of 1 to 0.8 of water saturation, the non-linear decrease in the relative diffusion coefficient results was rapid. However, below a value of about 0.6 in degree of water saturation, the non-linear decrease in the relative diffusion coefficient for all concrete mixes was less rapid. When the experimental relative diffusion coefficient results were compared with the Millington and Quirk (1961) empirical model, it was found that the overall agreement between the Millington and Quirk (1961) model and the experimental results was not good for all types of mixes except for Mix E (20%SF). Moreover, a new empirical equation was developed in this study using a regression analysis method to represent the relative diffusion coefficient as a function of saturation and silica fume content in order to have a better agreement with the experimental results than the previously described model. In the comparison between the experimental relative diffusion coefficient and the results obtained by the Saetta et al. (1993) empirical equation and the equation proposed in this study, it was shown that the Saetta et al.

(1993) model overestimates the relative diffusion coefficient at high relative humidity levels and underestimates them at low relative humidity levels. In the same comparison, it was found that there is a good agreement between the experimental relative diffusion coefficient and the results obtained by the empirical equation developed in this study.

It was found that the addition of silica fume in the concrete mixes decreased the relative diffusion coefficient results, especially at high degrees of water saturation.

5.3 Conclusions

1) A relatively complete theoretical framework is proposed for modeling the major aspects of moisture flow and the transport and ionic species in unsaturated concrete. The proposed framework consists of using Richard's equation for moisture flow and a coupled equation for the advective-dispersive transport of ions.

2) Three experimental techniques have been used in this study to determine the key material parameters needed for modeling moisture flow and the transport of ions under unsaturated conditions, including the saturated permeability coefficient, the capillary pressure-moisture relationship, and the dependency of the effective diffusion coefficient on the degree of water saturation.

3) The experimental results of this study were used in different empirical models that have been originally developed for soils to examine whether they could be applied for concrete or not.

   3.1) The van Genuchten-Mualem model worked very nicely for representing the unsaturated hydraulic conductivity parameters and water retention data of concrete.

3.2) The Millington and Quirk model, on the on the other hand, although it has been successfully applied in many soils applications, did not work so nicely with the concrete specimens considered in this study, especially for the case of the saturation dependent tortuosity.

4) Following the failure of the Millington and Quirk model to represent the experimental data generated in this study, a more realistic empirical model was developed using a regression analysis and is proposed for predicting the relative diffusion coefficient as function of saturation and silica fume content.

5) The effects of using different proportions of silica fume (a supplementary cementing material), on the key hydraulic parameters of concrete were discussed, including its effect on the saturated permeability coefficient, the relative permeability coefficient, the moisture retention data, the relative diffusion coefficient, and the dependency of the effective diffusion coefficient on the degree of water saturation.

5.4 Recommendations for future work

1) The experimental work in this study could be extended to cover several types of concrete rather than evaluating the effect of only one type of supplementary cementing material on the hydraulic parameters of concrete (for example, cement type, types of aggregates, mineral admixtures, etc.).

2) Since the concrete sample holder designed and used in the centrifuge technique of this study has the ability to maintain water without any leakage under a relatively high angular speed (up 4000 RPM, the maximum speed that the used centrifuge machine could achieve), it could be used in the future for determining the saturated hydraulic

permeability of very low porosity concrete types, such as high performance concrete.

3) There is a need for a larger number of constitutive models that can reliably represent the relative diffusion coefficient of different types of concrete (concrete mixes) over a wide range of water saturation levels.

4) The experimental and the empirical hydraulic parameters determined in this study could easily be used by many predictive numerical codes available in the literature to evaluate the long-term effects of the service environment on the durability of concrete structures, such as the effects of chlorides, and moisture on the process of corrosion in the reinforcing steel bars.

6. References

ACI 211. 1-91, *Standard Practice for Selecting Proportions for Normal, Heavyweight, and Mass Concrete.* Farmington Hills, MI: American Concrete Institute, 1991.

Atkinson, A., and A. K. Nickerson. 1984. "The diffusion of ions through water saturated cement." *Journal of Materials Sciences* 19: 3068–78.

Barbour, S. L., P. C. Lim, and D. G. Fredlund. 1996. "A New Technique for Diffusion Testing of Unsaturated Soil." *Geotechnical Testing Journal* 19, no. 3: 247–58.

Basheer, Muhammed P. A. 2001. "Permeation Analysis." In *Handbook of Analytical Techniques in Concrete Science and Technology*, edited by V. S. Ramachandran and J. J. Beaudoin, 658–737. Norwich, NY: William Andrew Publishing/Noyes.

Bazant, Z. P., and L. J. Najjar. 1972. "Nonlinear Water Diffusion in Nonsaturated Concrete." *Materials and Structures* 5, no. 1: 3–20.

Brooks, R. H., and A. T. Corey. 1966. "Properties of porous media affecting fluid flow." *Journal of Irrigation and Drainage Div*. 72: 61–88.

Chung, D. D. L. 2002. "Review—Improving cement-based materials by using Silica Fume." *Journal of Materials Science* 37: 673–82.

Conca, J. L. and J. Wright. 1990. "Diffusion Coefficients in Gravel under Unsaturated Conditions." *Water Resource Research* 26, no. 5: 1055–66.

Crank, J. 1975. *The Mathematics of Diffusion*, 2nd ed. London: Oxford University Press.

Davis, G. B., M. G. Tefry, and B. M. Patterson. 2004. *Petroleum and solvent vapours: quantifying their behaviour assessment and exposure.* Perth: CSIRO Land and Water.

Dullien, F. A. L. 1992. *Porous Media: Fluid Transport and Pore Structures*, 2nd ed. New York, NY: Academic Press, Inc.

Durner, W. 1994. "Hydraulic conductivity estimation for soils with heterogeneous pore structure." *Water Resource Research* 32, no. 9: 211–23.

European Standard. 1996. *Building materials—Determination of hygroscopic sorption curves*. ISO/DIS 1257.

Garboczi, E. J. 1990. "Permeability, Diffusivity, and Microstructural Parameters: A Critical Review." *Cement and Concrete Research* 20: 591–601.

Gjrov, O. E. 1993. "Durability of concrete containing condensed silica fume." *ACI Special Publications* SP-79: 695–708.

Hall, C. 1989. "Water sorptivity of mortars and concretes: a review." *Magazine of Concrete Research* 41: 51–61.

Hall, C. 1994. "Barrier performance of concrete: A review of fluid transport theory." *Materials and Structures* 27: 291–306.

Hooton, R. D. 1993. “Influence of silica fume replacement of cement on physical properties and resistance to sulfate attack freezing and thawing, and alkali–silica reactivity.” *Journal of ACI Mater* 90, no. 2: 143–152.

Kelham, S. 1988. “A water absorption test for concrete.” *Magazine for Concrete Research* 40, 106–10.

Khaleel, R., J. F. Relyea, and J. L. Conca. 1995. “Evaluation of van Genuchten-Mualem relationships to estimate unsaturated hydraulic conductivity at low water contents.” *Water Resource Research* 31, no. 11: 2659–68.

Khanzode, R. M., S. K. Vanapalli, and D. G. Fredlund. 2002. “Measurement of soil-water characteristic curves for fine-grained soils using a small-scale centrifuge.” *Canadian Geotechnology Journal* 39: 1209–17.

Kitowski, C. J., and H. G. Wheat. 1997. “Effect of Chlorides on Reinforcing Steel Exposed to Simulated Concrete Solutions.” *Corrosion* 53, no. 3: 216–26.

Kosugi K. 1996. “Lognormal distribution model for unsaturated soil hydraulic properties.” *Water Resource Research* 32, no. 9: 2697–703.

Labuza, T. 1963. “Creation of Moisture Sorption Isotherms for Hygroscopic materials. Sorption Isotherm Methods.” *International Symposium on Humidity and Moisture*. www.fsci.umn.edu/Ted_Labuza/PDF_files/papersCreation_Moisture_Isotherms.PDF

Ludirdja, D., R. L. Berger, and J. F. Young. 1989. “Simple method for measuring water permeability of concrete.” *ACI Material Journal* 86: 433–9.

Mainguy, M., O. Coussy, and V. Baroghel-Bouny. 2001. “Role of Air Pressure in Drying of Weakly Permeable Materials.” *Journal of Engineering Mechanics* 127, no. 6: 582–92.

Martys, N. S. 1995. *Survey of Concrete Transport Properties and Their Measurement (NISTIR 5592).* Gaithersburg, MD: U.S. Department of Commerce, National Institute of Standards and Technology.

Martys, N. S. 1999. “Diffusion in partially-saturated porous material.” *Materials and Structures* 32: 555–62.

McCarter, W. J., T. M. Chrisp, A. Butler, and P. A. M. Basheer. 2001. “Near-surface sensors for conduction monitoring of cover-zone concrete.” *Construction and Building Materials* 15: 115–24.

Meyer, P. D., K. P. Saripalli, and V. L. Freedman. 2004. *Near-Field Hydrology Data Package for the Integrated Disposal Facility 2005 Performance Assessment (PNNL-14700).* Richland, WA: Pacific Northwest National Laboratory.

Millington, R. J., and J. P. Quirk. 1961. “Permeability of Porous Solids.” *Transactions of the Faraday Society* 57: 1200–7.

Monlouis-Bonnaire, J. P., J. Verdier, and B. Perrin. 2004. “Prediction of the relative permeability to gas flow of cement-based material.” *Cement and Concrete Research* 34: 737–44.

Monfore, G. E. 1968. “The Electrical Resistivity of Concrete.” *Journal of the PCA Research and Development Laboratories*, 35–48.

Mualem, Y. 1976. “A new model for predicting the hydraulic conductivity of unsaturated porous media.” *Water Resource Research* 12: 513–22.

Mualem, Y. 1976. “Hysteresis models for prediction of the hydraulic conductivity of unsaturated porous media.” *Water Resource Research* 12, no. 6: 1248–54.

Perraton, D., and P. C. Aitcin. 1992. *Permeability as seen by the researcher. High Performance Concrete: From Material to Structure*. London: E. & F.N. Spon.

Perraton, D., P. C. Aitcin, and D. Vezina. 1988. “Permeabilities of silica fume concretes.” *ACI Special Publications* SP-108: 63–84.

Polder, R. B., and W. H. A. Peelen. 2002. “Characterisation of chloride transport and reinforcement corrosion in concrete under cyclic wetting and drying by electrical resistivity.” *Cement and Concrete Composite* 24: 427–35.

Pont, S. D., and A. Ehrlacher. 2004. “Numerical and experimental analysis of chemical dehydration, heat and mass transfer in a concrete hollow cylinder submitted to high temperatures.” *International Journal of Heat and Mass Transfer* 47: 135–47.

Puyate, Y. T. and C. J. Lawrence. 1998. “Wick action at moderate Peclet number.” *Physics of Fluids* 10, no. 8: 2114–2116.

Richards, L. A. 1941. “A pressure-membrane extraction apparatus for soil solution.” *Soil Science* 51, no. 5: 377–86.

Richards, Lorenzo A. 1931. “Capillary conduction of liquids through porous mediums.” *Physics* 1: 318–33.

Richardson, M. G. 2002. *Fundamental of durable concrete, modern concrete technology*. London: Spon Press.

Romero, E., A. Gens, and A. Lloret. 2001. “Temperature effects on the hydraulic behaviour of an unsaturated clay.” *Geotechnical and Geological Engineering* 19: 311–32.

Saetta, A. V., R. V. Scotta, and R. V. Vitaliani. 1993. “Analysis of Chloride Diffusion into Partially Saturated Concrete.” *ACI Materials Journal* 90: 441–51.

Sallam, A., W. A. Jury, and J. Letey. 1984. “Measurements of gas diffusion coefficient under relatively low air-filled porosity.” *Soil Sciences Society of America Journal* 48, 3–6.

Samson, E., J. Marchand, K. A. Snyder, and J. J. Beaudoin. 2005. “Modeling ion and fluid transport in unsaturated cement systems in isothermal conditions.” *Cement and Concrete Research* 35: 141–53.

Schaefer, C. E., R. R. Arands, H. A. van der Sloot, and D. S. Kosson. 1995. "Prediction and experimental validation of liquid-phase diffusion resistance in unsaturated soils." *Journal of Contaminate Hydrology* 20: 145–66.

Scheidegger, A. E. 1974. *The Physics of Flow Through Porous Media*. Toronto: University of Toronto Press.

Shackelford, C. D. 1991. "Laboratory diffusion testing for waste disposal: A review." *Journal of Contaminate Hydrology* 7: 177–217.

Siddique, R, and Khan, M. I. 2011. *Supplementary cementing materials*. Heidelberg: Springer. http://public.eblib.com/EBLPublic/PublicView.do?ptiID=691006.

Šimůnek, J., M. Šejna, H. Saito, M. Sakai, and M. Th. van Genuchten. 2008. *The HYDRUS-1D Software Package for Simulating the Movement of Water, Heat, and Multiple Solutes in Variably Saturated Media* (Version 4.08, HYDRUS Software Series 3). Riverside, CA: Department of Environmental Sciences, University of California Riverside.

Tang, A., and Y. Cui. 2005. "Controlling suction by the vapour equilibrium technique at different temperatures and its application in determining the water retention properties of MX80 clay." *Canadian Geotechnology Journal* 42: 287–96.

The Concrete Society. 1988. *Permeability testing of site concrete—a review of methods and experiences (Technical Report 3)*. London: The Concrete Society.

Trangchirapat, W., and C. Janturapitakkul. 2010. “Strength, Dry Shrinkage, and Water Permeability of Concrete Incorporating Ground Palm Oil Fuel Ash.” *Cement and Concrete Composite* 32: 767–74.

van Genuchten, M. Th. 1980. “A closed-form equation for predicting the hydraulic conductivity of unsaturated soils.” *Soil Sciences Society of America Journal* 44: 892–8.

van Genuchten, M. Th., F. J. Leij, and S. R. Yates. 1991. *The RETC Code for Quantifying the Hydraulic Functions of Unsaturated Soils*. Riverside, CA: U.S. Salinity Laboratory, U.S. Department of Agriculture, Agricultural Research Service.

Vogel, T., and M. Císlerová. 1988. “On the reliability of unsaturated hydraulic conductivity calculated from the moisture retention curve.” *Transport in Porous Media* 3: 1–15.

Whitaker, S. 1998. “Coupled transport in multiphase systems: a theory of drying.” In *Advances in Heat Transfer*, edited by J.P. Hartnett et al., 1–104. San Diego, CA: Academic Press.

Whittington, H. W., J. McCarter, and M. C. Forde. 1981. “The conduction of electricity through concrete.” *Magazine of Concrete Research* 33, no. 114: 48–60.

7. Appendix A Saturated Permeability Measurements

Table 7.1: Saturated permeability measurements for Mix A (0% silica fume).

Sample #	**1**	**2**	**3**
Sample diameter	0.043 m	0.043 m	0.043
Sample length	0.15 m	0.15 m	0.15 m
Sample area	1.45E-3 m^2	1.45E-3 m^2	1.45E-3 m^2
Water tube diameter	0.15 m	0.15 m	0.15 m
Tube cross-sectional area	1.77E-4 m^2	1.77E-4 m^2	1.77E-4 m^2
Initial height of water in the tube	5.65E-2 m	5.65E-2 m	5.65E-2 m
Operative radius	0.19 m	0.19 m	0.19 m
Angular speed	2600 RPM	2600 RPM	2600 RPM
Angular velocity	272 rad/s	272 rad/s	272 rad/s
Acceleration	13737 m/s^2	13775 m/s^2	13737 m/s^2
Scale factor N	1400	1404	1400
Drop of water level in the tube	4E-3 m	5E-3 m	4E-3 m
Final height of water in the tube	5.25E-2 m	5.15E-2 m	5.25E-2 m
Periods of checking data	4 hr	4 hr	4 hr
Saturated permeability	6.6E-12 m/s	7.8E-12 m/s	6.6E-12 m/s

Table 7.2: Saturated permeability measurements for Mix B (5% silica fume).

Sample #	**1**	**2**	**3**
Sample diameter	0.043 m	0.043 m	0.043
Sample length	0.15 m	0.15 m	0.15 m
Sample area	1.45E-3 m^2	1.45E-3 m^2	1.45E-3 m^2
Water tube diameter	0.15 m	0.15 m	0.15 m
Tube cross-sectional area	1.77E-4 m^2	1.77E-4 m^2	1.77E-4 m^2
Initial height of water in the tube	5.65E-2 m	5.65E-2 m	5.65E-2 m
Operative radius	0.19 m	0.19 m	0.19 m
Angular speed	2800 RPM	2800 RPM	2800 RPM
Angular velocity	293 rad/s	293 rad/s	293 rad/s
Acceleration	15932 m/s^2	15975 m/s^2	15932 m/s^2
Scale factor N	1624	1628	1624
Drop of water level in the tube	3E-3 m	3.5E-3 m	3E-3 m
Final height of water in the tube	5.35E-2 m	5.3E-2 m	5.35E-2 m
Periods of checking data	4 hr	4 hr	4 hr
Saturated permeability	4.3E-12 m/s	4.6E-12 m/s	4.3E-12 m/s

Table 7.3: Saturated permeability measurements for Mix C (10% silica fume).

Sample #	**1**	**2**	**3**
Sample diameter	0.043 m	0.043 m	0.043
Sample length	0.15 m	0.15 m	0.145 m
Sample area	1.45E-3 m^2	1.45E-3 m^2	1.45E-3 m^2
Water tube diameter	0.15 m	0.15 m	0.145 m
Tube cross-sectional area	1.77E-4 m^2	1.77E-4 m^2	1.77E-4 m^2
Initial height of water in the tube	5.65E-2 m	5.65E-2 m	5.65E-2 m
Operative radius	0.19	0.19	0.19
Angular speed	2800 RPM	2800 RPM	2800 RPM
Angular velocity	293 rad/s	293 rad/s	293 rad/s
Acceleration	15932 m/s^2	15932 m/s^2	15945 m/s^2
Scale factor N	1624	1624	1626
Drop of water level in the tube	4E-3 m	4E-3 m	3.5E-3 m
Final height of water in the tube	5.35E-2 m	5.3E-2 m	5.35E-2 m
Periods of checking data	6 hr	6 hr	6 hr
Saturated permeability	3.8E-12 m/s	3.8E-12 m/s	3.2E-12 m/s

Table 7.4: Saturated permeability measurements for Mix D (15% silica fume).

Sample #	**1**	**2**	**3**
Sample diameter	0.043 m	0.043 m	0.043
Sample length	0.15 m	0.15 m	0.15 m
Sample area	1.45E-3 m^2	1.45E-3 m^2	1.45E-3 m^2
Water tube diameter	0.15 m	0.15 m	0.15 m
Tube cross-sectional area	1.77E-4 m^2	1.77E-4 m^2	1.77E-4 m^2
Initial height of water in the tube	5.65E-2 m	5.65E-2 m	5.65E-2 m
Operative radius	0.19	0.19	0.19
Angular speed	2800 RPM	2800 RPM	2800 RPM
Angular velocity	293 rad/s	293 rad/s	293 rad/s
Acceleration	15932 m/s^2	15932 m/s^2	15932 m/s^2
Scale factor N	1624	1624	1624
Drop of water level in the tube	3E-3 m	3E-3 m	4E-3 m
Final height of water in the tube	5.35E-2 m	5.3E-2 m	5.25E-2 m
Periods of checking data	10 hr	10 hr	10 hr
Saturated permeability	1.7E-12 m/s	1.7E-12 m/s	2.3E-12 m/s

Table 7.5: Saturated permeability measurements for Mix E (20% silica fume).

Sample #	**1**	**2**	**3**
Sample diameter	0.043 m	0.043 m	0.043
Sample length	0.15 m	0.15 m	0.15 m
Sample area	1.45E-3 m^2	1.45E-3 m^2	1.45E-3 m^2
Water tube diameter	0.14 m	0.15 m	0.15 m
Tube cross-sectional area	1.77E-4 m^2	1.77E-4 m^2	1.77E-4 m^2
Initial height of water in the tube	5.65E-2 m	5.65E-2 m	5.65E-2 m
Operative radius	0.19	0.19	0.19
Angular speed	2900 RPM	2900 RPM	2900 RPM
Angular velocity	304 rad/s	304 rad/s	304 rad/s
Acceleration	17137 m/s^2	17091 m/s^2	17091 m/s^2
Scale factor N	1747	1742	1742
Drop of water level in the tube	3E-3 m	3E-3 m	4E-3 m
Final height of water in the tube	5.35E-2 m	5.3E-2 m	5.25E-2 m
Periods of checking data	14 hr	14 hr	14 hr
Saturated permeability	1.1E-12 m/s	1.1E-12 m/s	1.5E-12 m/s

8. Appendix B Degree of Saturation Measurements

Table 8.1: The measurements of the degrees of water saturation for Mix A (0%SF).

Sample #	SSD mass (g)	Oven dry mass (g)	Relative humidity %	Equilibrium mass at RH%	Saturation %
1	30.0748	28.157	97.3	30.070	99.750
2	28.6222	26.234		28.620	99.916
3	31.5952	30.000		31.500	94.032
1	31.0631	29.270	93.5	31.060	99.827
2	27.3347	25.714		27.310	98.476
3	27.6559	26.003		27.630	98.433
1	28.5871	26.861	84.3	28.444	91.722
2	31.2392	29.317		31.021	88.672
3	29.3330	27.399		29.165	91.304
1	28.7920	27.095	78.5	28.485	81.920
2	31.1493	29.037		30.709	79.159
3	30.5890	28.813		30.271	82.095
1	29.7009	28.0093	75.3	29.3597	79.830
2	26.2776	24.7249		25.9605	79.578
3	26.9879	25.3925		26.685	81.014
1	30.1557	28.257	68.9	29.5925	70.338
2	31.1441	29.8299		30.7095	66.930
3	30.5052	28.5338		29.9195	70.290
1	27.4304	25.7112	57.6	26.7706	61.622
2	28.2208	26.4148		27.5328	61.905
3	26.6418	25.1486		26.0989	63.642

Table 8.1 (Cont.): The measurements of the degrees of water saturation for Mix A (0%SF).

Sample #	SSD mass (g)	Oven dry mass (g)	Relative humidity %	Equilibrium mass at RH%	Saturation %
1	27.3327	25.7679	43.2	26.6564	56.780
2	30.8390	29.0389		30.0371	55.452
3	28.7088	27.1177		27.9969	55.257
1	31.3654	29.5971	32.9	30.326	41.226
2	31.1350	29.352		30.128	43.494
3	26.5538	24.9635		25.635	42.225
1	28.7682	27.0366	22.5	27.594	32.190
2	30.7142	28.9226		29.514	33.004
3	28.5051	26.6085		27.222	32.358
1	27.5049	25.7438	11.3	26.199	25.836
2	31.7317	29.8391		30.339	26.398
3	28.2416	26.556		26.990	25.765
1	29.6488	27.7341	8.2	28.194	23.999
2	28.8210	26.8287		27.292	23.234
3	28.5858	26.7341		27.162	23.098

Table 8.2: The measurements of the degrees of water saturation for Mix B (5%SF).

Sample #	SSD mass (g)	Oven dry mass (g)	Relative humidity %	Equilibrium mass at RH%	Saturation %
1	30.3035	28.151	97.3	30.240	97.050
2	30.7656	28.643		30.690	96.439
3	30.3769	28.171		30.271	95.200
1	28.8101	26.707	93.5	28.760	97.618
2	29.9785	27.904		29.960	99.108
3	29.7308	27.700		29.720	99.468
1	28.9767	27.059	84.3	28.854	93.583
2	28.8603	26.685		28.668	91.156
3	30.2288	28.001		30.062	92.496
1	27.2272	25.375	78.5	26.982	86.781
2	28.8322	26.738		28.473	82.862
3	30.0177	28.0254		29.698	83.953
1	29.9919	27.8305	75.3	29.5877	81.299
2	28.7533	26.8821		28.4184	82.102
3	30.6799	28.4777		30.3206	83.684
1	30.8013	28.7458	68.9	30.2646	73.890
2	29.0208	27.1573		28.555	75.004
3	29.3429	27.2973		28.8325	75.049
1	28.2068	26.355	57.6	27.5695	65.585
2	30.2554	28.2033		29.5141	63.876
3	28.7506	26.6914		28.0234	64.685

Table 8.2 (Cont.): The measurements of the degrees of water saturation for Mix B (5%SF).

Sample #	SSD mass (g)	Oven dry mass (g)	Relative humidity %	Equilibrium mass at RH%	Saturation %
1	31.9117	29.8938	43.2	31.0363	56.618
2	31.4358	29.2397		30.4981	57.302
3	29.0100	27.075		28.1792	57.065
1	28.1084	26.1536	32.9	26.977	42.122
2	30.4880	28.5831		29.3764	41.645
3	29.4764	27.5007		28.3409	42.527
1	28.1143	26.3103	22.5	26.8923	32.262
2	28.8892	26.8254		27.499	32.639
3	28.9251	27.0219		27.6213	31.494
1	28.4711	26.5153	11.3	27.0107	25.330
2	27.9672	26.0675		26.5455	25.162
3	31.0444	29.0283		29.5333	25.048
1	29.3497	27.218	8.2	27.6941	22.334
2	29.0996	27.0634		27.5407	23.441
3	29.3915	27.3506		27.7945	21.750

Table 8.3: The measurements of the degrees of water saturation for Mix C (10%SF).

Sample #	SSD mass (g)	Oven dry mass (g)	Relative humidity %	Equilibrium mass at RH%	Saturation %
1	30.0002	27.932	97.3	29.997	99.826
2	30.7415	28.467		30.740	99.947
3	29.0899	26.884		29.089	99.964
1	29.4546	27.222	93.5	29.457	100.125
2	29.5306	27.336		29.511	99.116
3	28.8523	26.836		28.847	99.737
1	29.8596	27.559	84.3	29.675	91.984
2	28.3343	26.238		28.181	92.703
3	29.9123	27.662		29.694	90.307
1	29.8906	27.682	78.5	29.568	85.378
2	27.2587	25.208		27.009	87.808
3	28.7248	26.8451		28.4914	87.583
1	27.0472	24.9561	75.3	26.7095	83.851
2	28.8992	26.836		28.5743	84.253
3	30.3957	28.317		30.0849	85.048
1	30.7056	28.6075	68.9	30.2706	79.267
2	29.1347	26.917		28.6357	77.499
3	27.7707	25.6		27.2549	76.238
1	29.1441	27.0907	57.6	28.501	68.681
2	30.5092	28.3401		29.8041	67.493
3	28.7863	26.878		28.1268	65.440

Table 8.3 (Cont.): The measurements of the degrees of water saturation for Mix C (10%SF).

Sample #	SSD mass (g)	Oven dry mass (g)	Relative humidity %	Equilibrium mass at RH%	Saturation %
1	28.5902	26.5206	43.2	27.7174	57.828
2	29.5315	27.5558		28.6829	57.048
3	28.0541	25.9997		27.14	55.505
1	30.5848	28.5106	32.9	29.4624	45.888
2	30.5789	28.4298		29.4278	46.438
3	28.2957	26.0897		27.074	44.619
1	30.2319	27.9151	22.5	28.7029	34.004
2	29.9685	27.797		28.5189	33.244
3	29.1577	26.9904		27.6758	31.625
1	29.8829	27.71	11.3	28.2457	24.654
2	29.8720	27.7144		28.2532	24.972
3	28.8092	26.6729		27.196	24.486
1	27.9976	25.911	8.2	26.3732	22.151
2	27.9957	26.0139		26.4468	21.844
3	30.4656	28.308		28.7806	21.904

Table 8.4: The measurements of the degrees of water saturation for Mix D (15%SF).

Sample #	SSD mass (g)	Oven dry mass (g)	Relative humidity %	Equilibrium mass at RH%	Saturation %
1	30.5442	28.426	97.3	30.530	99.330
2	26.7479	24.855		26.718	98.420
3	27.8460	25.642		27.811	98.412
1	28.2070	26.103	93.5	28.115	95.614
2	28.3129	26.372		28.299	99.305
3	29.9220	27.869		29.912	99.513
1	29.5783	27.383	84.3	29.454	94.329
2	29.2008	26.961		29.074	94.322
3	27.2088	25.285		27.090	93.826
1	26.6289	24.766	78.5	26.413	88.430
2	28.3130	26.298		28.064	87.624
3	28.7880	26.7153		28.5502	88.527
1	29.8290	27.7396	75.3	29.5454	86.427
2	28.9551	26.5556		28.6339	86.614
3	29.8568	27.7172		29.5732	86.745
1	29.6300	27.5067	68.9	29.2115	80.290
2	28.9565	26.9803		28.5847	81.186
3	27.7507	25.639		27.299	78.610
1	25.4155	23.193	57.6	24.7566	70.353
2	29.0581	26.8873		28.4	69.684
3	27.1342	25.1134		26.4882	68.032

Table 8.4 (Cont.): The measurements of the degrees of water saturation for Mix D (15%SF).

Sample #	SSD mass (g)	Oven dry mass (g)	Relative humidity %	Equilibrium mass at RH%	Saturation %
1	26.3394	24.3814	43.2	25.5291	58.616
2	31.6785	29.6646		30.7935	56.055
3	31.6477	29.2583		30.5953	55.955
1	29.5885	27.5527	32.9	28.448	43.978
2	29.1205	27.091		28.0563	47.563
3	27.6590	25.7816		26.6174	44.519
1	29.8710	27.7166	22.5	28.4446	33.791
2	30.8866	28.7739		29.5345	36.001
3	28.4354	26.2704		27.027	34.947
1	27.3008	25.3187	11.3	25.7609	22.310
2	29.8595	27.7689		28.2444	22.745
3	27.5043	25.529		25.9972	23.703
1	29.4521	27.3419	8.2	27.7724	20.401
2	25.3266	23.4825		23.8751	21.290
3	29.2735	27.2797		27.698	20.980

Table 8.5: The measurements of the degrees of water saturation for Mix E (20%SF).

Sample #	SSD mass (g)	Oven dry mass (g)	Relative humidity %	Equilibrium mass at RH%	Saturation %
1	28.5260	26.669	97.3	28.516	99.462
2	30.6691	28.680		30.659	99.492
3	28.2130	26.466		28.200	99.273
1	24.3158	22.610	93.5	24.302	99.179
2	29.2576	27.344		29.228	98.448
3	28.1872	26.141		28.157	98.505
1	29.6022	27.646	84.3	29.465	92.993
2	30.5639	28.745		30.460	94.265
3	26.5970	24.983		26.511	94.647
1	26.5820	24.906	78.5	26.397	88.947
2	29.0170	27.023		28.762	87.224
3	27.0359	25.0442		26.8335	89.838
1	30.0484	27.9468	75.3	29.7253	84.626
2	28.4065	26.2298		28.1255	87.091
3	28.8702	26.966		28.6177	86.740
1	29.6777	27.7657	68.9	29.2931	79.885
2	30.2274	28.1592		29.8479	81.651
3	27.4258	25.6044		27.0891	81.514
1	31.2744	29.2377	57.6	30.7572	74.606
2	25.9265	24.2464		25.5077	75.073
3	25.9943	24.4362		25.5772	73.230

Table 8.5 (Cont.): The measurements of the degrees of water saturation for Mix E (20%SF).

Sample #	SSD mass (g)	Oven dry mass (g)	Relative humidity %	Equilibrium mass at RH%	Saturation %
1	28.4277	26.561	43.2	27.7003	61.033
2	30.9760	28.8756		30.156	60.960
3	29.6802	27.4879		28.8114	60.370
1	24.3745	22.6577	32.9	23.409	43.762
2	31.8269	29.9215		30.8533	48.903
3	27.6277	25.8331		26.6509	45.570
1	27.5895	25.934	22.5	26.4653	32.093
2	31.4485	29.5343		30.1956	34.547
3	29.8765	28.0228		28.6295	32.729
1	25.3850	23.6334	11.3	24.0406	23.247
2	26.1186	24.1639		24.6204	23.354
3	29.6005	27.6004		28.0872	24.339
1	29.5060	27.5703	8.2	27.9775	21.036
2	27.9422	26.0117		26.4458	22.486
3	31.7185	29.4578		29.9605	22.236

9. Appendix C Electrical Resistivity Measurements

Table 9.1: Electrical resistivity measurements for Mix A (0%SF).

Sample #	Electrical current (amp) at 2.5V	Electrical current (amp) at 5V	Potential voltage (V)	Resistivity (ohm)	Sample area cm^2	Sample thickness (cm)	RH (%)	Electrical resistivity K.ohm.cm
1	1.30E-03	3.63E-03	1.11	1072	19.6	0.50	97.3	42
2	1.01E-03	2.65E-03	0.96	1524	19.6	0.65		46
3	1.04E-03	2.76E-03	0.98	1455	19.6	0.60		48
1	9.50E-04	2.32E-03	0.77	1825	19.6	0.60	93.5	60
2	1.14E-03	3.26E-03	1.16	1179	19.6	0.55		42
3	1.26E-03	3.20E-03	0.88	1289	19.6	0.60		42
1	8.70E-04	2.15E-03	0.80	1953	19.6	0.65	84.3	59
2	8.70E-04	1.90E-03	0.39	2427	19.6	0.70		68
3	8.90E-04	2.15E-03	0.73	1984	19.6	0.70		56
1	8.20E-04	1.84E-03	0.49	2451	19.6	0.70	78.5	69
2	7.80E-04	2.00E-03	0.90	2049	19.6	0.60		67
3	9.30E-04	2.18E-03	0.64	2000	19.6	0.60		65
1	7.70E-04	1.87E-03	0.75	2273	19.6	0.60	75.3	74
2	8.50E-04	2.13E-03	0.84	1953	19.6	0.50		77
3	7.80E-04	1.90E-03	0.76	2232	19.6	0.60		73
1	6.20E-04	1.29E-03	0.19	3731	19.6	0.70	68.9	105
2	6.70E-04	1.45E-03	0.35	3205	19.6	0.60		105
3	6.90E-04	1.55E-03	0.49	2907	19.6	0.60		95

Table 9.1 (Cont.): Electrical resistivity measurements for Mix A (0%SF).

Sample #	Electrical current (amp) at 2.5V	Electrical current (amp) at 5V	Potential voltage (V)	Resistivity (ohm)	Sample area cm^2	Sample thickness (cm)	RH (%)	Electrical resistivity K.ohm.cm
1	6.90E-04	1.44E-03	0.20	3333	19.6	0.60	57.6	109
2	8.30E-04	1.72E-03	0.17	2809	19.6	0.50		110
3	6.70E-04	1.50E-03	0.48	3012	19.6	0.50		118
1	6.50E-04	1.40E-03	0.33	3333	19.6	0.50	43.2	131
2	6.00E-04	1.34E-03	0.47	3378	19.6	0.50		133
3	6.00E-04	1.45E-03	0.74	2941	19.6	0.50		115
1	3.00E-04	6.80E-04	0.53	6579	19.6	0.60	32.9	215
2	2.00E-04	6.00E-04	1.25	6250	19.6	0.60		204
3	2.50E-04	6.40E-04	0.90	6410	19.6	0.60		210
1	4.00E-04	8.00E-04	0.00	6250	19.6	0.60	22.5	204
2	2.00E-04	4.80E-04	0.71	8929	19.6	0.60		292
3	3.90E-04	6.50E-04	-1.25	9615	19.6	0.70		270
1	2.58E-04	5.30E-04	0.13	9191	19.6	0.65	11.3	278
2	2.34E-04	4.69E-04	0.01	10638	19.6	0.70		298
3	2.90E-04	5.93E-04	0.11	8251	19.6	0.65		249
1	2.72E-04	5.75E-04	0.26	8251	19.6	0.50	8.2	324
2	2.50E-04	5.43E-04	0.37	8532	19.6	0.50		335
3	2.61E-04	5.59E-04	0.31	8389	19.6	0.50		329

Table 9.2: Electrical resistivity measurements for Mix B (5%SF).

Sample #	Electrical current (amp) at 2.5V	Electrical current (amp) at 5V	Potential voltage (V)	Resistivity (ohm)	Sample area cm^2	Sample thickness (cm)	RH (%)	Electrical resistivity K.ohm.cm
1	6.73E-04	1.71E-03	0.88	2408	19.6	0.70	97.3	68
2	7.30E-04	1.95E-03	1.00	2056	19.6	0.65		62
3	9.40E-04	2.10E-03	0.47	2155	19.6	0.70		60
1	1.08E-03	2.58E-03	0.70	1667	19.6	0.50	93.5	65
2	9.90E-04	2.15E-03	0.37	2155	19.6	0.60		70
3	1.03E-03	2.11E-03	0.12	2315	19.6	0.70		65
1	9.20E-04	2.05E-03	0.46	2212	19.6	0.55	84.3	79
2	7.90E-04	1.81E-03	0.56	2451	19.6	0.60		80
3	8.20E-04	1.82E-03	0.45	2500	19.6	0.60		82
1	7.20E-04	1.53E-03	0.28	3086	19.6	0.60	78.5	101
2	7.50E-04	1.65E-03	0.42	2778	19.6	0.50		109
3	7.80E-04	1.60E-03	0.12	3049	19.6	0.60		100
1	7.00E-04	1.40E-03	0.00	3571	19.6	0.60	75.3	117
2	6.20E-04	1.41E-03	0.54	3165	19.6	0.60		104
3	6.80E-04	1.41E-03	0.17	3425	19.6	0.60		112
1	5.40E-04	1.10E-03	0.09	4464	19.6	0.60	68.9	146
2	6.10E-04	1.24E-03	0.08	3968	19.6	0.60		130
3	6.00E-04	1.24E-03	0.16	3906	19.6	0.60		128
1	5.10E-04	1.09E-03	0.30	4310	19.6	0.50	57.6	169
2	5.80E-04	1.16E-03	0.00	4310	19.6	0.55		154
3	5.50E-04	1.10E-03	0.00	4545	19.6	0.60		149

Table 9.2 (Cont.): Electrical resistivity measurements for Mix B (5%SF).

Sample #	Electrical current (amp) at 2.5V	Electrical current (amp) at 5V	Potential voltage (V)	Resistivity (ohm)	Sample area cm^2	Sample thickness (cm)	RH (%)	Electrical resistivity K.ohm.cm
1	2.80E-04	6.60E-04	0.66	6579	19.6	0.65	43.2	199
2	2.75E-04	6.70E-04	0.76	6329	19.6	0.70		177
3	2.93E-04	6.80E-04	0.61	6460	19.6	0.70		181
1	2.80E-04	6.00E-04	0.31	7813	19.6	0.60	32.9	256
2	2.80E-04	6.00E-04	0.31	7813	19.6	0.60		256
3	3.60E-04	7.30E-04	0.07	6757	19.6	0.50		265
1	1.80E-04	3.80E-04	0.25	12500	19.6	0.70	22.5	350
2	1.85E-04	3.69E-04	0.00	13543	19.6	0.70		380
3	1.82E-04	3.75E-04	0.13	13001	19.6	0.70		364
1	1.91E-04	3.87E-04	0.06	12755	19.6	0.65	11.3	385
2	1.93E-04	3.94E-04	0.10	12438	19.6	0.70		349
3	1.92E-04	3.91E-04	0.08	12594	19.6	0.65		380
1	1.27E-04	2.80E-04	0.42	16340	19.6	0.70	8.2	458
2	1.20E-04	2.80E-04	0.62	15625	19.6	0.65		472
3	1.00E-04	2.55E-04	0.89	16129	19.6	0.75		422

Table 9.3: Electrical resistivity measurements for Mix C (10%SF).

Sample #	Electrical current (amp) at 2.5V	Electrical current (amp) at 5V	Potential voltage (V)	Resistivity (ohm)	Sample area cm^2	Sample thickness (cm)	RH (%)	Electrical resistivity K.ohm.cm
1	7.60E-04	1.60E-03	0.24	2976	19.6	0.70	97.3	83
2	6.20E-04	1.46E-03	0.65	2976	19.6	0.60		97
3	7.50E-04	1.62E-03	0.34	2874	19.6	0.65		87
1	7.40E-04	1.64E-03	0.44	2786	19.6	0.50	93.5	109
2	7.40E-04	1.73E-03	0.63	2525	19.6	0.50		99
3	7.30E-04	1.55E-03	0.26	3067	19.6	0.60		100
1	6.23E-04	1.34E-03	0.33	3487	19.6	0.50	84.3	137
2	6.12E-04	1.23E-03	0.04	4026	19.6	0.65		122
3	6.19E-04	1.24E-03	0.01	4026	19.6	0.65		122
1	5.60E-04	1.19E-03	0.26	4000	19.6	0.50	78.5	157
2	5.71E-04	1.19E-03	0.21	4019	19.6	0.50		158
3	5.81E-04	1.20E-03	0.15	4039	19.6	0.50		159
1	5.70E-04	1.14E-03	0.00	4386	19.6	0.60	75.3	143
2	5.70E-04	1.18E-03	0.16	4098	19.6	0.50		161
3	5.00E-04	1.02E-03	0.08	4845	19.6	0.55		173
1	4.46E-04	9.00E-04	0.04	5507	19.6	0.60	68.9	180
2	4.70E-04	9.70E-04	0.15	5000	19.6	0.60		164
3	4.58E-04	9.35E-04	0.10	5241	19.6	0.60		171
1	3.40E-04	7.00E-04	0.14	6944	19.6	0.60	57.6	227
2	4.00E-04	8.10E-04	0.06	6098	19.6	0.50		239
3	4.60E-04	9.50E-04	0.15	5102	19.6	0.50		200

Table 9.3 (Cont.): Electrical resistivity measurements for Mix C (10%SF).

Sample #	Electrical current (amp) at 2.5V	Electrical current (amp) at 5V	Potential voltage (V)	Resistivity (ohm)	Sample area cm^2	Sample thickness (cm)	RH (%)	Electrical resistivity K.ohm.cm
1	1.85E-04	3.70E-04	0.00	13514	19.6	0.65	32.9	408
2	1.25E-04	3.50E-04	1.11	11111	19.6	0.60		363
3	2.10E-04	4.35E-04	0.17	11111	19.6	0.60		363
1	1.50E-04	3.00E-04	0.00	16667	19.6	0.60	22.5	545
2	1.45E-04	3.00E-04	0.16	16129	19.6	0.60		528
3	1.40E-04	3.70E-04	0.98	10870	19.6	0.50		427
1	1.44E-04	2.88E-04	0.00	17361	19.6	0.60	11.3	568
2	1.40E-04	3.00E-04	0.31	15625	19.6	0.60		511
3	1.42E-04	2.94E-04	0.16	16447	19.6	0.60		538
1	1.17E-04	2.35E-04	0.02	21186	19.6	0.60	8.2	693
2	1.70E-04	3.40E-04	0.00	14706	19.6	0.45		641
3	1.06E-04	2.34E-04	0.43	19531	19.6	0.70		548

Table 9.4: Electrical resistivity measurements for Mix D (15%SF).

Sample #	Electrical current (amp) at 2.5V	Electrical current (amp) at 5V	Potential voltage (V)	Resistivity (ohm)	Sample area cm^2	Sample thickness (cm)	RH (%)	Electrical resistivity K.ohm.cm
1	7.00E-04	1.49E-03	0.28	3165	19.6	0.65	97.3	96
2	7.00E-04	1.46E-03	0.20	3289	19.6	0.60		108
3	6.30E-04	1.30E-03	0.15	3731	19.6	0.65		113
1	6.50E-04	1.38E-03	0.27	3425	19.6	0.60	93.5	112
2	7.00E-04	1.40E-03	0.00	3571	19.6	0.60		117
3	6.50E-04	1.40E-03	0.33	3333	19.6	0.60		109
1	5.14E-04	1.04E-03	0.06	4753	19.6	0.70	84.3	133
2	5.75E-04	1.17E-03	0.06	4237	19.6	0.60		139
3	5.71E-04	1.17E-03	0.10	4195	19.6	0.60		137
1	4.70E-04	9.46E-04	0.03	5252	19.6	0.60	78.5	172
2	4.80E-04	9.60E-04	0.00	5208	19.6	0.60		170
3	4.60E-04	9.40E-04	0.10	5208	19.6	0.60		170
1	4.45E-04	9.02E-04	0.06	5476	19.6	0.60	75.3	179
2	4.40E-04	8.80E-04	0.00	5682	19.6	0.60		186
3	4.50E-04	9.23E-04	0.12	5285	19.6	0.60		173
1	4.00E-04	8.08E-04	0.05	6127	19.6	0.60	68.9	200
2	3.83E-04	8.00E-04	0.20	5995	19.6	0.55		214
3	4.40E-04	8.95E-04	0.08	5495	19.6	0.55		196
1	3.68E-04	7.42E-04	0.04	6684	19.6	0.50	57.6	262
2	3.14E-04	6.40E-04	0.09	7669	19.6	0.60		251
3	3.63E-04	7.30E-04	0.03	6812	19.6	0.55		243

Table 9.4 (Cont.): Electrical resistivity measurements for Mix D (15%SF).

Sample #	Electrical current (amp) at 2.5V	Electrical current (amp) at 5V	Potential voltage (V)	Resistivity (ohm)	Sample area cm^2	Sample thickness (cm)	RH (%)	Electrical resistivity K.ohm.cm
1	2.35E-04	4.75E-04	0.05	10417	19.6	0.60	43.2	341
2	2.35E-04	4.70E-04	0.00	10638	19.6	0.60		348
3	2.45E-04	5.00E-04	0.10	9804	19.6	0.60		321
1	1.65E-04	3.40E-04	0.14	14286	19.6	0.60	32.9	467
2	1.80E-04	3.75E-04	0.19	12821	19.6	0.55		457
3	1.90E-04	3.90E-04	0.12	12500	19.6	0.55		446
1	1.60E-04	3.25E-04	0.08	15152	19.6	0.50	22.5	595
2	1.69E-04	3.30E-04	-0.12	15528	19.6	0.50		609
3	1.65E-04	3.20E-04	-0.14	16077	19.6	0.50		631
1	1.80E-04	3.00E-04	-1.25	20833	19.6	0.55	11.3	743
2	1.89E-04	3.30E-04	-0.85	17730	19.6	0.50		696
3	1.85E-04	3.15E-04	-1.03	19157	19.6	0.50		752
1	1.10E-04	2.00E-04	-0.56	27778	19.6	0.70	8.2	779
2	1.40E-04	2.90E-04	0.17	16667	19.6	0.45		727
3	1.34E-04	2.70E-04	0.04	18382	19.6	0.50		722

Table 9.5: Electrical resistivity measurements for Mix E (20%SF).

Sample #	Electrical current (amp) at 2.5V	Electrical current (amp) at 5V	Potential voltage (V)	Resistivity (ohm)	Sample area cm^2	Sample thickness (cm)	RH (%)	Electrical resistivity K.ohm.cm
1	4.36E-04	9.55E-04	0.40	4817	19.6	0.60	97.3	158
2	3.90E-04	8.50E-04	0.38	5435	19.6	0.65		164
3	3.90E-04	9.00E-04	0.59	4902	19.6	0.65		148
1	3.66E-04	9.00E-04	0.79	4682	19.6	0.50	93.5	184
2	3.10E-04	8.00E-04	0.92	5102	19.6	0.55		182
3	3.38E-04	8.50E-04	0.85	4883	19.6	0.50		192
1	3.20E-04	7.40E-04	0.60	5952	19.6	0.55	84.3	212
2	3.20E-04	7.40E-04	0.60	5952	19.6	0.60		195
3	3.10E-04	6.73E-04	0.37	6887	19.6	0.65		208
1	3.00E-04	6.20E-04	0.16	7813	19.6	0.60	78.5	256
2	3.05E-04	7.30E-04	0.71	5882	19.6	0.50		231
3	3.00E-04	7.30E-04	0.76	5814	19.6	0.50		228
1	3.20E-04	6.60E-04	0.15	7353	19.6	0.55	75.3	262
2	3.30E-04	7.00E-04	0.27	6757	19.6	0.50		265
3	2.70E-04	5.90E-04	0.39	7813	19.6	0.50		307
1	2.20E-04	5.90E-04	1.01	6757	19.6	0.45	68.9	295
2	3.50E-04	6.80E-04	-0.15	7576	19.6	0.50		297
3	2.55E-04	5.60E-04	0.41	8197	19.6	0.50		322
1	1.90E-04	4.00E-04	0.24	11905	19.6	0.60	57.6	389
2	2.10E-04	4.30E-04	0.11	11364	19.6	0.60		372
3	1.82E-04	3.90E-04	0.31	12019	19.6	0.60		393

Table 9.5 (Cont.): Electrical resistivity measurements for Mix E (20%SF).

Sample #	Electrical current (amp) at 2.5V	Electrical current (amp) at 5V	Potential voltage (V)	Resistivity (ohm)	Sample area cm^2	Sample thickness (cm)	RH (%)	Electrical resistivity K.ohm.cm
1	2.10E-04	4.20E-04	0.00	11905	19.6	0.40	43.2	584
2	1.14E-04	2.30E-04	0.04	21552	19.6	0.60		705
3	1.10E-04	2.25E-04	0.11	21739	19.6	0.70		609
1	1.40E-04	2.80E-04	0.00	17857	19.6	0.50	32.9	701
2	1.18E-04	2.36E-04	0.00	21186	19.6	0.55		756
3	1.29E-04	2.58E-04	0.00	19380	19.6	0.50		761
1	5.50E-05	1.40E-04	0.88	29412	19.6	0.50	22.5	1154
2	7.00E-05	1.45E-04	0.17	33333	19.6	0.50		1308
3	7.60E-05	1.50E-04	-0.07	33784	19.6	0.55		1205
1	1.00E-04	1.80E-04	-0.63	31250	19.6	0.50	11.3	1227
2	9.50E-05	1.90E-04	0.00	26316	19.6	0.40		1291
3	9.75E-05	1.85E-04	-0.29	28571	19.6	0.50		1121
1	4.40E-05	1.00E-04	0.54	44643	19.6	0.55	8.2	1593
2	3.50E-05	9.00E-05	0.91	45455	19.6	0.60		1487
3	3.95E-05	9.00E-05	0.54	49505	19.6	0.65		1495